The Pennsylvania State University

The Graduate School

Department of Materials Science and Engineering

LONGITUDINAL PIEZOELECTRIC CHARACTERIZATION AND DOMAIN WALL CONTRIBUTIONS IN LEAD ZIRCONATE TITANATE THIN FILMS

A Thesis in

Materials Science and Engineering

by

Fei Xu

Submitted in Partial Fulfillment

of the Requirements

for the Degree of

Doctor of Philosophy

August 1999

Abstract

Lead zirconate titanate (PZT) films have been used in a number of novel MEMS (microelectromechanical systems) devices due to the superior electromechanical properties of ferroelectric PZT. For the proper design of such devices, precise knowledge of the electromechanical properties of PZT films, including the longitudinal piezoelectric coefficients d_{33} are required. However, most of the current piezoelectric characterization techniques are not directly applicable to the measurement of piezoelectric thin films due to the existence of a substrate and the limitations imposed by the sample geometry. In this work, a pneumatic pressure charge technique was developed for characterization of the effective d_{33} of piezoelectric films using the direct piezoelectric effect. A stress normal to the film plane was applied to the PZT films through the pneumatic pressure rig and the induced charge was measured for calculation of the effective d_{33}. It was found that additional in-plane stresses were also applied to the film due to friction between the O-ring and film surfaces; most of the stress was released quickly through O-ring sliding. The remanent in-plane stresses were minimized by proper design and operation of the pressure rig. A measurement procedure which eliminated the charge induced by the in-plane stress was then introduced. Using this procedure, accurate d_{33} coefficients were measured for both bulk and thin film PZT specimens, as was indicated by calibrations using laser interferometry and the Berlincourt method.

Effective d_{33} coefficients of sol-gel derived PZT films with compositions near the morphotropic phase boundary were investigated. The films had small grain sizes (~0.1 μm) and strong preferred orientation (either [111] or [100]). The dielectric constant and the remanent polarization increased when the film thickness increased from 0.25 μm to

3.4 μm, while the grain size and preferred orientation of the film didn't change. Before poling, the films showed very weak piezoelectricity with an effective d_{33} less than 10 pC/N. The effective d_{33} increased with both poling time and field and saturated as the poling field exceeded three times the coercive field. With an increase of film thickness, the effective d_{33} increased, primarily due to the increase of the remanent polarization. The maximum effective d_{33} was measured at a Zr/Ti ratio of 52/48 with typical values between 100 pC/N to 120 pC/N for films 1 μm thick. The effective d_{33} was larger on the tetragonal side of the morphotropic phase boundary than on the rhombohedral side. It was also found that PZT films with <111> preferred orientation had larger effective d_{33} than films with <100> preferred orientation. The effective d_{33} of PZT films measured by the pneumatic pressure charge technique was slightly larger than that by laser interferometry, due to differences in the mechanical boundary conditions on the thin film. Theoretical analysis showed that substrate clamping is partially responsible for the small effective d_{33} in PZT films.

The effective d_{33} coefficients of PZT films are smaller than those of their bulk counterparts, especially when the film thickness is small. In part, this is due to substrate clamping. Limited extrinsic contributions to the piezoelectric properties may also reduce piezoelectricity in PZT films. To investigate this, domain wall motion and the extrinsic contribution to the dielectric and piezoelectric response in PZT films were examined. The temperature dependence of the dielectric properties showed that the intrinsic dielectric constant was similar for all the PZT films and 25% to 50% of the dielectric response at room temperature arises from the extrinsic contribution. The extrinsic contribution to the dielectric constant in PZT films was mostly from 180° domain wall motion, and it

increased with both film thickness and grain size. On the other hand, ferroelastic non-180° domain wall motion was found to be limited in fine grain PZT films, suggesting that the extrinsic contribution to the piezoelectric coefficient in the fine grain PZT films was small. However, as the films became thicker (> 5 μm), non-linear behavior between the piezoelectric coefficient and the electric driving field was observed. This indicated that there was significant ferroelectric non-180° domain wall motion under high external excitation in thicker films. The activity of the non-180° domain walls was studied through non-180° domain switching. For fine grained films with film thicknesses less than 2 μm, non-180° switching was negligible, indicating that either the pinning of non-180° domain walls was very strong or that there were few present in the films. As the films became thicker, non-180° domain switching was observed when the poling field exceeded a threshold field. The threshold field decreased with an increase in film thickness, suggesting more non-180° domain wall mobility in thicker films. Non-180° domain switching in the large grained PZT films was found to be much easier and more significant than in fine grained PZT films. Transmission electron microscope plane view micrographs showed domain fringes in fine grained films. The majority of the grains which had domain fringes only had one set of parallel stripes. More complex domain fringes were observed in some large grains. Near the films surface, very few grains which had domain structures were found.

TABLE OF CONTENTS

List of Figures ix
List of Tables xiii
Acknowledgment xiv

Chapter 1. Introduction and Statement of Goals 1

1.1 Introduction 1
1.2 Statement of Goals 3

Chapter 2. Literature Review 6

2.1. Microelectromechanical Systems (MEMS) 6
2.2. Piezoelectric and Electrostrictive Effects 9
2.3 Ferroelectric Effect and Ferroelectric Materials 12
2.4 Lead Zirconate Titanate (PZT) 16
2.5 Ferroelectric Domain Structure 20
2.6 Intrinsic and Extrinsic Contributions 23
2.7 Phenomenological Theory of PZT System 29
2.8 Special Issues in PZT Thin Film Properties 33
2.8.1 Grain Size 34
2.8.2 Stress 38
2.8.3 Crystallographic Orientation of the Films 43
2.8.4 Clamping and Interface Effect 46

Chapter 3. Experimental Procedure 48

3.1 PZT Film Deposition 48
3.2 Film Structure Characterizations 51
3.2.1 X-Ray Diffraction 52
3.2.2 Scanning Electron Microscope 52
3.2.3 Transmission Electron Microscope 52

3.2.4. Film Thickness Measurements 53
3.3 Electrical Properties Evaluations 53
3.3.1 Low Field Electrical Characterization 54
3.3.2. High Field Electrical Characterization 54
3.4 Piezoelectric Property Measurements 54
3.4.1 The Pneumatic Pressure Charge Technique 55
3.4.2 Double Beam Laser Interferometry 59
3.4.3 Calibration using Berlincourt Meter 61
3.5 Low and High Temperature Property Measurements 62
3.6 Uniaxial Stress Measurement 63
3.7 Electrical Field Dependence Measurement 64

Chapter 4. The Pneumatic Pressure Charge Method for the Longitudinal Piezoelectric (d_{33}) Measurement of Thin PZT Films 65

4.1. Introduction 65
4.2 The Design of the Stress Rig 68
4.2.1 Problems in Stress Application for Thin Film Specimens 68
4.2.2 The Pneumatic Pressure Rig 71
4.3 Charge Response and Stress Analysis 72
4.4 Remnant In-Plane Stress Analysis 78
4.5 Self-Compensation of the Remnant In-Plane Stress 83
4.6 Calibration of the Pneumatic Pressure Charge Technique 86
4.7 Summary 89

Chapter 5. The Piezoelectric Characteristics of Sol-Gel Derived PZT Films on Platinum-coated Silicon Substrates 91

5.1 Structural Analysis 91
5.2 Dielectric and Ferroelectric Characterization 95
5.3 The Longitudinal Piezoelectric Properties 104
5.4 Summary 116

Chapter 6. Domain Wall Motion and its Contribution to the Dielectric and Piezoelectric Properties of PZT Films 118

6.1 Film Preparation and Properties 119
6.2 Temperature Dependence of the Dielectric and Ferroelectric Properties 123
6.3 Stress and Field Dependence of Dielectric and Piezoelectric Properties 133
6.4 Non-180° Domain Switching in PZT Films 141
6.5 Direct Observation of Microstructure and Domain Structures 146
6.6 Summary 150

Chapter 7. Conclusions and Recommendations for Future Work 152

7.1 Conclusions 152
7.1.1 Pneumatic Pressure Charge Technique for Piezoelectric d_{33} Measurement 152
7.1.2 The Piezoelectric Characteristics of Sol-Gel Derived PZT Films 153
7.1.3 Domain Wall Motion and Extrinsic Contributions to the Dielectric and Piezoelectric Properties of PZT Films 155
7.2 Recommendations for Future Work 157

References 162

LIST OF FIGURES

Figure 2.1 Cross section of a micromachined sensor structure with active ferroelectric thin films. From Polla [28]..... 8

Figure 2.2 PZT piezoelectric micropump with input and output ports. After Polla [2]..... 9

Figure 2.3 The perovskite unit cell of PZT. From Kingery et al. [39]..... 13

Figure 2.4 An illustration of the polarization hysteresis (P-E) loop of a ferroelectric material..... 15

Figure 2.5 The lead zirconate titanate phase diagram. After Jaffe et al. [26]..... 17

Figure 2.6 (a) The ferroelectric distortion of a tetragonal perovskite. (b) The ferroelectric distortion of a rhombohedral perovskite. After Shepard [14]..... 18

Figure 2.7 Variation of room temperature properties with composition for PZT. (a) piezoelectric coefficients, (b) dielectric constant. After Jaffe et al [26]..... 19

Figure 2.8 (a) 180° domain structure in a ferroelectric single crystal, from Mitsui et al. [43]. (b) 90° domain structure formed in a cubic grain, from Arlt [46]..... 22

Figure 2.9 (a) Intrinsic contribution due to the response from lattice. (b) Extrinsic contribution due to 180° domain wall motion. (c) Extrinsic contribution due to 90° domain wall motion..... 24

Figure 2.10 Temperature dependence of the dielectric constant of PZT ceramics modified by different dopants. After Zhang et al. [58]..... 28

Figure 2.11 Temperature dependence of the transverse piezoelectric coefficient of PZT ceramics modified by different dopants. After Zhang et al. [58]..... 29

Figure 2.12 The effects of applied uniaxial compressive stress on the dielectric constant of PZT-4 (left side) and PZT 5A (right side). From Krueger [86]..... 41

Figure 2.13 (a) Intrinsic piezoelectric d_{33} of tetragonal 48/52 PZT crystal along any crystallographic direction. (b) Intrinsic piezoelectric d_{33} of rhombohedral 52/48 PZT crystal along any crystallographic direction. From Du et al. [92]..... 45

Figure 3.1 Flow chart of the sol-gel method for the preparation of PZT thin films using 2-methoxyethanol solvent and RTA..... 51

Figure 3.2 A schematic of the experimental set-up for the d_{33} measurement..... 56

Figure 3.3 Schematic of the electric charge integrator..... 57

Figure 3.4 A schematic of a double beam interferometer. After Pan et al. [11]. 60

Figure 3.5 Schematic of the experimental setup for uniaxial stress measurements. 64

Figure 4.1 Simultaneous bending of thin film sample during the application of normal load. 70

Figure 4.2 (a) Normal stress applied to the sample by the pneumatic pressure rig.
(b) Calculated charge induced by the normal component of the stress.
(c) Total induced charge measured during the pressure change. 73

Figure 4.3 Charge measured on releasing pressure after applying pressure for different periods of time. 76

Figure 4.4 In-plane strain as a function of time during pressure changes in the pneumatic pressure rig. 77

Figure 4.5 The dimensions of: (a) the O-ring groove and (b) O-ring.. 81

Figure 4.6 The effect of O-ring compression on the pressure-induced charge. 82

Figure 4.7 Remnant in-plane stress produced by pneumatic pressure during:
(a) procedure in which pressure was switched between 0 and P_1.
(b) procedure with remnant in-plane stress self-compensation mechanism 84

Figure 4.8 Influence of the pre-loading pressure P_2 on the measured charge for a pressure change from $P = P_1$ to $P = 0$. 86

Figure 4.9 Charge induced in a bulk PZT-5A ceramic specimen as a function of applied pressure. 87

Figure 4.10 Influence of O-ring compression on the measured d_{33} coefficient of a bulk PZT-5A specimen. 88

Figure 5.1 XRD patterns of PZT 52/48 films prepared by 2-methoxyethanol solution and RTA on Si substrates with <111> and <100> oriented Pt bottom electrodes. 93

Figure 5.2 Microstructure of (111) oriented 52/48 PZT films: (a) SEM surface morphology of as-deposited film. (b) SEM surface morphology after chemical etching. (c) TEM plan view image (Courtesy of Z. Xie et al.). (d) TEM cross-sectional image (Courtesy of S. C. Cheng). 94

Figure 5.3 Thickness dependence of the dielectric constant for <111> and <100> oriented PZT 52/48 films. 96

Figure 5.4 Thickness dependence of the remanent polarization for <111> and <100> oriented PZT 52/48 films. 97

Figure 5.5 Temperature dependence of the dielectric constant of PZT 52/48 films. 99

Figure 5.6 The effect of excess Pb in solution on the Curie temperature of PZT 52/48 films. 101

Figure 5.7 The remanent polarization of a lead-deficient PZT 52/48 thin film as a function of the number of sequential measurements performed. 102

Figure 5.8 Charge response of PZT films to the applied pressure measured by the pneumatic pressure charge technique. 105

Figure 5.9 Induced charge as a function of pressure change for a 1μm PZT film poled at 150 kV/cm for 1 min. 106

Figure 5.10 Induced charge as a function of the poling field of a 1.3 μm thick <111> oriented PZT 52/48 film. 112

Figure 5.11 Effective d_{33} as a function of film thickness for 52/48 PZT films with <111> preferred orientation. 112

Figure 6.1 XRD patterns of PZT films deposited using acetylacetone modified 2-mothoxyethanol solution and RTA process (Courtesy of W. Ren). 120

Figure 6.2 SEM pictures of a 7 μm PZT 52/48 film prepared using acetylacetone modified 2-mothoxyethanol solution and RTA (Courtesy of W. Ren) 121

Figure 6.3 AFM picture of the film surface of a 3 μm <100> PZT 52/48 film prepared using acetic acid solution and conventional furnace annealing. 122

Figure 6.4 The temperature dependence of the dielectric constant of sol-gel PZT 52/48 films. 123

Figure 6.5 Reciprocal of the measured capacitance as a function of film thickness for <111> oriented fine-grained PZT films. 125

Figure 6.6 The dependence of the dielectric constant of PZT films on the amplitude of the ac electric driving field. 127

Figure 6.7 Temperature dependence of the dielectric loss of PZT 52/48 films 130

Figure 6.8 (a) P-E hysteresis loops at different temperatures. (b) Saturation and remanent polarizations as a function of temperature for PZT 52/48 films. 131

Figure 6.9 The coercive field of a 0.6 μm <111> oriented PZT film as a function of temperature. 132

Figure 6.10 The effect of applied normal stress on the dielectric constant of a poled <111> fine grained PZT 52/48 film. 134

Figure 6.11 The effect of stress amplitude on the d_{33} coefficients of a 1 μm thick <111> oriented fine grained PZT film and a PZT-5A bulk ceramic. 136

Figure 6.12 The effective d_{33} of PZT films as a function of film thickness at 1kHz. The films had an average grain size on the order of 0.1 μm. 138

Figure 6.13 Normalized effective d_{33} of PZT films as a function of sub-coercive ac electric field at 1kHz. 138

Figure 6.14 The normalized dielectric constant of PZT films as a function of ac electric field at 1 kHz. 140

Figure 6.15 Weak field dielectric constant of PZT films as a function of dc poling field at 1 kHz. 142

Figure 6.16 The threshold electric field for non-180° domain switching as a function of film thickness. 144

Figure 6.17 The threshold electric field for non-180° domain switching as a function of grain size. 145

Figure 6.18 The temperature dependence of the dielectric constant before and after dc poling. 147

Figure 6.19 TEM Plane view of PZT 52/48 films prepared by 2-methoxyethanol solution and RTA. (a) Domain fringes which have one set of parallel stripes. (b) Domain fringes which have four sets of variants related to each other by nearly 90°. 149

LIST OF TABLES

Table 2.1. Elastic, dielectric and piezoelectric constants of poled $Pb(Ti_{0.48}Zr_{0.52})O_3$ ceramics. From [26]..... 20

Table 2.2 The theoretical properties of PZT at 25°C. From [37]. 33

Table 4.1 Friction factors in O-ring seals. From [109]..... 81

Table 5.1 Elastic properties of PZT and silicon substrate. From [26] and [114]. 109

Table 5.2 Typical values for the dielectric constant, remanent polarization and d_{33} of 1 μm thick PZT films with different Zr/Ti ratios near the MPB. 114

Acknowledgment

I would like to express my gratitude to Dr. Susan Trolier-McKinstry for the encouragement, advice and support she provided me during the past four years. It has been so pleasant to work with her and the STM group. I would also like to thank other members of my committee, Dr. Clive Randall, Dr. Eric Cross, Dr. Qiming Zhang, and Dr. David Green, for their helpful discussions and guidance.

This work would not be possible without the help from many colleagues, friends and the technical staff in the Materials Research Laboratory. Among them, Dr. Wei Ren and Dr. Fan Chu deserve special thanks for their assistance and discussions. Thanks also go to Dr. Joseph Shepard, Jr., Dr Jon-Paul Maria, Dr. Jianzhong Zhao, Dr. Baomin Xu, and Dr. Zeliang Xie for their help in various ways.

Finally and most importantly, I would like to thank my beloved wife, Zhaoning, and my parents, for their love and supports. This thesis is dedicated to them.

Financial support for this research from the National Science Foundation is greatly appreciated.

Chapter 1. Introduction and Statement of Goals

1.1 Introduction

The demands for miniaturized mechanical devices and components which are integrated with microelectronics have led to great interest in the design and construction of microelectromechanical systems (MEMS). The ability to machine micro-sized and high-precision mechanical structures on silicon and the advances in IC microfabrication technology make it possible to realize high-reliability and low-cost MEMS devices based on silicon. Incorporating smart materials such as ferroelectrics into MEMS designs is an effective way to enhance the performance of sensing and actuation functions of the devices. Among the ferroelectric materials, lead zirconate titanate (PZT) is especially attractive for MEMS applications as a result of its large piezoelectric coefficients and high energy densities [1, 2]. Numerous MEMS designs based on PZT thin films deposited on silicon substrates are found in the literature and a number of prototype devices have been demonstrated [3-6].

For the proper design of novel microelectromechanical systems (MEMS) which utilize piezoelectric thin films to realize its mechanical functions, it is essential to have precise knowledge of the elastic and electromechanical properties of both the substrate and thin film, including the longitudinal (d_{33}) and transverse (d_{31} and d_{32}) piezoelectric

coefficients. Despite the tremendous efforts devoted to the development of piezoelectric PZT thin films in the past ten years, the electromechanical behavior of PZT films is still poorly understood. As a result, the electromechanical properties of bulk PZT ceramics are often used in designing MEMS devices, due to the difficulties in thin film piezoelectric measurements and the lack of piezoelectric data available for PZT thin films. Since the piezoelectric properties of ferroelectric materials including PZT are strongly dependent on grain size, defect chemistry, crystallographic orientation, and mechanical boundary conditions [7-9], it may not be appropriate to use the bulk values of these properties to substitute for those of thin films. However, most of the current techniques capable of measuring the piezoelectric properties of bulk materials are not directly applicable to the measurement of piezoelectric thin films, due to the existence of a substrate and the limitations induced by the sample geometry. In addition, thin film piezoelectric measurements are much more liable to errors since the strains or charges to be measured are extremely small. As a result, piezoelectric measurements on thin films are not common in the literature and the reported data are widely scattered. Until recently, the only established technique which was widely accepted for thin film longitudinal piezoelectric d_{33} measurements was double beam laser interferometry [10, 11]. However, this technique requires a sophisticated optical system and meticulous operation to measure the extremely small field-induced strain. Therefore, a quick, reliable, and convenient technique is highly desirable for routine measurements of thin film piezoelectric d_{33} coefficients.

Recently, there are reports from a few research groups in which the measured longitudinal and transverse piezoelectric coefficients d_{33} and d_{31} of PZT thin films are

considerably smaller than those of their bulk counterparts [12-14]. It is suggested that the primary reason for the reduced piezoelectricity in ferroelectric thin films is the inability to activate the non-180° domain wall motion, which results in limited extrinsic contributions to the piezoelectric properties [15, 16]. However, experimental evidence of the reduced extrinsic contributions in PZT thin films is needed to verify this hypothesis. To do this, discrimination between the intrinsic and extrinsic contributions to the dielectric and piezoelectric responses in PZT films is required. Furthermore, separation of the intrinsic and extrinsic properties in PZT films will enable a quantitative evaluation of both the intrinsic and the domain wall contributions to the dielectric and piezoelectric properties. Such quantitative analysis can provide important information about the influence of the grain size, preferred orientation, the film thickness, and the mechanical boundary conditions on the intrinsic responses, the domain structures, and domain wall motion in these films. An understanding of the effect of the above factors on film properties is very important in the development of PZT films for MEMS applications since it provides guidance on how to improve the piezoelectric properties of PZT films.

1.2 Statement of Goals

Based on the above discussion, the objectives of this thesis can be divided into the following categories:

1. The development of a measurement technique for characterization of the longitudinal piezoelectric coefficient of thin films.

A direct piezoelectric measurement technique for thin films is proposed which applies pneumatic pressure to the piezoelectric films and measures the induced charge. The stresses imposed on the films by the pneumatic pressure will be analyzed and a procedure for accurate thin film d_{33} measurement will be developed based on the stress analysis. Calibration will be made using other established techniques. In addition, a detailed error analysis will be given and the methods which reduce the measurement error in this technique will be discussed.

2. Investigation of the extrinsic contributions to the dielectric and piezoelectric properties of PZT films.

The intrinsic and extrinsic dielectric properties of PZT films will be investigated through studying the temperature dependence of the dielectric constant. The extrinsic contribution to the piezoelectric properties in PZT films will be investigated by studying the stress and electric field dependence of the piezoelectric coefficients. The ferroelectric and ferroelastic activity of the non-180° domain walls in PZT films will be evaluated though the investigation of the influence of unaxial stress and dc electric poling field on their dielectric properties. The effect of the grain size and the film thickness on non-180° domain wall pinning and extrinsic contributions to the dielectric and piezoelectric properties of PZT films will be discussed.

3. Investigations into the piezoelectric characteristics of sol-gel derived PZT films.

The d_{33} coefficient of PZT films with different compositions, grain sizes, orientations, and film thicknesses will be measured using the pneumatic pressure charge technique and double beam laser interferometry. The influence of the mechanical boundary condition on the effective d_{33} of PZT films will be discussed by comparing the effective d_{33} values measured by the two different techniques. The effect of the poling field, film thickness, film composition and orientation on the effective d_{33} of the PZT films will also be investigated.

Chapter 2. Literature Review

2.1. Microelectromechanical Systems (MEMS)

With the rapid development of silicon micromachining technologies in recent years, the field of microelectromechanical systems (MEMS) has drawn a great deal of attention for its potential to revolutionize many industrial products, such as surgical tools, military devices, miniature instrumentation, sensors and actuators [17]. MEMS devices generally refer to miniaturized mechanical devices and components such as micro-sensors and micro-actuators which are usually fabricated on silicon substrates. Due to the advances in silicon micromachining and microfabrication technologies, MEMS devices with various mechanical structures can be formed with high precision and low fabrication cost [18]. In addition, the excellence of both the electrical and mechanical properties of silicon single crystals makes it possible to integrate the miniature mechanical components with IC electronics monolithically, which further improves the reliability of the system.

Most MEMS devices are fabricated using silicon substrates and compatible thin film materials, such as silicon dioxide, polysilicon, silicides, titanium nitride, and noble metals, etc. These devices usually utilize electrostatic forces or piezoresistive effects to realize the actuation and sensing functions [19, 20]. Through proper design and engineering of micromachined structures such as membranes, cantilevers, beams, and diaphragms, a variety of sensors and actuators can be fabricated [21]. Although many

kinds of MEMS devices such as microphones [22], inkjet print heads [23], comb-drive actuators [24], microscanners [25] and accelerometers [20] have been successfully built using these materials, the relatively low energy densities and forces which can be generated using electrostatic actuation limit their performance. In contrast, MEMS design based on the piezoelectric effect is an attractive alternative since it may provide much larger forces and energy densities than electrostatic devices. In addition, piezoelectric MEMS devices offer the potential for integrating sensing and actuation in a single device using a single material. By incorporating a piezoelectric material into a MEMS device, both sensing and actuation can be performed by this material through either the direct or converse piezoelectric effects, which may result in better integration of the system and simplicity in the design.

Among available piezoelectric materials, ferroelectric lead zirconate titanate (PZT) ceramics are very attractive for MEMS applications since they have large piezoelectric constants and electromechanical coupling coefficients [26] and PZT thin film deposition on silicon substrates has been well developed. Compared to the most commonly used piezoelectric thin film, zinc oxide, which has a bulk longitudinal piezoelectric coefficient of about 12 pC/N [27], PZT ceramics have more than one order of magnitude larger piezoelectric coefficients. Thus they can provide much higher energy densities and transmitted forces when used as the active material in MEMS designs. In addition, unlike zinc oxide, which does not possess piezoelectricity in randomly oriented polycrystals, PZT films can be poled to be strongly piezoelectric due to the reorientable polar axis.

During the past decade, extensive efforts have been devoted to the development of piezoelectric PZT films for MEMS applications. A variety of MEMS designs based on PZT thin films have been reported in the literature and several prototype devices have been demonstrated in recent years. Figure 2.1 shows the structure of a micromachined acoustic or thermal sensor which was developed at the University of Minnesota [28], and Figure 2.2 describes the structure of micropumps designed by the same institution [2]. Among other MEMS devices using PZT thin films as the active layer are micromotors, accelerometers, scanning force microscopy tips, and micro-sonar arrays, etc. [29-32].

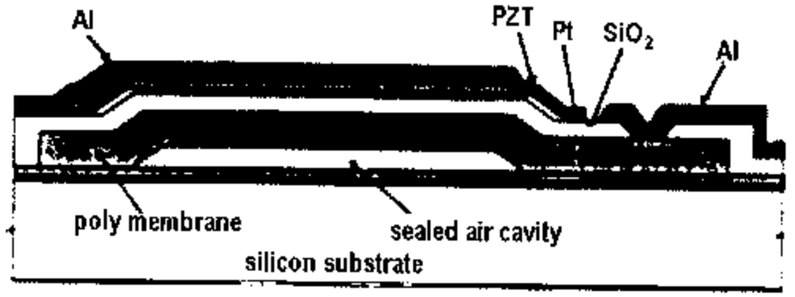

Figure 2.1. Cross section of a micromachined sensor structure with active ferroelectric thin films. The piezoelectric material is PZT for mechanical microsensor application and $PbTiO_3$ for pyroelectric detector applications. The air gap is formed by micromachining to allow either mechanical deformation or thermal isolation [28].

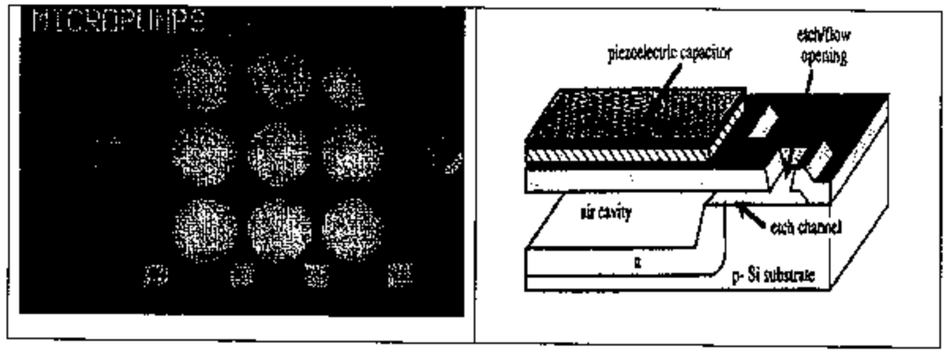

Figure 2.2. PZT piezoelectric micropump with both input and output ports [2].

2.2. Piezoelectric and Electrostrictive Effects

Materials which develop an induced electric polarization when exposed to an applied stress are called piezoelectric materials. In addition, in piezoelectric materials a strain is induced in response to an applied electric field. Therefore, a piezoelectric material always displays its piezoelectricity in two ways: the direct piezoelectric effect, which is the linear relationship between electric polarization and applied mechanical stress, and the converse piezoelectric effect, which is the linear relationship between mechanical strain and electric field. In both cases, the proportionality constants are the piezoelectric coefficients and they are numerically identical to each other [33]. They can be described as follows:

$$P_i = d_{ijk}\,\sigma_{jk} \qquad (2.1)$$

$$x_{jk} = d_{ijk}\,E_i \qquad (2.2)$$

where P, is the induced electric polarization (C/m^2), σ_{jk} is the applied mechanical stress (N/m^2), x_{jk} is the field induced strain, E_i is the applied electric field (V/m), and d_{ijk} is the piezoelectric coefficient (C/N for the direct effect and m/V for the converse effect). The piezoelectric coefficients are third rank tensors as described in the above equations. But for convenience, it is more common to use the reduced subscript matrix format rather than the tensor format.

Microscopically, the piezoelectric effect originates from a coupling between the elastic and electric behavior of the crystal. When mechanical stress is applied to a crystal, it distorts the lattice. An electric dipole moment can accompany this strain when the change in the unit cell leads to a shift of the center of positive and negative charge. Similarly, when an electric field is applied to the crystal, it deforms the crystal structure in addition to altering the electric dipole moment in the unit cell. The piezoelectric coefficient tensor must have symmetry equal to or higher than the symmetry of the crystal itself according to Neumann's principle [34]. To satisfy this condition, invariance of the piezoelectric tensor components under all the symmetry element operations of the crystal must be maintained. An examination of all 32 point groups shows that the 11 centrosymmetric classes are all nonpiezoelectric. Of the remaining 21 non-centrosymmetric classes, 20 classes have non-zero components in their piezoelectric coefficient tensors and therefore can exhibit the piezoelectric effect. The only exception is point group 432. Although it is non-centrosymetric, the combination of all the symmetry element operations results in zero for all the piezoelectric tensor components. The non-zero components and their relationship in each of the 20 classes are determined by the symmetry of each class and can be found in the literature [33].

Unlike the piezoelectric effect which only appears in non-centrosymmetric crystals, electrostriction is a quadratic effect and occurs in all crystals [34]. When an electric field is applied to the crystal, it produces strains proportional to the square of the polarization. This is called the electrostrictive effect, and can be defined as:

$$x_{ij} = Q_{ijkl} P_k P_l \qquad (2.3)$$

The proportionality constant in the above equation, Q_{ijkl}, is the electrostrictive coefficient. Fundamentally, the electrostrictive effect is a universal phenomenon and it is the origin of the coupling between electrical and mechanical components. The piezoelectric effect in ferroelectric materials can be viewed as biased electrostriction in crystals which have a polarization. In these materials, the total polarization in the unit cell is the sum of the spontaneous polarization at zero electric field and the electric field induced polarization (P_{ind}). Therefore, for an applied electric field E_3, e.g. in the z direction, the total strain in the z direction can be written as [8]:

$$x_3 = Q_{33} (P_3 + P_{ind})^2 \approx Q_{33} P_3^2 + (2 Q_{33} P_3) P_{ind}$$
$$= Q_{33} P_3^2 + 2 Q_{33} P_3 \varepsilon_0 \varepsilon_{33} E_3 \qquad (2.4)$$

where P_3 is the spontaneous polarization and $\varepsilon_0 \varepsilon_{33}$ is the permittivity of the crystal in the z direction. Obviously only the second term in equation 2.4 is the strain due to the applied field. It can be seen that the induced strain is linearly related to the applied field, which is by definition the piezoelectric effect. Thus the piezoelectric coefficients of ferroelectric

materials are generally determined by the electrostrictive coefficients, the spontaneous polarization, and the permittivity of the crystal [35-36]. Since ferroelectric materials (see Section 2.3) usually have much larger permittivities than other materials, they also have larger piezoelectric coefficients even though they have relatively small electrostrictive coefficients [26, 37].

2.3 Ferroelectric Effect and Ferroelectric Materials

Ferroelectric materials are spontaneously electrically polarized under equilibrium conditions. In addition, the spontaneous polarization in a ferroelectric material has more than one possible crystallographic orientation and it can be switched among these directions by an achievable electric field [38]. At sufficiently high temperatures, most ferroelectric materials have a higher symmetry crystal structure (paraelectric phase) which does not have a reorientable spontaneous polarization. As the material cools through the Curie temperature (T_c), a phase transformation occurs where it evolves from the paraelectric phase into a lower symmetry ferroelectric phase with a spontaneous polarization [35]. At the transition temperature T_c, the dielectric constant reaches a maximum for most ferroelectric materials. At temperatures above the Curie temperature, the dielectric constant, K, obeys the Curie-Weiss law:

$$K = C/(T-T_0) \qquad (2.5)$$

where C is the Curie constant, which is typically on the order of $10^3 - 10^5$ K [8], T is the temperature, and T_0 is the Curie-Weiss temperature. In a first order ferroelectric material, $T_c > T_0$, while in a second order ferroelectric material $T_c = T_0$.

Perhaps the most important ferroelectric prototype is the perovskite oxide structure (Figure 2.3). Ferroelectrics such as barium titanate and PZT all belong to this family. PZT has a cubic structure in the high temperature paraelectric phase, in which the central atom is either Zr^{4+} or Ti^{4+}, the corner atoms are Pb^{2+}, and the face centered atoms are O^{2-} [39]. During the phase transition at T_c, the cubic unit cell distorts into a tetragonal or rhombohedral structure. The relative shift of the oxygen octahedra and the cation atoms due to the structural distortion results in the generation of an electric dipole moment in the ferroelectric phases [8].

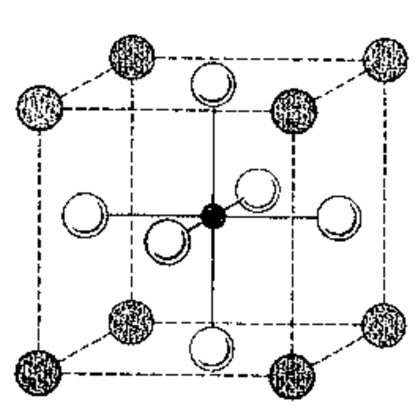

Figure 2.3. The perovskite unit cell of PZT [38]. The central atom is either Zr^{4+} or Ti^{4+}, the corner atoms are Pb^{2+}, and the face centered atoms are O^{2-}.

For ferroelectric materials, since there is more than one crystallographic direction along which the spontaneous polarization is stable, on cooling through the transition temperature from the paraelectric phase, the material may evolve into a pattern that is composed of regions with different polarization vectors. This is called a domain structure [40]. A domain is a region where all of the polarization vectors are aligned along the same crystallographic direction. The relative orientation of the different domains is dictated by the symmetry of the paraelectric phase and the symmetry elements lost at the transition [38]. Domain structures are developed in both polycrystalline and single crystal samples to minimize the free energy, and they significantly influence the properties of ferroelectric materials (see section 2.5 and section 2.6). Under an external electric field, the closer the polarization vector is to the electric field, the lower the free energy of the domain. Therefore, the polarization vector of the ferroelectric domains can be switched to a more energetically favorable direction by the application of a large dc electric field. This is the poling process [40].

The trademark of ferroelectricity is the polarization electric-field (P-E) hysteresis loop. This loop is the evidence showing that the spontaneous polarization can be reoriented among the possible crystallographic orientations. The hysteresis in the P-E relation results from the stability of the polarization along the preferred crystallographic orientations and its resistance to reorientation. From the P- E hysteresis loop (shown in Figure 2.4), several distinctive characteristics of ferroelectric materials can be described.

The saturation polarization, P_{sat}, defined as the linear extrapolation of the polarization at high field back to the zero field point, refers to the total polarization that can be attributed to the reversal of the spontaneous polarization. The remanent

polarization, P_r, is the polarization remaining in a ferroelectric material after the external electric field is released. It reflects the degree of alignment of the dipole moments in a given ferroelectric. The coercive field, E_c, refers to the electric field at which $P_{net} = 0$ [41].

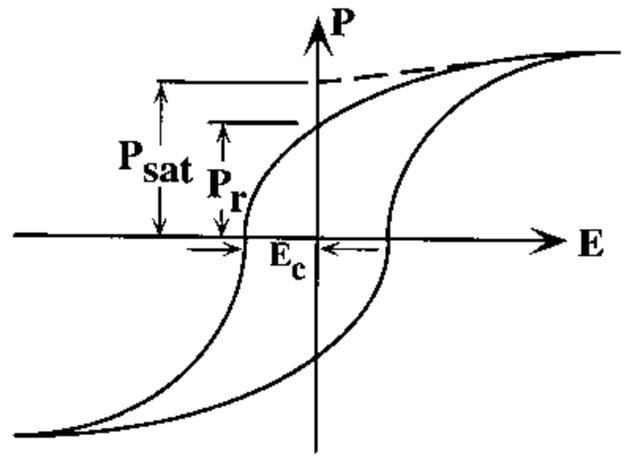

Figure 2.4. An illustration of the polarization hysteresis (P-E) loop of a ferroelectric material. The saturation polarization P_s, the remanent polarization P_r, and the coercive field E_c are shown as defined.

All ferroelectric crystals are piezoelectric since they all have polar structures. However, randomly oriented polycrystalline ferroelectric ceramics are initially not piezoelectric because they have a centrosymmetric ∞∞m symmetry due to the random distribution of polarization vectors after cooling through T_c. However since the material has a reorientable polarization, by switching the domains to the energetically favorable

directions through dc poling, its symmetry can be reduced to a noncentrosymmetric ∞m, where m lies along the poling axis [34]. Therefore, ferroelectric ceramics can be piezoelectric after poling. The piezoelectric activity induced by the poling process increases monotonically with the degree of the alignment of the polar vectors in all the grains, which is indicated by the ratio of the remanent polarization to the spontaneous polarization [26].

2.4 Lead Zirconate Titanate (PZT)

Lead zirconate titanate, $Pb(Zr_{1-x},Ti_x)O_3$, is a solid solution system between $PbTiO_3$ and $PbZrO_3$ which has the perovskite structure. After being developed in the 1950's, this material has become the most important and widely used piezoelectric ceramic due to its superior dielectric and piezoelectric properties. In this solid solution system, by changing the zirconium/titanium ratio, both the structure and properties of the material can be adjusted. The phase diagram of the system is shown in Figure 2.5 [26].

At temperatures above T_c, the cubic paraelectric structure (m3m) is stable for all the compositions. On cooling through T_c, the paraelectric cubic phase transforms to a tetragonal phase (4mm) for titanium-rich compositions ($0<x<0.52$) and a rhombohedral phase (3m or 3c) for zirconium-rich compositions ($0.52<x<0.94$). The distortions of the cubic unit cell to tetragonal and rhombohedral unit cells are illustrated in Figures 2.6a and 2.6b. In tetragonal PZT, there are six possible orientations for the spontaneous polarization which are the six <100> directions in the paraelectric cubic structure, while

in rhombohedral PZT there are eight possible orientations for the spontaneous polarization which are the eight <111> directions in the paraelectric cubic structure. Therefore, 90° and 180° domains may be formed in tetragonal PZT while 71°, 109°, and 180° domains may be formed in rhombohedral PZT [42].

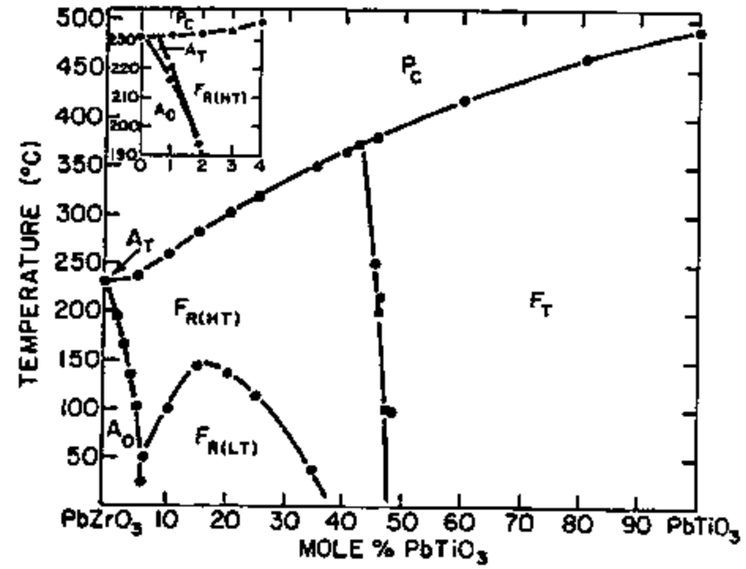

Figure 2.5. The lead zirconate titanate phase diagram [26]. P_c is the paraelectric cubic phase, F_T is the ferroelectric tetragonal phase, $F_{R(HT)}$ is the high temperature ferroelectric rhombohedral phase, $F_{R(LT)}$ is the low temperature ferroelectric rhombohedral phase, A_O is the antiferroelectric orthorhombic phase, and A_T is the antiferroelectric tetragonal phase.

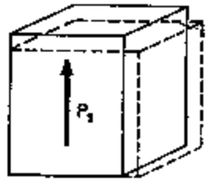

Figure 2.6a.

The ferroelectric distortion of a tetragonal perovskite. The polarization direction is along one of the <100> directions of the prototype unit cell [14].

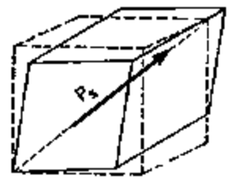

Figure 2.6b.

The ferroelectric distortion of a rhombohedral perovskite. The polarization direction is along one of the <111> directions of the prototype unit cell [14].

The most important feature in the PZT solid-solution system is the existence of a morphotropic phase boundary (MPB). The MPB refers to an abrupt structural change with variation in composition, but which is nearly independent of temperature. In the PZT system, the MPB lies between the Zr/Ti ratios of 52/48 and 53/47, and it separates the rhombohedral and tetragonal phases. The appearance of an MPB can be related to the instability of one ferroelectric phase against another upon a critical composition change. At the MPB composition, two phases coexist since they have identical free energies. Due to the structural instability of the material at compositions near this boundary, many physical properties will be either greatly enhanced or suppressed. In PZT, the dielectric constants, the piezoelectric coefficients, and the electromechanical coupling factors all reach their highest value at compositions near the MPB [26]. Figure 2.7 shows the dependence of the dielectric constants and the piezoelectric coefficients of undoped PZT ceramics on compositions near the MPB. Table 2.1 lists the physical properties of undoped $Pb(Ti_{0.48}Zr_{0.52})O_3$ ceramics after poling.

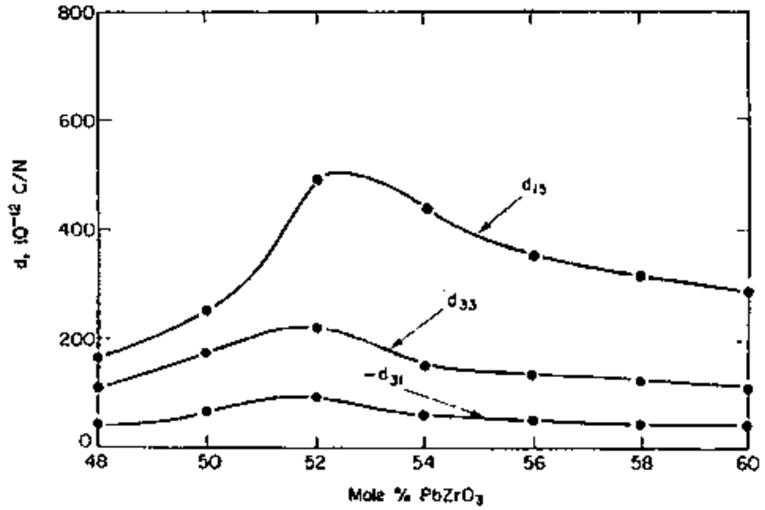

(a)

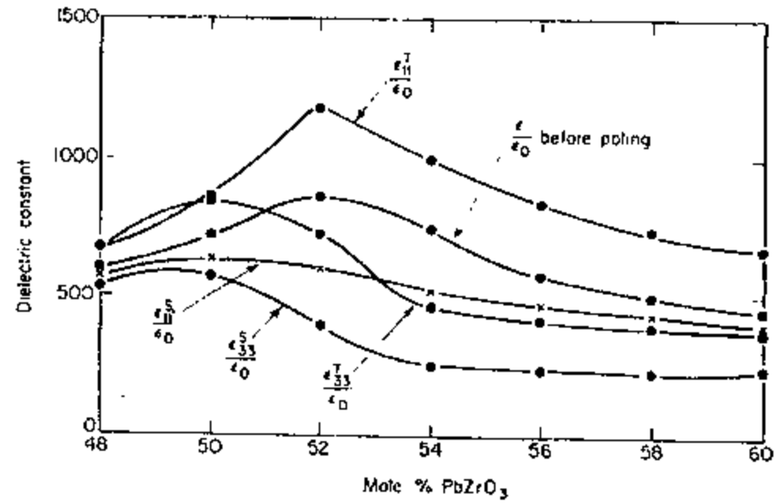

(b)

Figure 2.7. Variation of room temperature properties with composition for PZT.

(a) piezoelectric coefficients, (b) dielectric constant. From [26].

Table 2.1. Elastic, dielectric and piezoelectric constants of poled $Pb(Ti_{0.48}Zr_{0.52})O_3$ ceramics [26].

T_c (°C)	ε_{11}	ε_{33}	d_{33} (pC/N)	d_{31} (pC/N)	s^E_{11}(pm^2/N)	s^E_{12} (pm^2/N)	s^E_{13} (pm^2/N)
386	1180	730	223	-93.5	13.8	-4.07	-5.80

2.5 Ferroelectric Domain Structure

Ferroelectric materials usually form domain structures in an attempt to minimize their free energy. On cooling down through T_c, ferroelectric distortion of the unit cell results in both spontaneous polarization and spontaneous strain in the structure. Due to the existence of surfaces, imperfections and mechanical constraints on ferroelectric crystals, there are electrostatic and elastic energies associated with the spontaneous polarization and the spontaneous strain in the crystal [40]. The electrostatic energy is caused by depolarization fields resulting from the uncompensated polarization at the surfaces. This energy can be reduced by forming a 180° domain structure in the crystal (shown in Figure 2.8a). In such a structure, the electrostatic energy, W_d, can be described as [43]:

$$W_d = 2.71P^2dV/\varepsilon_0 t[1 + (\varepsilon_x\varepsilon_z)^{1/2}] \qquad (2.6)$$

where t and V are the thickness and volume of the crystal, P is the polarization, d is the domain width, ε_x and ε_z are the dielectric constants along the x and z axis respectively. It

is shown in the above equation that the electrostatic energy associated with the depolarization field is proportional to the domain width, therefore a multi-domain structure has less electrostatic energy than the single domain state. However, the formation of 180° domain structures also introduces domain walls into the crystal which have an associated free energy. If the energy per unit area of the domain wall is σ, then the domain wall energy in the structure shown in Figure 2.8a can be expressed as [40]:

$$W_w = (\sigma/d)V \qquad (2.7)$$

Therefore, a stable 180° domain configuration should minimize the sum of the electrostatic energy and domain wall energy. This leads to the following relation between the 180° domain width and crystal (grain) size, t [40]:

$$d \propto t^{1/2} \qquad (2.8)$$

Whether the 180° domain configuration is formed or not in a ferroelectric crystal or ceramic depends on whether there are enough free electric carriers to compensate the spontaneous polarization (so that the depolarization field is screened). For materials with large free carrier concentrations and a high mobility at the Curie temperature, 180° domains are absent, as has been observed in $PbTiO_3$ and $K(TaNb)O_3$ single crystals [44]. For material has low free carrier concentrations at the Curie temperature such as $BaTiO_3$, 180° domain structures are often observed [8].

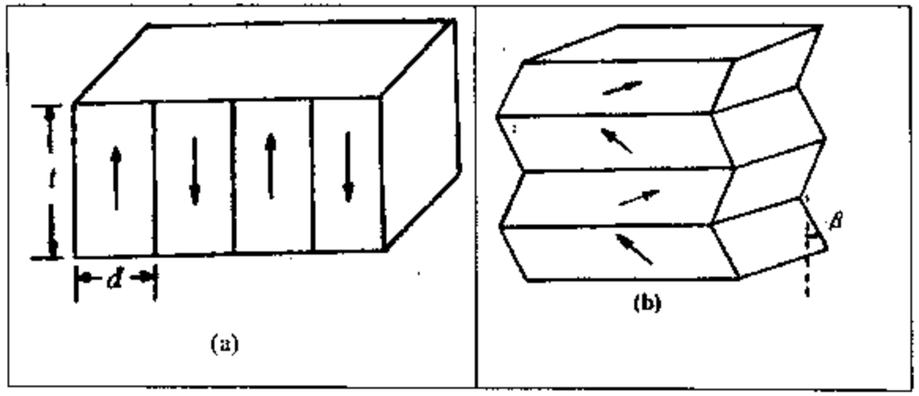

Figure 2.8. (a) 180° domain structure in a ferroelectric single crystal, from [43].

(b) 90° domain structure formed in a cubic grain, from [46].

The elastic energy associated with the development of the spontaneous strain can be reduced by the formation of non-180° domains. In ferroelectric ceramics, this energy is significant since each grain is constrained by its neighbors. Therefore non-180° domain patterns are often formed to minimize the intergranular stresses in ferroelectric ceramics. Arlt calculated the elastic energies and domain wall energy in a clamped $BaTiO_3$ grain which was comprised of an array of twinned 90° domains (Figure 2.8b) [45, 46]. Minimization of the total energy gave:

$$d = (\sigma_{90} g / 2kc\beta_1^2)^{1/2} \qquad (2.9)$$

where g is the grain size, k is a constant, d is the domain width, β_1 is the shear angle of the domain, σ_{90} is the energy per unit area of the 90° domain walls, and c is the stiffness.

Both equation 2.7 and equation 2.8 show that the 180° and 90° domain width in a stable configuration are proportional to the square root of the grain size, which is in agreement with the experimental results in $BaTiO_3$ and PZT ceramics [47, 48]. The equilibrium domain pattern formed in a particular ferroelectric material depends on the exact stress states, any uncompensated surface charge and imperfections in the structure. The domain configurations also change with the grain size. Fine grain PZT ceramics (grain sizes below 1μm) were found to have domain structures much simpler than those formed in the larger grain ceramics [49]. Very finely twinned domains (~ 10nm) were observed at a grain size of 0.2 μm for Nb-doped PZT [7].

As the grain size decreases to some level, the decrease in elastic energy due to the formation of domains becomes smaller than the energy expense associated with domain wall formation itself. In ferroelectric ceramics which have grain sizes smaller than this value, the twinned domain structures with non-180° domain walls have more free energy than the single domain state so that they should not appear. This critical grain size has been calculated to be 40nm for $BaTiO_3$ [45] and 8nm for $PbTiO_3$ [50].

2.6 Intrinsic and Extrinsic Contributions

It has been found that the room temperature dielectric and piezoelectric properties of ferroelectric materials are from both intrinsic and extrinsic sources [51-53]. The dielectric and piezoelectric properties of a single domain single crystal under the appropriate boundary conditions are defined as the intrinsic properties (volume

contribution) of that material. As illustrated in Figure 2.9a, the application of an electric field will cause changes in both the spontaneous polarization and the spontaneous strain of the ferroelectric unit cell, resulting in an induced charge or strain in each domain. This is the origin of the intrinsic dielectric and piezoelectric response. For ferroelectric polycrystalline materials the intrinsic dielectric and piezoelectric responses are the appropriate average of the intrinsic properties of all the domains in every grain in that material. The phenomenological theory developed by Devonshire relates the intrinsic piezoelectric coefficients to the intrinsic dielectric properties and polarization as follows [35]:

$$d_{ijk} = 2Q_{ijkl}\,\varepsilon_0\varepsilon_{kl}P_l \qquad (2.10)$$

where Q_{ijkl} is the electrostrictive coefficient, ε_0 is the permittivity of free space, ε_{kl} is the intrinsic dielectric constant, and P_l is the polarization.

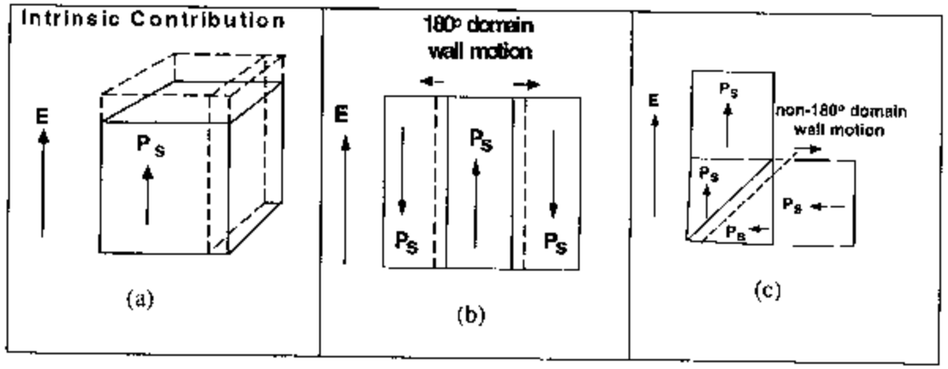

Figure 2.9. (a) Intrinsic contribution due to the response from lattice.

(b) Extrinsic contribution due to 180° domain wall motion

(c) Extrinsic contribution due to 90° domain wall motion

On the other hand, the dielectric and piezoelectric responses that originate from sources other than the intrinsic contribution are lumped as extrinsic properties of the materials. It is believed that the majority of the extrinsic contributions originate from domain wall motions [52]. As discussed in the previous section, domain wall motion in response to applied electric fields or stresses can result in induced charge or strain. This, in turn, gives rise to a dielectric and piezoelectric response in addition to the response from the distortion of the unit cell (Figure 2.9b and 2.9c). It is very important to point out here that 180° domain walls are purely ferroelectric walls. They can be excited electrically, and their movements lead to a polarization change only. Thus the 180° domain walls contribute only to the dielectric properties of ferroelectric materials. In contrast, non-180° domain walls are both ferroelectric and ferroelastic: they can be excited by both external electrical and mechanical signals. Such wall motion can cause changes in the polarization and the strain, so that it can contribute to both the dielectric and piezoelectric properties. The primary source of the extrinsic piezoelectric response in ferroelectric materials is believed to be the non-180° domain wall motion [54,55].

To understand how the dielectric and piezoelectric properties of ferroelectric materials are influenced by domain structure and domain wall motion, quantitative evaluation of the intrinsic and extrinsic contributions to dielectric and piezoelectric response is needed. In general, there are two kind of experimental methods which can be used to separate intrinsic and extrinsic responses in ferroelectric ceramics. The first one is measurement of the frequency dispersion of the dielectric response [56, 57]. In this experiment the upper bound of the frequency of the applied electric field is high enough so that the domain wall motion and defect reorientation can no longer respond to the

change in the applied field. At this frequency, the response from the material is totally due to the ionic motion of the lattice and electronic displacement of the atoms, which is the intrinsic response. However, this experiment requires frequencies in the range of GHz, and can only give information about the dielectric properties. In addition, the dielectric constant measured at high frequencies is a clamped dielectric constant, which is different from the dielectric constant measured below the resonance frequency. The other experiment to discriminate the intrinsic and extrinsic response is a measurement of the temperature dependence the dielectric and piezoelectric constants [7,58]. Since domain wall motion and defect reorientation are thermally activated processes, they can be frozen out at temperature near zero Kelvin. Therefore the piezoelectric and dielectric properties measured at this temperature are completely from the intrinsic contribution. This method can provide information on both dielectric and piezoelectric responses. But it should be noticed here that the properties measured near zero Kelvin may not be directly related to the properties at high temperatures.

There have been many studies conducted on the extrinsic contributions to dielectric and piezoelectric characteristics in ferroelectric materials [52, 56, 57, 58, 59-62]. The weak field (< 2 kV/cm) dielectric and piezoelectric responses of PZT ceramics have been investigated as a function of the amplitude of the electric driving field [59]. Both the dielectric and piezoelectric constants were found to increase with the driving field. Accompanied by the onset of this non-linearity, hysteresis loop started to appear. The increase of nonlinear effects was also accompanied by an increase in loss. By applying a dc bias field or decreasing the temperature, non-linearity was reduced. These

results suggest that the nonlinear behavior in ferroelectric ceramics is of extrinsic nature due to the domain wall motions [59].

The piezoelectric response of PZT ceramics to an applied ac stress was studied as a function of both the stress amplitude and frequency [60]. Nonlinear behavior was also observed under sub-coercive field stresses. The author attributed the piezoelectric hysteresis and the dependence of the piezoelectric coefficient on the applied ac stress to irreversible domain wall motions. It was found that the piezoelectric non-linearity under sub-coercive stress field could be described by the classical Rayleigh law which was developed for ferromagnetic materials. In this model, randomly distributed defects in the ferroelectric materials interact with the mobile ferroelastic domain walls and act as pinning centers to limit the non-180° domain wall motions [60].

To separate the extrinsic contribution from the total response in a ferroelectric material, the temperature dependence of dielectric and piezoelectric properties of PZT ceramics was investigated from 4.2 K to room temperature [58]. Although PZT ceramics modified with different dopants had much different dielectric and piezoelectric constants at room temperature, their dielectric and piezoelectric behaviors were almost identical at 4.2 K (Figure 2.10 and Figure 2.11). This result indicates that doping does little to change the intrinsic properties in PZT ceramics, but can significantly influence the extrinsic contributions to the room temperature properties of PZT ceramics. The dielectric constant measured at 4K agrees very well with the thermodynamically predicted value [7].

The investigation conducted by Zhang et al. [52] also showed that both the measured dielectric and piezoelectric constants of PZT ceramics decreased with decreasing temperature due to the reduced domain wall activities. The authors then tried

to quantitatively determine the relative contributions of the intrinsic and extrinsic response based on an assumption that domain wall motion under weak driving field does not produce a volume change in the materials. They suggested that the piezoelectric hydrostatic coefficient d_h does not have extrinsic contributions, and thus can be used to separate the intrinsic and extrinsic properties. Using this idea, the temperature dependence of both the intrinsic and extrinsic response of PZT ceramics was calculated, and the domain wall contributions from 180° and non-180° domains were analyzed. They concluded that at room temperature, more than 50% of the dielectric and piezoelectric response in PZT ceramic is from domain wall motion, and both 180° and non-180° domain wall contributions are likely present in soft PZT [52].

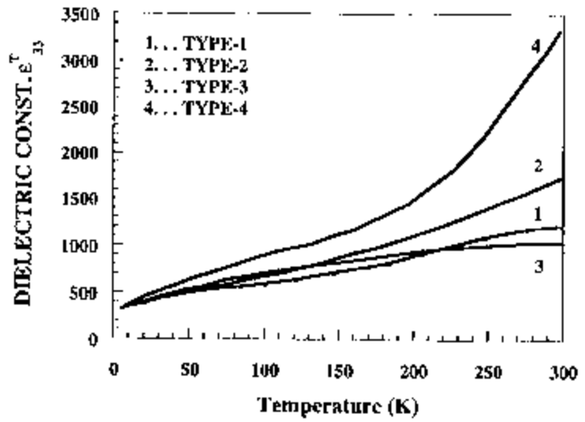

Figure 2.10 **Temperature dependence of the dielectric constant of P/T ceramics modified by different dopants [58].**

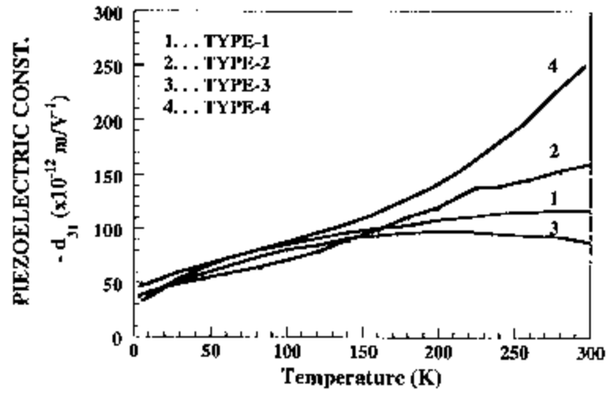

Figure 2.11 **Temperature dependence of the transverse piezoelectric coefficient of PZT ceramics modified by different dopants [58].**

2.7 Phenomenological Theory of PZT System

For a better understanding of the properties of multi-domain polycrystalline PZT ceramics or films, knowledge of the properties of single crystal single domain PZT is required. Since the growth of good quality PZT single crystals for the composition across the MPB has not been accomplished, single crystal data are not available from direct measurements. Although the dielectric and piezoelectric properties of single domain PZT can be deduced experimentally by low temperature measurements, it gives only the properties at temperatures near zero Kelvin. Therefore, thermodynamic

phenomenological theory has been developed to predict the single domain properties of PZT. This theory can then be used to separate the intrinsic and extrinsic contributions to the properties of a multi-domain polycrystalline material. It can also be used to study the effect of mechanical and electrical boundary conditions on the single domain properties, which is very important in understanding the behavior of ferroelectric thin films.

The principles of the thermodynamic theory for ferroelectrics is that the free energy of a ferroelectric single crystal can be expanded in terms of a power series in the order parameters which cause the phase transition [63]. For the paraelectric-ferroelectric phase transition in PZT system, the order parameter is the spontaneous polarization. From this energy function, the characteristics of ferroelectric phase transitions, the relationships between the coefficients in the power series and the macroscopic parameters of the crystal, and the temperature dependence of the macroscopic parameters can all be determined. Therefore the single domain properties of ferroelectric crystals and their relationships with each other can be described by just a few coefficients. This theory is purely macroscopic and phenomenological, and is applicable to almost all ferroelectric crystals independent of the crystal structure and the microscopic processes responsible for the ferroelectric phase transition. The details of the thermodynamic theory of ferroelectrics can be found in a number of books and reviews, and thus will not be repeated here [8, 40, 63-65].

The phenomenological theory for the PZT solid solution system have been developed and used to explain the properties and phase transitions in this system [37, 66-72]. Since the coefficients of the energy function cannot be determined by direct measurement from single crystals, the development of a complete thermodynamic theory

for the PZT system is complicated and must involve indirect methods to determine these coefficients. For a single domain PZT near the MPB, the elastic Gibbs free energy function under isothermal conditions can be expressed as a power series of the ferroelectric spontaneous polarization (P_i) and stress (X_j) [69]:

$$\begin{aligned}\Delta G = {} & \alpha_1 [P_1^2 + P_2^2 + P_3^2] + \alpha_{11} [P_1^4 + P_2^4 + P_3^4] + \alpha_{12} [P_1^2 P_2^2 + P_2^2 P_3^2 + P_3^2 P_1^2] \\ & + \alpha_{111} [P_1^6 + P_2^6 + P_3^6] + \alpha_{112} [P_1^4(P_2^2 + P_3^2) + P_2^4(P_1^2 + P_3^2) + P_3^4 (P_1^2 + P_2^2)] \\ & + \alpha_{123} P_1^2 P_2^2 P_3^2 - \tfrac{1}{2} s_{11}[X_1^2 + X_2^2 + X_3^2] - s_{12} [X_1X_2 + X_3X_2 + X_1X_3] \\ & - \tfrac{1}{2} s_{44} [X_4^2 + X_5^2 + X_6^2] - Q_{11} [X_1P_1^2 + X_2P_2^2 + X_3P_3^2] \\ & - Q_{12} [X_1 (P_2^2 + P_3^2) + X_2 (P_1^2 + P_3^2) + X_3 (P_1^2 + P_2^2)] \\ & - Q_{44} [X_4P_2 P_3 + X_5P_3 P_1 + X_6P_1 P_2] \end{aligned} \qquad (2.11)$$

There are three sets of coefficients in the above energy function to be determined: the ferroelectric dielectric stiffnesses at constant stress (α_i , α_{ij} , α_{ijk}), the elastic compliances at constant polarization (s_{ij}), and the electrostrictive coefficients between polarization and stress (Q_{ij}). Amin measured the spontaneous strains in ferroelectric phases by high temperature X-ray diffraction and calculated the spontaneous polarization through the electrostrictive constants. The dielectric stiffness coefficients (α_{11} and α_{111}) were then determined from these data. The polarization interaction dielectric stiffness coefficients (α_{12}, α_{112}, α_{123}) were determined through the aid of the morphotropic phase boundary data. Using these coefficients, a thermodynamic theory for the PZT system from $PbTiO_3$ to the MPB was established, and the elastic, dielectric, piezoelectric, and thermal properties of the single domain ferroelectric PZT were calculated [69]. This

theory was modified later to account for the composition dependence of the Curie constant which was found from a combination of calorimetric and phenomenological data, and resulted in a better agreement between the theoretical and experimental dielectric data near the morphotropic phase boundary [70].

A thermodynamic theory for the entire PZT system was developed later by Haun et al. using an energy function including additional order parameters, such as terms for the octahedral tilt angle, antiferroelectricity, and coupling terms [37]. To determine the coefficients of the energy function and their composition dependence, pure and homogeneous PZT powders across the phase diagram were prepared by the sol-gel method. PZT ceramics were also fabricated using these powders and their dielectric, piezoelectric, elastic, pyroelectric, and electrostrictive properties were measured for the evaluation of the coefficients of the energy function. The resulting energy function can be used to model the phase transitions and single domain properties of the PZT system across the entire composition. The spontaneous polarizations, spontaneous strains, the dielectric and piezoelectric properties of the single domain PZT were calculated by solving the energy function [37]. It was found that both the dielectric susceptibility coefficients and the dielectric anisotropy reached a maximum at the PZT 50/50 composition, due to the peak in the Curie constant at this composition and the change in the ratios of the dielectric stiffness coefficient as a function of composition. Because of the significant composition dependence of the dielectric susceptibility coefficients, the piezoelectric charge coefficients, d_{ij}, were also functions of the composition, and showed large peaks at compositions near the MPB due to the large dielectric susceptibility

coefficients there. Table 2.2 summarizes the theoretical single domain properties of PZT at 25°C.

Table 2.2 The Theoretical Properties of PZT at 25°C. From Haun [37].

	Mole Fraction $PbTiO_3$ in PZT*									
	0.1	0.2	0.3	0.4	0.5	0.6	0.7	0.8	0.9	1.0
P_S (C/m^2)	0.57	0.66	0.65	0.50	0.50	0.57	0.64	0.70	0.74	0.75
θ_S (Deg.)	5.42	7.36	6.64	—	—	—	—	—	—	—
η_{33} or η_{33}'	219.	277.	280.	295.	382.	197.	116.	86.4	72.9	66.6
η_{11} or η_{11}'	195.	262.	360.	529.	1721.	498.	218.	143.	121.	124.
g_{33} (10^{-3} Vm/N)	26.8	30.9	34.6	41.9	96.6	92.9	101.	114.	124.	134.
g_{31} (10^{-3} Vm/N)	- 8.13	- 9.53	- 11.2	- 15.6	- 46.0	- 33.8	- 31.8	- 34.2	- 37.1	- 39.2
g_{15} (10^{-3} Vm/N)	12.9	14.3	15.5	18.1	41.0	38.4	40.8	44.9	48.6	50.9
d_{33} (10^{-12} C/N)	47.2	72.1	107.	189.	327.	162.	104.	87.2	81.2	79.2
d_{31} (10^{-12} C/N)	- 13.3	- 21.6	- 38.5	- 80.5	- 156.	- 58.9	- 32.6	- 26.2	- 23.9	- 23.1
d_{14} (10^{-12} C/N)	1.81	3.27	- 7.26	- 25.1	—	—	—	—	—	—
d_{15} (10^{-12} C/N)	24.2	34.5	42.0	60.0	624.	169.	78.6	57.0	52.1	56.1

*The values listed from 0.1 to 0.4 were calculated from the high-temperature rhombohedral equations, except for P_S and θ_S from 0.1 to 0.3 which were calculated from the low-temperature rhombohedral equations. The values listed from 0.5 to 1.0 were calculated from the tetragonal equations. $P_S = P_3$ in the tetragonal state, but $P_S = 3^{1/2} P_3$ in the rhombohedral states. $\theta_S = 3^{1/2} \theta_3$. η_{11} and η_{33} were used in the tetragonal state, and η_{11}' and η_{33}' (see Section 2.5) were used in the rhombohedral state. The piezoelectric coefficients are all based on the cubic axes.

2.8 Special Issues in PZT Thin Film Properties

The properties of PZT thin films are usually different from those of polycrystalline bulk ceramics since there are dissimilarities between bulk and thin film

PZT in many aspects. Depending on the deposition technique and the substrate used, PZT thin films can be made either epitaxial, textured, or randomly oriented. They may have grain sizes much different from the typical grain sizes in bulk PZT ceramics. There are often large biaxial stresses in thin films due to the volume change during the phase transition of PZT and the thermal expansion coefficient mismatch between the substrate and the film. In addition, the substrate and electrode adjacent to the PZT films may also cause surface/interface effects and clamping in PZT films. All these are known to affect the dielectric, piezoelectric and ferroelectric properties of PZT films by altering both the intrinsic and extrinsic contributions in these films. Therefore these issues must be taken into consideration in an investigation of thin film PZT properties. In this section, each of these factors will be discussed individually and brief overviews on their effects on the properties of PZT ceramics and thin films will be given.

2.8.1 Grain Size

The grain size of PZT films may have a very wide variation due to differences brought about by the processing procedure and the choice of substrate. For PZT films deposited on single crystal substrates which have a lattice match to PZT, e. g., metal oxides with oxygen octahedra backbones, the films may be epitaxially grown on top of the single crystal substrates. These films can be viewed as 2 dimensional single crystals with the presence of low angle grain boundaries within them. Therefore, the "grain size" in the lateral direction may be enormously large compare to those in PZT ceramics. One the other hand, PZT films deposited on polycrystalline substrates usually are also

polycrystalline, and they often have smaller grain sizes than bulk PZT ceramics due to both the high nucleation density and the fact that the crystallization temperatures used for thin film processes are considerably lower than the temperatures used for ceramic processing. To reduce the thermal budget and interdiffusion between the film and the substrate, rapid thermal annealing is often used for the crystallization of the PZT films. Films annealed by this process typically have very small grain sizes since the soaking time at high temperature is extremely short. Therefore, grain size effects are very important in studying the properties of PZT thin films.

The effect of grain size on the properties of PZT ceramics has been the subject of a number of investigations [7, 73-79]. It was found that the crystal tetragonality (c/a ratio) of PZT ceramics decreased with decreasing grain size, resulting in a decrease of the average unit cell volume [7]. The observed result was attributed to internal stresses which inhibited the development of a fully unclamped tetragonal structure on cooling through the Curie temperature. With decreasing grain size, non-180° domain formation becomes difficult, which results in an increased internal stress. The remanent polarization was found to increase with increasing grain size below 1μm, saturate above 1μm, and then drop slightly above 3μm [7]. The coercive field was found to increase with decreasing grain size. The sharp decrease in the remanent polarization and increase in the coercive field for the fine grain-sized ceramics was believed to be due to the clamping of domains exhibited by neighboring grains and grain boundaries [7, 76, 80]. The observed decrease in the remanent polarization of the coarse grain-sized materials was attributed to relatively free domain reversal processes just after the removal of field [7].

As for grain size effects on the dielectric properties of PZT, there are contrary works in the open literature. Earlier works [73, 77, 78] showed an increased dielectric constant with increasing grain size. The authors explained this behavior using either a space-charge distribution model [77] or a Gaussian distribution of the Curie temperature model [78]. However, Webster and Weston reported that the dielectric constants of both rhombohedral and tetragonal compositions increased with decreasing grain size, and the above authors explained this behavior using an internal stress [76]. It is believed that the discrepancy described above may be due to artifacts associated with the processing. Recently, Kim investigated grain size effects on the dielectric properties of carefully prepared PZT ceramics which had a wide range of grain size [7]. It was found in this work that the dielectric constant and loss of undoped PZT increased with decreasing grain size. It was also noticed that the grain size dependence of the dielectric constant appeared to diminish when the composition approached the MPB. The author concluded that there are both intrinsic (internal stress) and extrinsic (domain wall motion, grain boundary phase, defects) causes for the observed size effects in the dielectric constant, and that the extrinsic sources often dominate at room temperature. The increase of loss with decreasing grain size was attributed to space charge in the grain boundary phases. Dielectric measurements at 15K showed that the grain size dependence of the dielectric constant of PZT ceramics was retained at this temperature and higher dielectric constants were observed in fine grain specimens than in the coarse grain ones. This result supports the internal stress model which explains the increase of intrinsic dielectric constant with decreasing grain size [7].

The dependence of phase transition parameters on grain size in PZT ceramics has also been investigated. Most results showed that the dielectric maximum K_m at the Curie temperature decreased and the peak became broadened with decreasing grain size. At the same time, an increase of the Curie temperature was observed [7, 77-79]. The reason for the broadening and decrease of K_m with decreasing grain size is still unclear. It appears that more than one mechanism can account for this behavior, including a change in domain wall motion and the presence of a low dielectric constant grain boundary phase. The dependence of the Curie temperature on grain size is believed to be due to space charge accumulated in the grain boundary phases [77, 80]. It was reported that little change of the Curie temperature with grain size was found in Nb-doped PZT in which the space charge layer in the grain boundary phases was minimized by donor doping [7].

The piezoelectric and related properties of PZT ceramics were consistently found to decrease with decreasing grain size in the literature. This behavior is believed to be due to the clamping of domain walls in fine-grained PZT. In addition, the switching of non-180° domains during the poling process is suppressed by the neighboring grains in fine grain PZT ceramics. These same mechanical forces tend to cause relaxation of the domains (depoling), thus leading to a fast initial aging rate of the piezoelectric properties at the early stage after the removal of the poling field. Furthermore, space charge associated with defects can accumulate at the grain boundaries. The space-charge layer, which is seen to increase with decreasing grain size, may degrade the poling efficiency. These effects, coupled together, seem to lead to the observed grain size dependence of the piezoelectric-related properties over a wide range of temperatures (300K, 100K, 15K).

With decreasing temperature, the extrinsic contribution such as domain wall motion was frozen out, and the piezoelectric properties became independent of the grain size [7].

In review of grain size effects on the properties of PZT system, there are some investigations on PZT bulk ceramics. However, there are still some unresolved problems due to the contrary results. As for grain size effects in thin film PZT, there is no systematic study reported in the open literature to the author's best knowledge.

2.8.2 Stress

Thin film materials deposited on a different substrate usually are mechanically stressed. The origin of these stresses (which are primarily of biaxial nature) can be sorted as thermal, intrinsic, and extrinsic stresses [81]. The intrinsic stress is commonly referred to as the growth stress, and is determined by the nature of both the film and substrate and is fundamentally related to the film deposition process. Large intrinsic stresses are usually found in films prepared by physical vapor deposition processes (e.g. sputtering). Extrinsic stresses are caused by structural changes which have an accompanying dimensional change, such as the crystallization of an amorphous phase or the paraelectric-ferroelectric phase transition. Thermal stresses are due to the thermal expansion mismatch between the film and the substrate. As the specimen is cooled down from the deposition or crystallization temperature, residual strain develops in the film due to thermal expansion mismatch, which results in a biaxial stress in the film. Stress measurements on sol-gel derived PZT films deposited on Pt-coated silicon substrates [82] showed that the residual stress present in these films is mainly thermal stress. The

residual stress was measured to be tensile and had a magnitude of about 100 MPa for submicron PZT films with MPB composition, which was in good agreement with the calculated thermal stress [82, 83].

Due to the ferroelastic nature of non-180° domain walls in ferroelectric materials including PZT, it is reasonable to expect that the properties of these materials can be influenced by mechanical stresses. Both the intrinsic and extrinsic properties of a ferroelectric material can be changed by mechanical stresses through alterations in the domain structure, Curie point, domain wall activity, and switching properties [81].

The effects of both biaxial stress and uniaxial stress on the dielectric and piezoelectric characteristics of PZT ceramics have been the subject of many investigations [84-90]. The results from compressive biaxial stress experiments showed that as the applied stress increased, there were decreases in the dielectric constant but increases in the loss factor for both hard and soft PZT ceramics [84]. The reduction of the dielectric constant with an applied biaxial stress in soft PZT ceramics was much stronger than that in hard PZT ceramics, and could not be recovered after the removal of the stress. These effects can be explained by non-180° domain reorientation as a result of the applied stress. Under an applied compressive stress, domains which have polarization vectors perpendicular to the stress are energetically more favorable than those with polarization vectors parallel to the stress. Therefore a compressive biaxial stress tends to reorient the polarization vector of the domains to a direction more perpendicular to the plane. Since the dielectric properties of PZT are very anisotropic ($\varepsilon_c < \varepsilon_a$), the dielectric constant of PZT ceramics decreases due to the reorientation of the non-180° domains. Similar experiments on the piezoelectric measurements showed that the d_{31} coefficients

of PZT ceramics also decreased with increasing applied compressive biaxial stress [85]. This behavior was also attributed to the non-180° domain reorientation due to the stress application. A compressive stress would reorient ferroelectric domains whose polarization vectors are parallel to the stress to directions perpendicular to it. However, these reoriented domains tend to arrange themselves antiparallel to each other (i. e., forming 180° domain configurations) to reduce the electrostatic energy associated with the depolarization field. Therefore, the net polarization of the material and its piezoelectric coefficients are reduced due to the non-180° domain reorientation [91].

Uniaxial stress effects on the dielectric and piezoelectric characteristics of PZT ceramics have also been investigated [86-90]. Krueger studied the effects of the amplitude and the sequence of the applied uniaxial stress parallel to the poling direction on the dielectric constant and d_{33} coefficient for both hard and soft PZT [86]. The results on the dielectric constant are shown in Figure 2.12. During the first stress cycle, there was a significant increase in the dielectric constant with the increase of applied compressive stress for hard PZT ceramics. However for soft PZT, the dielectric constant initially increased with applied compressive stress, then reached a maximum at about 55 MPa, followed by a large decrease as the applied stress continue to increase during the first stress application. The dependence of the dielectric constant on the applied stress retained a similar behavior for hard PZT in later cycles, with only a slight decrease in the magnitude of the changes and a small increase in the dielectric constant after stress removal. In contrast, the dielectric constant of soft PZT showed little change as the applied stress increased during the later cycles.

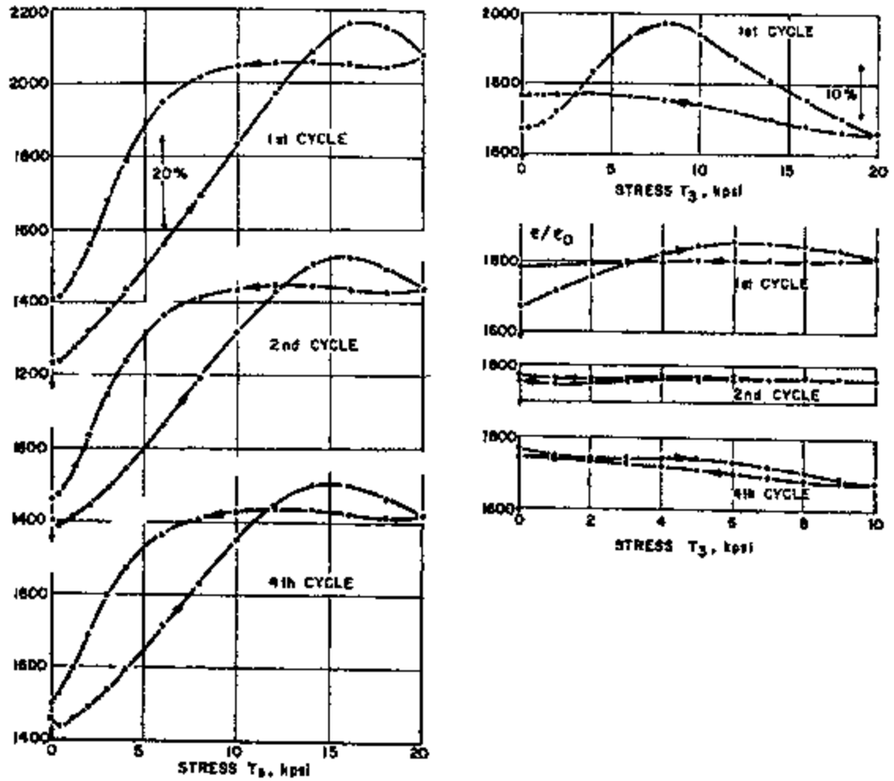

Figure 2.12 The effects of applied uniaxial compressive stress on the dielectric constant of PZT-4 (left side) and PZT 5A (right side). Stress was applied parallel to the polar axis. Data were taken from Krueger [86].

An increase in the dielectric constant with applied compressive uniaxial stress in soft PZT ceramics was also observed by Nishi and Zhang et al. [89, 90]. This behavior is believed to be due to the increased domain wall contributions to the dielectric and piezoelectric properties caused by the applied uniaxial stress. In hard PZT, the defect

dipoles are reorientable due to the mobile nature of these defects. They tend to align with the polarization vectors of the domains to stabilize the domain structure. A displacement of the domain walls then increases the material's free energy so that the domain walls in hard PZT are inactive against external excitation. Small domain wall contributions in hard PZT lead to reduced dielectric constants and piezoelectric coefficients. However, by applying a compressive stress parallel to the polarization vector, the ferroelectric domains tend to reorient to directions more perpendicular to the stress, which results in a metastable domain configuration. Therefore the domain wall motion is much enhanced by the compressive stress, so that the dielectric constant and tan δ increase as extrinsic contributions increase [90].

The unaxial stress behavior of soft PZT ceramics also can be explained by domain processes occurring in soft PZT ceramics in response to an applied stress. At the initial stage where the applied stress is small, domain wall mobility increases with applied stress, which is similar to what happens in the hard PZT ceramics but less significant. This results in an increased dielectric constant with applied stress. As the applied stress continues to increase, substantial non-180° domain switching occurs due to the reorientation of the ferroelectric domains to more energetically favorable directions. As the domains with polarization vectors parallel to the stress reorient to directions perpendicular to it, the piezoelectric coefficient decreases due to depoling [86, 90].

The effects of biaxial stress on the properties of sol-gel derived PZT thin films were investigated by Shepard et al. recently [14]. Through bending the substrate using a uniform pneumatic pressure rig, both tensile and compressive biaxial stresses were applied to the films. It was found that the dielectric constant changed very little with the

applied biaxial stress (<10% for ±100 MPa) and that the changes were reversible. Contrary to what was observed in PZT ceramics, the dielectric constant of PZT thin films increased when the applied biaxial stress was compressive, and decreased when the stress was tensile. The change of the remanent polarization with applied biaxial stress was also reversible, and the remanent polarization decreased with tensile stress and increased for compressive stress. In addition, a small increase (less than 10%) in the coercive field was observed with applied compressive stress, while the change in the coercive field was even smaller for tensile stress. All these results, including the small changes in the dielectric properties in PZT films due to the applied stress and the reversible nature of the stress effects on both the high field and low field characteristics, suggest that unlike the situation in bulk PZT ceramics, non-180° ferroelastic domain wall motions play little role in the thin film properties over the stress range studied [14].

The effects of uniaxial stress on the properties of PZT films have not been reported in the literature. This kind of experiment is also very helpful for investigating the ferroelastic activity of the non-180° domain walls in these films.

2.8.3 Crystallographic Orientation of the Films

Through adjusting the processing parameters during the preparation procedure and/or choosing appropriate substrates, highly oriented or epitaxial PZT films can be deposited by many deposition techniques. Due to the large anisotropy of PZT crystals (calculated on the basis of phenomenological theory), all the properties of these films are expected to be strongly dependent on the crystallographic orientation. Furthermore, since

there are several directions which are equivalent in the high temperature paraelectric phase but different in the room temperature ferroelectric phases, the dielectric, piezoelectric, and the ferroelectric properties of PZT films are also strongly influenced by the domain structures formed in the films during the phase transition. Thus PZT films may have the same crystallographic orientation in the high temperature paraelectric phase, but develop into different domain patterns on different substrates (e.g., *a*-domains which have polarization vectors parallel to the film surface and *c*-domains which have polarization vectors perpendicular to the film surface).

The intrinsic values of the dielectric and piezoelectric properties of PZT crystals along any crystallographic direction can be calculated by projecting the values along the principal axis into that direction using the tensor transformation method. The dependence of the intrinsic dielectric constants and piezoelectric coefficients on crystallographic orientation has been calculated [92] using data from the phenomenological theory [37] for PZT of both tetragonal and rhombohedral compositions near the MPB. Their calculations showed that for both tetragonal and rhombohedral PZT, the dielectric constant monotonically increases with the angle from the spontaneous polarization direction. The minimum and maximum values are found in directions which are parallel and perpendicular to the polarization direction respectively. Similarly the piezoelectric constant d_{33} is found to have a maximum value along the polarization direction and decrease as the crystal is rotated away from that axis for tetragonal PZT (Figure 2.13a). However, for rhombohedral PZT, the calculation shows (Figure 2.13b) that d_{33} has the maximum value in a direction 59.4° away from the polarization direction [111], which is close to the paraelectric cubic perovskite equivalent axis [100].

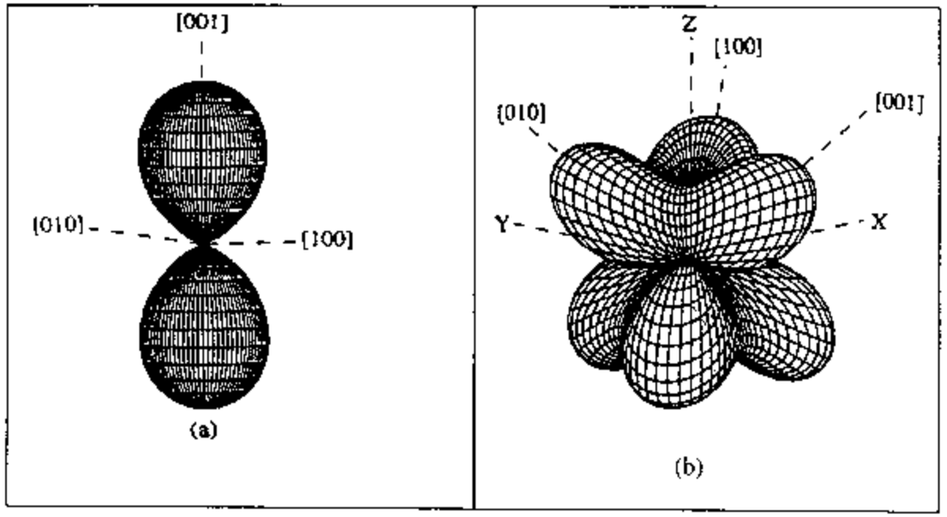

Figure 2.13 **(a) Intrinsic piezoelectric coefficient d_{33} of tetragonal 48/52 PZT crystal along any crystallographic direction [92].**

(b) Intrinsic piezoelectric coefficient d_{33} of rhombohedral 52/48 PZT crystal along any crystallographic direction [92].

The influence of non-180° domain formation on the dielectric and ferroelectric properties of PZT thin films has been demonstrated by B. Tuttle et al. [83, 93]. Their results on sol-gel prepared tetragonal PZT thin films showed that films which are predominantly *a*-domain have low remanent polarizations and high dielectric constants while films which are predominantly *c*-domains have large remanent polarizations and low dielectric constants. These results are consistent with the directional dependence of the properties in a tetragonal PZT crystal. The formation of *a* and *c*-domains is believed to be determined by the biaxial stress in the films at temperatures in the vicinity of the

Curie temperature. PZT films under tension at the transformation temperature are preferentially *a*-domain oriented, whereas films under compression at the transformation temperature are *c*-domain oriented. Since X-ray diffraction measurements of PZT films as a function of electric field showed that electrical switching of 90° domains in these submicron films is severely limited, the original orientation and assembly of these 90° domains have significant impact on the film properties.

2.8.4 Clamping and Interface Effect

It is well known that the elastic constants, the dielectric constants and the piezoelectric constants of a piezoelectric are all functions of the electrical and mechanical boundary conditions. For a piezoelectric thin film deposited on a rigid substrate which is much thicker than the film itself, the film is always mechanically clamped to some extent by the substrate. Therefore the measured dielectric and piezoelectric constants in thin films are those under partially clamped mechanical boundary conditions (which are different from either the constants under free boundary condition or the constants under totally clamped conditions). The exact mechanical boundary condition under which the dielectric and/or piezoelectric measurements on PZT thin films are performed varies according to the geometry of the sample, the elastic constants of the film and the substrates, and the piezoelectric constants of the film. Since little elastic data on PZT thin films been reported in the literature, quantitative modeling of the mechanical boundary condition in these films is not possible. Furthermore, there have been no experimental results on the influence of the substrate clamping on the properties of PZT thin films

reported in the literature. Therefore, the effect of the clamping effect imposed by the substrate on film properties is still not well understood. However such information is very important in understanding the piezoelectric behavior of PZT films, and initial work is imperative.

The film/substrate and film/top electrode interface is another factor which may influence the properties of PZT films. As has been pointed out previously, local stresses at these interfaces can pin the domain walls, which will result in a small extrinsic contributions to both the dielectric and piezoelectric responses in these films. Space charge at the interfaces may also cause domain wall pinning, as indicated by imprint in these films. In addition, low permittivity layers may form at these interfaces, which can result in a low measured dielectric constant. These layers may result from the volatilization of PbO at the surface during annealing, the formation of an amorphous phase during the sputtering of the top electrode, or the formation of TiO_2 phase at the bottom electrode due to the interdiffusion during annealing.

Chapter 3. Experimental Procedure

This chapter describes experimental procedures used in film preparation, structural analysis, and electrical and piezoelectric characterization for the investigations performed in this thesis.

3.1 PZT Film Deposition

The sol-gel process is one of the prime methods among all ferroelectric thin film deposition techniques due to its precise compositional and doping control, good homogeneity and uniformity for large area deposition, low processing temperatures, and low manufacturing costs. In addition, the grain size of sol-gel derived PZT films can be controlled to some extent during annealing of the pyrolyzed amorphous films. These advantages make the sol-gel process a suitable film deposition technique for the purpose of the investigations performed in this study. Therefore, all the PZT films investigated in this thesis were fabricated through the sol-gel spin-on technique.

In general, the sol-gel process involves the following steps:

a) dissolution and reaction of the cation precursors in a suitable solvent

b) monitoring the solution characteristics, including viscosity and solids content

c) film deposition by spin coating

d) low temperature heat treatment for organic pyrolysis

e) high temperature annealing for film densification and crystallization

In this study, three sol-gel methods (which were different in both solution chemistry and annealing process) were chosen for the preparation of the PZT films. The first one used sol-gel solutions made by the methoxyethanol process described by Budd et al. [94] and modified by Brooks et al. [95]. Lead acetate trihydrate, $Pb(CH_3COO)_2{\cdot}3H_2O$, zirconium n-propoxide, $Zr[OCH(CH_3)_2]_4$, and titanium isopropoxide, $Ti[OCH(CH_3)_2]_4$ (Aldrich Chemical, Milwaukee, WI) were used as the elemental precursors. Figure 3.1 details this method. First, lead acetate trihydrate was dissolved in 2-methoxyethanol, and the water of hydration was distilled at 110°C under a vacuum of 130mbar. Appropriate quantities of zirconium n-propoxide and titanium isopropoxide corresponding to the targeted stoichiometry of the PZT films were then mixed in 2-methoxyethanol and refluxed with the lead acetate solution at 110°C for 2.5 hours. The preparation of the precursor solution was carried out in a Rotary Evaporator (Labconco). A 0.4 Molar solution containing 12% excess lead was prepared for film fabrication. 4% formamide in volume was added to this solution to adjust the surface tension to reduce the likehood of cracking of the film during pyrolysis and annealing [94]. PZT films were deposited by spin coating the precursor solution on substrates at 3000 rpm for 30 seconds. Each PZT layer was pyrolyzed at 340°C for 60 second on hot plate. After four layers were spin coated and pyrolyzed, the deposited film was crystallized at 700°C for 30 sec using an AG Associates, Heatpulse 210 rapid thermal annealing system (RTA), and a PZT film of approximately 0.25 μm in thickness was obtained. Thicker films were fabricated by repeating this procedure. PZT films with composition across the morphotropic phase boundary (zirconium to titanium ratios of

56/44, 52/48, and 48/52) and thickness from 0.25 μm to 3.4 μm were prepared by this method.

However, for films thicker than 4 μm prepared by the above method, cracks often occurred due to the stress accumulation. To make thicker films, a second sol-gel method was used which added additional acetylacetone into the precursor solution used in the first method. In addition, a 600°C to 650°C pre-annealing step was introduced into this process for densification of the spin-coated layers to prevent further shrinkage during the final annealing at 700° by RTA [96]. This adjustment enabled preparation of PZT films up to 10 μm thick.

The third sol-gel method also used the same precursors as the first two but a different solvent (acetic acid, CH_3COOH). Ethylene glycol and deionized water were added to the solution to control the viscosity and surface tension. This method was proposed by Yi et al. [97] and modified by Chen et al. [98] and was also capable of preparing PZT films 10 μm or thicker without cracks. In addition, conventional box furnace annealing at 700°C for 1 hour rather than RTA was used for the final crystallization of the PZT films in this method. The details of this sol-gel process can be found elsewhere [98].

The substrates used for this work were Pt(111)/Ti/SiO_2/Si and Pt(100)/SiO_2/Si wafers commercially produced by Nova Electronics and Tong Yang Central Laboratories, respectively. For the Pt(111)/Ti/SiO_2/Si substrates, the thickness of SiO_2, Ti and Pt layers were 1 μm, 0.02 μm and 0.12 μm respectively. For the Pt(100)/SiO_2/Si substrates, the thickness of SiO_2 and Pt layers were 0.3 μm and 0.15 μm respectively. In both cases, the wafers were single-side polished.

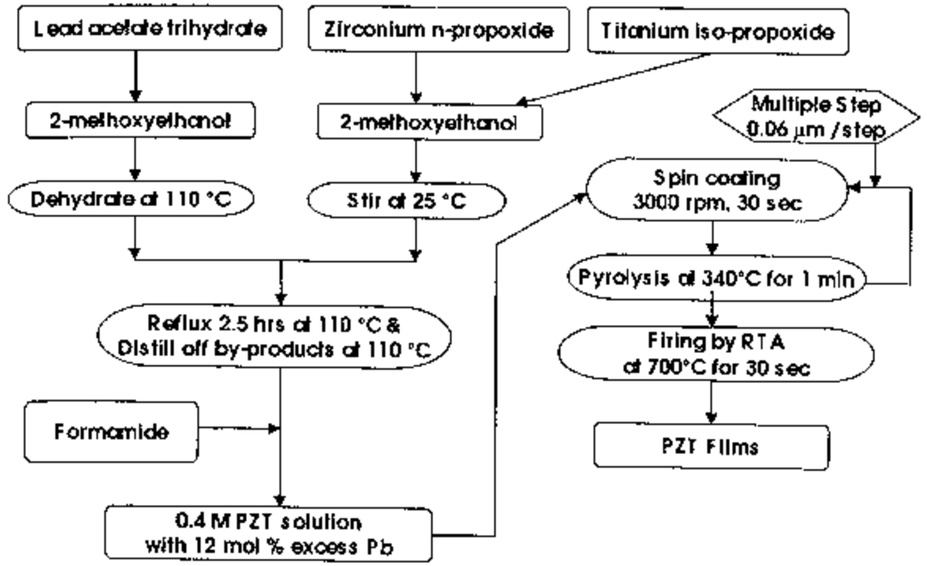

Figure 3.1 **Flow chart of the sol-gel method for the preparation of PZT thin films using a 2-methoxyethanol solvent.**

3.2 Film Structure Characterization

The elastic, dielectric, piezoelectric and ferroelectric properties of PZT films are all closely related to the structure and microstructure of the materials. Thus, the phase structure, the crystallographic orientation, the grain size, and the domain configuration of the PZT films were characterized since all of them are important factors governing the properties of the films.

3.2.1 X-Ray Diffraction

The x-ray diffraction (XRD) patterns of PZT films were recorded at room temperature with a Scintag DMC-105 diffractometer (Scintag, Inc., Sunnyvale, CA) using Cu Kα radiation to determine the extent of crystalline structure and the preferred orientation of the films. A scan rate of 2 degrees per minute was used throughout the structure analysis.

3.2.2 Scanning Electron Microscope

The surface morphology and cross-sectional microstructure of the PZT films were examined using a JEOL JSM6300F field-emission scanning electron microscope (FE-SEM). A thin gold film was sputtered on top of the PZT film surface to increase the surface conductivity. Such a continuous conducting layer is necessary to provide better surface details and to prevent sample charging.

3.2.3 Transmission Electron Microscope

Transmission electron microscopy (TEM) was used to reveal the microstructure of the films, such as growth textures, grain sizes, and domain structures. To prepare the cross-section TEM specimens, the films were first ground to a thickness of about 0.1 mm and then dimpled to about 10 μm thick. After that, argon ion milling was used to thin the sample to electron transparency. The cross-section TEM images were observed using a field-emission Hitachi HF-2000 TEM [99]. The plane view TEM samples were prepared

by grinding and ion milling from the substrate side followed by a short time ion milling at the top surface. The condition of ion milling is as follows: HV = 5 kV, current = 0.5 mA, at 12.5° with liquid nitrogen cooling [100].

3.2.4. Film Thickness Measurements

In this study, an Alpha-Step 500 surface profilometer from Tencor Instruments (Mountain View, CA) was used to measure the actual film thickness. This measurement employs a sensitive stylus which glides over the substrate surface across the step between the deposited film and the bottom electrode. The step height is determined by the vertical displacement of the stylus. In order to form a thickness step profile, PZT films were patterned by wet chemical etching in a dilute mixture of hydrofluoric acid and hydrochloride acid.

3.3 Electrical Properties Evaluations

To examine the high and low field electrical properties of the PZT films, a simple metal-insulator-metal (MIM) sandwich configuration for the capacitor was used. To facilitate the electrical property evaluations, top contact electrodes of platinum, approximately 600 Å in thickness and usually 1.6 mm in diameter, were sputter-deposited on top of the PZT film surface through a shadow mask. The sputtering system used was a Blazers SCD 040 from Blazers Corp. (Hudson, NH).

3.3.1 Low Field Electrical Characterization

The dielectric constant and loss tangent of the PZT films were measured using either a Hewlett Packard 4274A multi-frequency LCR meter or a 4192A LF impedence analyzer. All low-field tests were conducted at a frequency of 1kHz and ac rms electric field of 0.5 kV/cm. In some cases, the dependence of the dielectric constant and loss tangent on the amplitude of the applied electric field was measured at 1kHz. For these measurements, electrical contacts were made using point probes.

3.3.2. High Field Electrical Characterization

The polarization hysteresis loops of the PZT films were measured using a Radiant Technologies RT66A ferroelectric tester, from which the saturated polarization, P_{sat}, the remanent polarization, P_r, and the coercive field, E_c, were determined. Typically, the maximum electric field was 500 kV/cm and the measurement frequency was 30 Hz for the hysteresis measurements. An external amplifier (AVC Instrumentation 790 Series Power Amplifier) was used to allow high field measurements on thicker films.

3.4 Piezoelectric Property Measurements

In order to measure the longitudinal piezoelectric coefficient d_{33} of the PZT films, a pneumatic pressure charge method was developed in this study. Laser interferometry

and a Berlincourt meter were used for the calibration and error analysis of the pneumatic pressure charge method. To investigate the influence of mechanical boundary conditions on the effective d_{33} coefficient of PZT films, both the pneumatic pressure charge method and double beam interferometry were used to measure the effective d_{33} of the same sample at the same position.

3.4.1 The Pneumatic Pressure Charge Technique

The pneumatic pressure charge technique is a simple and inexpensive method for evaluating the effective longitudinal piezoelectric coefficient, d_{33}, of piezoelectric films. It is a direct piezoelectric measurement which applies a static normal stress perpendicular to the film and measures the surface charge induced by the applied stress.

The experimental set-up of the pneumatic pressure charge technique is schematically shown in Figure 3.2. There were two major parts in this set-up: a pneumatic pressure rig which was designed to apply a uniform normal stress to the tested specimen and a home-made charge integrator for induced-charge collection. The stress rig consisted of two identical aluminum components machined with cavities. The sample was placed between the aluminum fixtures with cavities both above and beneath it. O-rings (Parker Seals, Lexington, KY) were used to seal both sides of the sample in the housing. By introducing high-pressure nitrogen gas into these cavities simultaneously, equal and uniform forces were exerted on both sides of the sample. Thus a uniform compressive normal stress was applied to the specimen. Similarly, releasing the pressure from the cavities resulted in a decreased compressive normal stress on the specimen. The

pressure inside the two cavities was measured using Omega PX602 pressure transducers. The pressure applied in this experiment ranged from 0.1 to 1.2 MPa.

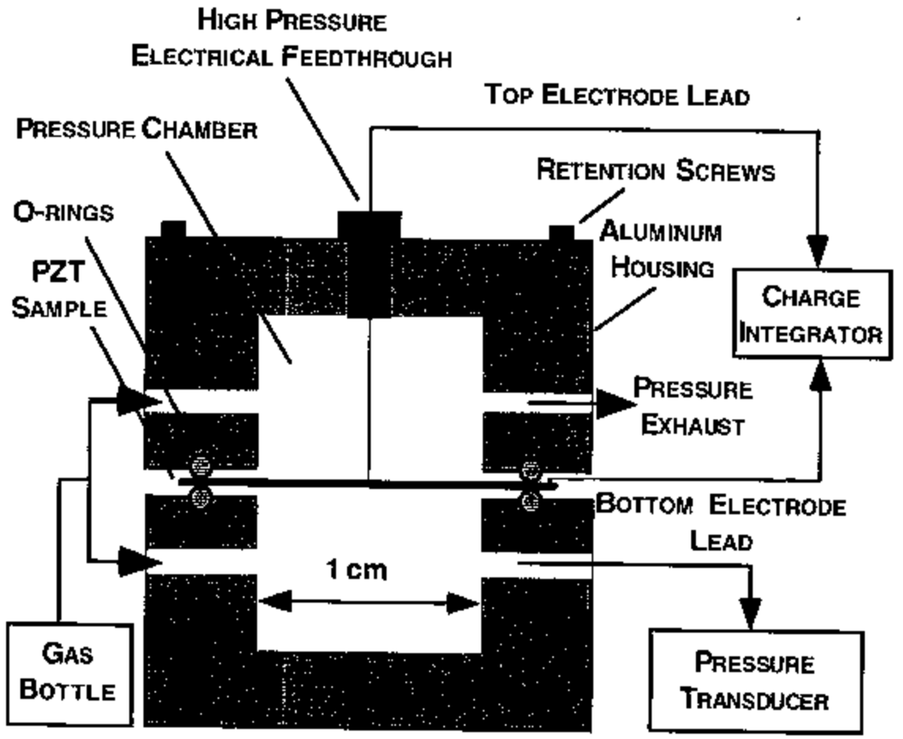

Figure 3.2 A schematic drawing of the experimental set-up for the d_{33} measurement.

The induced piezoelectric charge was collected using a charge integrator (Figure 3.3). The electronics converted the collected charge into a variation of voltage on a capacitor of known size placed in series with the stressed specimen. The polypropylene reference capacitor had very good temperature stability and low dielectric absorption. Since the circuit runs in a virtual ground mode, the voltage between the two electrodes of the specimen was always zero, so that almost all the induced charge was driven to the capacitor. The voltage output from the charge integrator was monitored in real time using a Hewlett Packard 54600A oscilloscope.

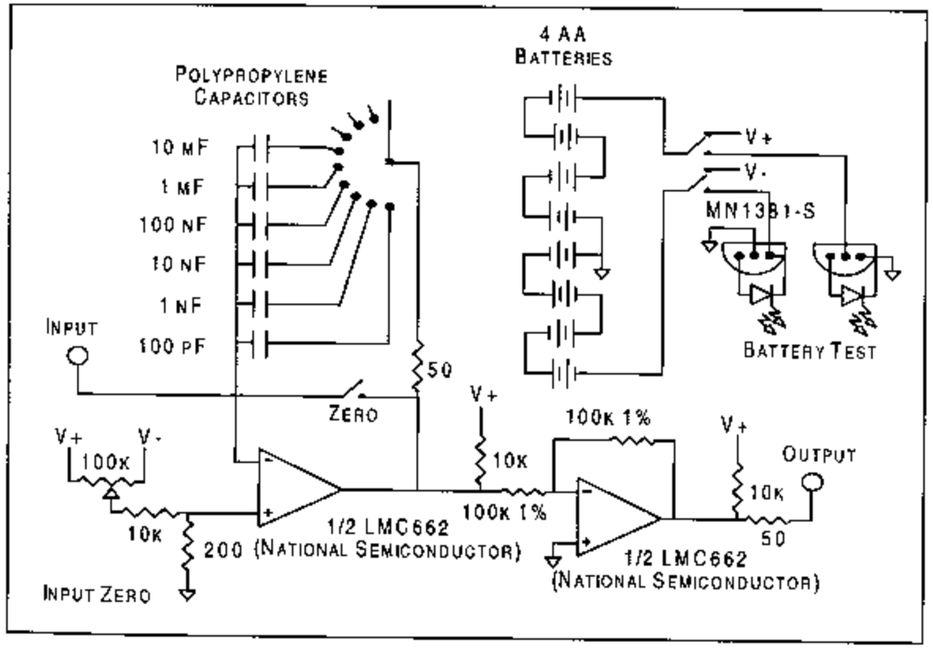

Figure 3.3 **Schematic of the electric charge integrator.**

To characterize the pneumatic stress rig, resistance strain gauges (Omega pre-wired strain gauge, type KFG-1N-120-C1-11L3M3R) were used to monitor the in-plane strains presented in the sample mounted into the stress rig through a 3800 wide range strain indicator (Vishay Measurements Group, Raleigh, NC). The strain gauge was attached to the center of the sample surface using super glue. The in-plane strain in the sample was measured as a function of time after the pressure was introduced or released from the cavities.

The effective piezoelectric coefficient d_{33} of the tested PZT films can be determined from:

$$d_{33} = Q/\Delta P \cdot A \qquad (3.1)$$

where Q is the pressure-induced charge collected by the charge integrator, ΔP is the pressure change inside the cavities, and A is the area of the top electrode.

For the piezoelectric measurements, PZT films were poled under various field levels at room temperature for 1 min to 10 minutes. It was found that the back of the silicon wafer should be polished with 1 μm alumina powder to improve the accuracy of the results. Air dry silver epoxy was used to contact the top and bottom electrodes of the thin film capacitor to the electrical leads. The top electrodes were sputtered Pt films 1.6 mm in diameter.

3.4.2 Double Beam Laser Interferometry

A modified double beam laser interferometer system, which is capable of resolving AC displacement on the order of 10^{-2} Å with a lock-in amplifier, was adopted to measure the electric field-induced longitudinal strain [11]. The effective piezoelectric coefficient d_{33} of the PZT films was evaluated from the strain response to the external driving E-field by:

$$d_{33} = x_3/E_3 \tag{3.2}$$

where x_3 is the longitudinal field-induced strain and E_3 is the amplitude of the external ac driving field.

The measurement set-up is schematically shown in Figure 3.4. This method is based on the interference between two coherent laser beams, of which one is the reference beam and another is a beam reflected from both the surfaces of a piezoelectric sample. An electric-field-induced strain of the piezoelectric sample results in a change in the optical path length of the second laser beam, which leads to a variation of the light intensity of the interfered pattern of the two laser beams. The light intensity is detected by the photo-detector and can be expressed as [10]:

$$I = \frac{1}{2}(I_{max} + I_{min}) + \frac{1}{2}(I_{max} - I_{min})\sin(\frac{4\pi\Delta L}{\lambda}) \tag{3.3}$$

where I_{max} and I_{min} are the maximum and minimum intensities of the interference fringes, ΔL is the optical path length difference induced by strain oscillation of the piezoelectric

sample, and λ is the wavelength of the laser light. When the displacement ΔL is much less than the full fringe range, the sine function in equation 3.3 can be replaced with its argument. The light intensity from the photo-detector is converted to a voltage which is expressed as

$$V_{out}(t) = V_{dc} + (\frac{2\pi}{\lambda})V_{pp}\Delta L(t) \qquad (3.4)$$

where V_{pp} is the peak-to-peak voltage corresponding to the full fringe displacement (i.e. I_{max} - I_{min}) and V_{dc} is the dc offset. From knowledge of the peak-to-peak voltage, which is obtained by moving the reference mirror over a distance of greater than λ/2, and the wavelength of the laser, the change in the optical path length (ΔL) is measured. This gives the surface displacement of the piezoelectric sample, from which the field-induced strain and the effective piezoelectric coefficients can be characterized.

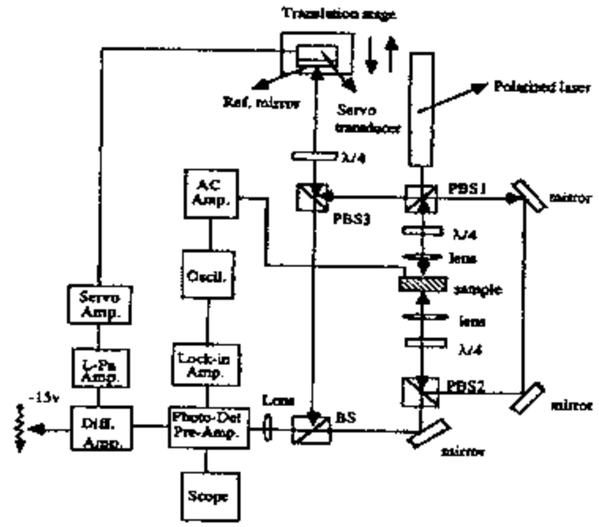

Figure 3.4. A schematic of a double beam Mach-Zehnder interferometer [11].

A Helium-Neon laser (Model 127, Spectra-Physics Lasers, Inc., Piscataway, NJ) with a wavelength of 632.8 nm was used in this system. A small piece of Pt-coated silicon substrate was adhered to the backside of the specimen to increase the reflectance from the back surface. The tested sample was mounted to a sample holder using super glue. The top electrodes were 1.6mm in diameter and silver epoxy was used to contact the lead from both the top and bottom electrodes. A bipolar ac electric field of 1kHz was applied between the two electrodes to generate an ac longitudinal strain in the specimen. The intensity of the interfered laser beams was detected by a photo-diode, then amplified and measured using a lock-in amplifier.

3.4.3 Calibration using Berlincourt Meter

A ZJ-2 piezoelectric d_{33} meter (Institute of Acoustics, Academia Sinica) was also used to measure the d_{33} value of bulk PZT specimens for calibration of the pneumatic pressure charge technique. The bulk specimen used was a piece of PZT-5A ceramic which was 25 mm by 25 mm by 2 mm in size and polished using 1μm alumina powder on both sides. A thin layer of Pt was sputtered on the whole area of one side as bottom electrode. On the other side, a 7.5 mm diameter top electrode was also formed using sputtered Pt. The sample was poled at 100°C for 10 min under an electrical field of 20 kV/cm. This sample was used as a standard for the calibration of the pneumatic pressure charge technique.

3.5 Low and High Temperature Property Measurements

The temperature dependence of the dielectric constant and loss tangent of PZT films was measured both above and below room temperature. For the high temperature measurements, PZT films were heated at ~ 2°C/min up to 450°C in a computer controlled oven. Samples were mounted onto alumina chip carriers with air-dry silver paint. Connections between the sample electrodes and chip carrier bonding pads were made by ultrasonic wire bonding (wedge bonder Model 4123, Kulicke and Soffa Industries, Inc.). The chip carriers were inserted into the oven and contacted with spring loaded probes. For the low temperature measurements, the samples were mounted onto a copper rod (cold finger) using low temperature grease. By inserting the cold finger into a liquid helium dewer and manually lowering it towards the cryogen, the temperature of the sample was continuously decreased to liquid helium temperature (4.2 K). The cooling rate was about 6°C/min. Silver paint was also used for the electrical contact between the electrodes and the leads connected to the measurement bridge. The bridge used to make dielectric constant and loss measurements was a Hewlett Packard 4284A LCR meter. The oscillation signal used was typically 1 kHz in frequency and 0.5 kV/cm in amplitude.

The high field electrical properties of PZT films, including the spontaneous polarization, the remanent polarization and the coercive field, were also measured as a function of temperature down to 4.2 K. The measurements were made using a RT66A ferroelectric tester at discrete temperatures. In some cases, the dielectric nonlinearity of PZT films at low temperature was also measured.

3.6 Uniaxial Stress Measurement

The dielectric properties of PZT films were measured as a function of applied compressive uniaxial stress. The measurement setup is shown schematically in Figure 3.5. A hydraulic stress rig was constructed and used to apply uniaxial stress to PZT films. The fixture is very similar in design to the pneumatic stress rig used for d_{33} measurements. The sample was put between two stainless steel parts, with cavities both above and beneath it. By pumping hydraulic oil into these cavities, high pressure was exerted on both sides of the sample, thus imposing compressive normal stress on the sample. Instead of using a high pressure electrical feedthrough, the top electrode was directly connected to the stainless steel housing. Low field dielectric measurements were made using a Hewlett Packard 4192A LF Impedance Analyzer at a frequency of 10 kHz and an amplitude of 1 kV/cm. High field ferroelectric hysteresis loop measurements were made using a RT66A ferroelectric tester. A two minutes waiting time was allowed before any measurements were made and the data were recorded as the average of 5 readings. The maximum pressure applied was 20 MPa. Larger pressures often resulted in sample breakage.

The piezoelectric coefficient d_{33} of both PZT bulk ceramics and thin films was measured as a function of stress amplitude. Static pressures from 1 to 12 MPa were applied to the samples using the pneumatic pressure rig described in section 3.4.1 and the induced charge was measured using the in-plane stress self-compensation procedure. The d_{33} coefficient was calculated from the induced charge and the applied pressure using equation 3.1 and then plotted as a function of stress amplitude.

3.7 Electrical Field Dependence Measurement

The effect of dc poling on the dielectric and piezoelectric properties of PZT films was investigated to evaluate domain wall activity. For the dielectric property measurements, the samples were poled under various dc electric fields for one minute at room temperature and measured after five minutes aging. For the piezoelectric measurements, the samples were poled for ten minutes at room temperature and allowed 24 hours aging time before the measurements were performed. The dielectric constant and loss tangent were measured using a Hewlett Packard 4192A LF Impedance Analyzer at a frequency of 1 kHz and an amplitude of 0.5 kV/cm. d_{33} was measured using the pneumatic pressure charge technique.

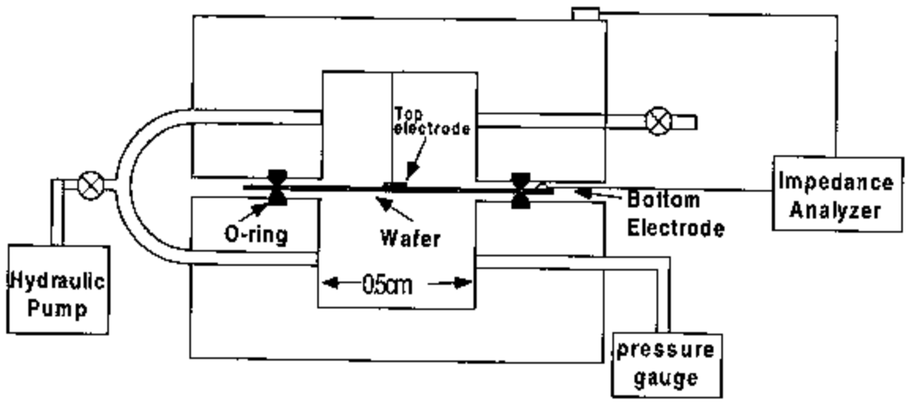

Figure 3.5 **Schematic drawing of the experimental setup for uniaxial stress measurements.**

Chapter 4. The Pneumatic Pressure Charge Method for the Longitudinal Piezoelectric (d_{33}) Measurement of PZT Thin Films

4.1. Introduction

For the proper design of MEMS devices, explicit knowledge of the piezoelectric properties, including the longitudinal (d_{33}) piezoelectric coefficient of the piezoelectric films is required. The d_{33} coefficient of bulk piezoelectrics can be determined by either resonance or static methods. In the resonance measurement, a specific sample geometry of fully electroded thin plates or bars is required, so that the vibration modes can be regulated and predicted [101]. Quasi-static methods include methods using the direct piezoelectric effect (such as the normal load and Berlincourt methods, which apply static or alternating stresses to the sample and collect the induced charge) and methods using the converse piezoelectric effect (such as laser interferometry, which involves direct strain measurements as a function of applied field). Compared to resonance techniques, the static methods have the advantage of enabling measurements at high excitation level and low frequency although they do not provide information about the elastic constants and coupling coefficients. Such measurements can provide important information concerning high-field piezoelectric properties, field induced structure transitions, non-

linearity of the piezoelectric response, and extrinsic contributions to piezoelectric response.

Unlike bulk piezoelectric measurements, thin film piezoelectric measurements are much more difficult due to the small values of the charge and strain to be measured and the complication caused by the substrate which is rigidly attached to the film. As a result, most of the piezoelectric measurement techniques established for bulk materials are not suitable for thin film piezoelectric measurements. The IEEE standard resonance method cannot be directly used to determine the piezoelectric coefficients of thin film materials. Since the piezoelectric vibration of thin film specimens is heavily loaded by the passive substrates, the resonance usually occurs at very high frequencies and a complex impedance spectrum is obtained which often contain peaks from a number of resonance modes. To determine the piezoelectric coefficients of thin films from resonance data, models must be developed to simulate the vibrational modes [102]. In addition, a minimum film thickness (more than 5 μm currently) is required for such measurements [103]. For converse static measurements, laser interferometry is able to measure the small field-induced displacements in piezoelectric thin films due to its superior resolution. However, the substrate makes accurate measurement of the longitudinal strain more difficult. Upon the application of an electric field, both longitudinal and transverse strains are induced in the piezoelectric thin film. Since the film is rigidly bonded to the substrate, and the electric field does not induce any strain in the passive substrate, substrate bending occurs due to the transverse strain in the film [10, 104]. Thus, the displacement of the film surface contains both the displacement due to the induced longitudinal strain in the piezoelectric film and the displacement due to substrate bending. To determine the

longitudinal piezoelectric coefficient d_{33}, the surface displacement due to substrate bending must be eliminated. This can be done by using a double-beam instrument which measures the net change in the distance between the two faces (front and back) of the specimen [10, 11]. However, it requires a more sophisticated optical system and a better laser source. As a result, the measurement is non-trivial and the instrumentation is extremely sensitive.

Compared to the difficulty in measuring the small field-induced strain in thin film piezoelectrics, the stress-induced charge is much easier to measure with modern electronics. This makes the piezoelectric measurement using the direct piezoelectric effect a simple, inexpensive alternative. However, only a few attempts to determine the piezoelectric d_{33} coefficient of thin films using the direct piezoelectric effect have been reported in the literature. Measurement techniques using this method for thin film d_{33} have not been well developed yet. The primary reason for the lack of success in direct piezoelectric thin film measurements is believed to be associated with the difficulty in ensuring that a uniaxial stress is applied to the thin film specimen (see Section 4.2.1).

Due to the lack of piezoelectric data for PZT films, electromechanical properties of bulk PZT ceramics are often used in MEMS designs. However, such approximation may introduce significant errors in the design since the piezoelectric coefficients of PZT films may be substantially different from those of bulk ceramics. Indeed, the lack of reliable and convenient measurement techniques for thin film piezoelectric characterization has become a major obstacle which hinders the development of piezoelectric films for MEMS application. In this chapter, a direct piezoelectric measurement technique was proposed for accurate d_{33} measurement on thin film samples.

The effective d_{33} coefficient is determined by applying pneumatic pressure to a piezoelectric film and measuring the induced charge in this technique. The stresses imposed on the films by the pneumatic pressure were analyzed through studying the induced charge signal and measuring the in-plane strain. The possible sources of error were then discussed and investigations for error reduction in these measurements were made. An experimental procedure which can measure d_{33} accurately for a thin film specimen was developed based on the above investigation. Finally, calibration of the pneumatic pressure charge technique was made using laser beam interferometry and the Berlincouter meter.

4.2 The Design of the Stress Rig

4.2.1 Problems in Stress Application for Thin Film Specimen

Measurement of the longitudinal piezoelectric coefficient d_{33} using the direct piezoelectric effect requires a uniaxial stress to be applied to the tested specimen. For thin film piezoelectric measurements, this requirement means that the applied stress must be perpendicular to the film plane and no other stress components (such as in-plane or shear stresses) can be imposed. A few different methods for the stress application have been reported. Surowiak and Czekaj tried to use a device similar to a Berlincourt meter to measure the d_{33} coefficients of PZT thin films by applying an ac stress to the film using solid hemispherical probe tips [105]. On the other hand, Lefki and Dormans used the

static normal load method in which a force perpendicular to the film was applied to the sample using a rectangular metallic tip [106]. However, this technique is destructive to the sample and the d_{33} coefficients calculated from the measured induced charge are questionable [107]. To avoid sample breakage and ensure a uniform stress, a conductive rubber tip was used to replace the metallic tip for the stress application [108]. Despite these efforts, inspection of these methods indicates that a true uniaxial stress is very difficult to achieve in thin films due to substrate bending and problems associated with stress alignment.

In a thin film sample, a very thin layer of piezoelectric material is rigidly stuck to a much thicker substrate. Therefore even a small amount of substrate bending can produce a very large biaxial stress in the film. Due to the intrinsic stress during film growth and the thermal expansion coefficient mismatch between the substrate and the piezoelectric material, thin film samples usually have small curvatures. During a normal load direct piezoelectric measurement, the thin film sample is simultaneously bent when force is applied perpendicular to the film plane to produce a normal stress (Figure 4.1), which imposes in-plane stresses on the piezoelectric film in addition to the out-of-plane stress. From the constitutive equations for piezoelectric materials, it can be seen that these in-plane stresses also produce charge through the transverse piezoelectric effect. Thus, the measured stress-induced charge is the sum of the charges due to the normal and in-plane stresses. Therefore an evaluation of d_{33} based on the total measured charge will be erroneous due to the presence of the in-plane stress.

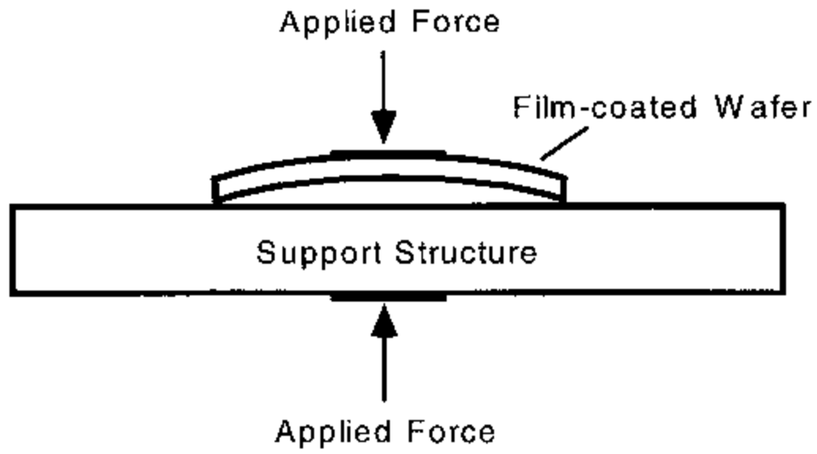

Figure 4.1 **Simultaneous bending of thin film sample during the application of normal load.**

Another problem for thin film d_{33} measurements using either the normal load method or the Berlincourt method is associated with stress alignment. To ensure that a true uniaxial stress is applied to a specimen, the longitudinal dimension of the specimen should be at least 3 times larger than its transverse dimension [101]. However, due to the small thickness of the substrate, this requirement cannot be fulfilled in thin film piezoelectric measurements. As a result, forces applied to the sample may not be perfectly perpendicular to the film plane, so that stress components other than the normal one may also be produced.

4.2.2 The Pneumatic Pressure Rig

As discussed in the previous section, the key issue in thin film d_{33} measurements using the direct piezoelectric effect is the application of a uniform, truly uniaxial stress. To overcome the problems associated with stress application, a pneumatic pressure rig was developed for thin film piezoelectric d_{33} measurements in this study.

The pneumatic pressure rig (shown in Figure 3.2) was originally designed to apply a uniaxial stress perpendicular to the tested thin film sample. The unique feature of this rig is that the force is applied by high-pressure gas over a large area of the sample. Since the pressure inside the two cavities is equal at equilibrium, the forces on the sample are uniform and act equally on the two faces. Because the applied forces are balanced everywhere across the surfaces of the sample, the pneumatic pressure does not bend the sample even if it has an initial curvature. In addition, normal stress perpendicular to the film plane can be obtained without the need to align the stress rig, even though the film thickness is much smaller than the lateral dimensions of the sample. Besides, unlike the normal load and the Berlincourt methods, there is no solid contact for stress application. Therefore, uniform stress can be obtained easily on a sample which does not have flat surfaces (which is usually the case for piezoelectric thin films due to the finite thickness of the top electrode).

4.3 Charge Response and Stress Analysis

The pneumatic pressure rig developed in this study was designed to apply only a normal (out-of-plane) stress to the tested sample. Changes in the stress applied to the tested sample were achieved by suddenly introducing or releasing high-pressure gas into the cavities. As the valve between the gas tank and the cavities was opened, the pressure in these cavities reached a preset value, and was held constant at that value until the high-pressure gas was released. The profile of the out-of-plane stress as a function of time during this process was shown in Figure 4.2a.

Ideally, if the out-of-plane stress was the only stress component produced on the tested sample by the pneumatic pressure, the induced charge should follow the same profile as the stress (i.e. the measured charge would be due only to the out-of-plane stress through the longitudinal piezoelectric effect). Figure 4.2b describes the signal which would be expected if this were the case. However, what was observed experimentally during the application and release of the pressure was much different, as shown in Figure 4.2c. When pressurized gas was introduced into the pressure rig, the induced charge quickly reached a maximum, followed by a continuous asymptotic decrease, until it stabilized after about 90 seconds. The pressure in both cavities was measured to be equal and constant throughout the signal stabilization. The signal measured after releasing the pressure was very similar to the signal on applying pressure, and the final values of the signal at stabilization were almost equal in magnitude, though opposite in sign. It should be emphasized here that the variation of the measured induced charge was not due to leakage either from the PZT sample or the electronics. This was verified by applying a

constant normal load to a bulk ceramic sample and measuring the induced charge using the same electronics. A step signal was indeed obtained in this case, as expected.

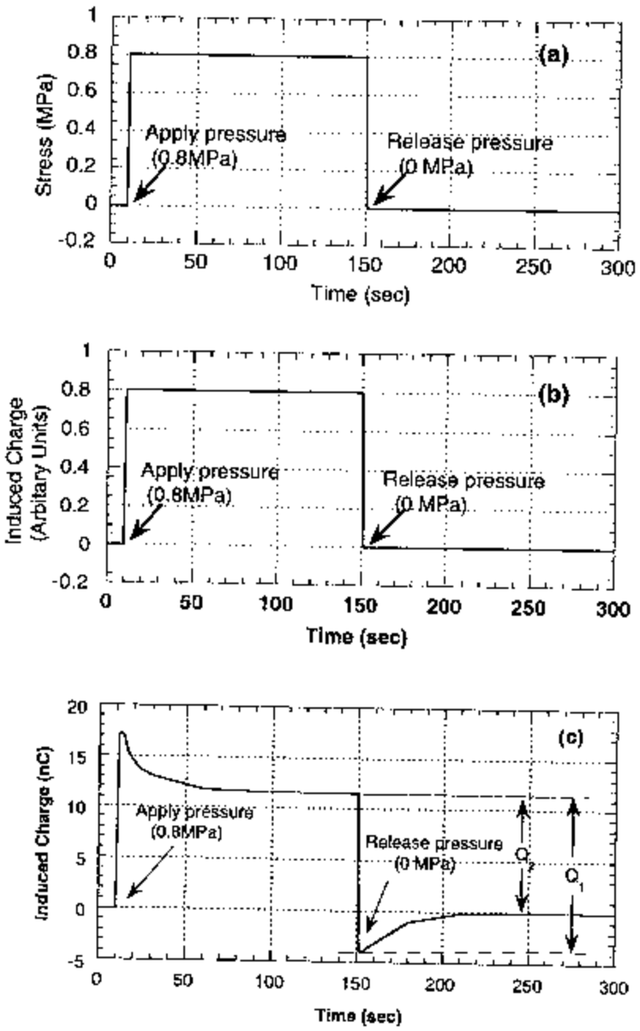

Figure 4.2 **(a) Normal stress applied to the tested sample by the pneumatic pressure rig**

(b) Calculated charge induced by the normal component of the stress

(c) Total induced charge measured during the pressure change

The experimental results above indicated that during the first 90 seconds after the pressure was introduced or released, the induced charge continuously changed with time although the pressure was constant inside the cavities. Since the out-of-plane stress on the sample was constant during this time, the change in the induced charge must come from sources other than the normal stress. This suggests that additional stress components were also generated by the pneumatic pressure change, and these stress components were responsible for the time dependence of the induced charge in the initial stage.

The constitutive equations for piezoelectricity show that the only other stress components which can induce charge in this measurement configuration are in-plane stresses. That is, shear stresses would not produce measured charge. There are two possible mechanisms which could lead to in-plane stress in piezoelectric thin films. The first is a pressure difference in the two cavities, which could induce in-plane stress through substrate bending. However, it was found that the time dependence of the induced charge could not be attributed to this mechanism. Due to the symmetry of the pressure rig, the pressure difference in the two cavities was negligible, as was indicated by the pressure gauges. Furthermore, a similar time dependence of the induced charge was also observed when a bulk ceramic PZT specimen was tested using the pneumatic pressure rig. Since there is no induced charge associated with bending in a bulk piezoelectric specimen (i.e. the net in-plane stress is zero), the in-plane stress must come from other sources.

Another mechanism which could be responsible for the pressure-induced in-plane stresses in the film is friction between the O-ring and the sample surface. Friction arises when there is a pressure change introduced into the cavities. The pneumatic pressure

generates a force which acts on all the surfaces exposed to it, including the O-ring cross-section. Increasing the pressure increases the force acting on the O-ring cross-section. This force is parallel to the film plane and pushes the O-rings outwards, thus generating a surface friction on both sides of the sample, so that a tensile in-plane stress is created. The in-plane stress decreases over time as the pneumatic pressure acting on the O-ring leads to O-ring sliding. O-ring sliding reduces the net force acting on the O-ring by creating a restoring force via deformation. Eventually the in-plane stress stabilizes as a force balance on the O-ring is reached. The net result is that in addition to the desired compressive normal stress component, there are also remnant tensile in-plane stresses present at steady state due to the pneumatic pressure change. For the same reason, a compressive in-plane stress arises when pressure is released from the cavity, since the unbalanced O-ring restoring forces cause the O-ring to slide back towards its original position. Since d_{31} and d_{33} have opposite signs for PZT, the piezoelectric charge induced by the normal stress component and the in-plane stress components add to each other. With the decrease in the in-plane stress over time, the total amount of induced charge also decreases. Finally at steady state, both stresses are constant and the signal no longer changes with time.

Experimental results demonstrated that the in-plane stress induced by the friction between the O-ring and the sample surfaces were responsible for the observed charge response in the pneumatic pressure rig. Figure 4.3 shows the induced charge signal measured on releasing the pressurized gas as a function of the stabilization time at high pressure. When the gas was released right after being introduced, no peak appeared so that Q_1 was equal to Q_2 (Q_1 and Q_2 have been defined in Figure 4.2c). This can be

explained as follows: since there was no deformation in the O-ring because no time was allowed for the O-ring to slide, there was no restoration force produced in this case. Upon releasing the gas, the in-plane stress changed from tensile to zero, producing charge with the same polarity as that due to the change of the normal stress. Since the O-ring was already in its equilibrium position, there was no change of the stress with time. Therefore the gradual decrease of the charge signal was eliminated in this case. If the gas was released after a sufficient-long stabilization time, a gradual decrease of the signal was observed. This was because the O-ring was deformed to balance the force induced by the gas and it gradually returned to its original position after releasing the gas.

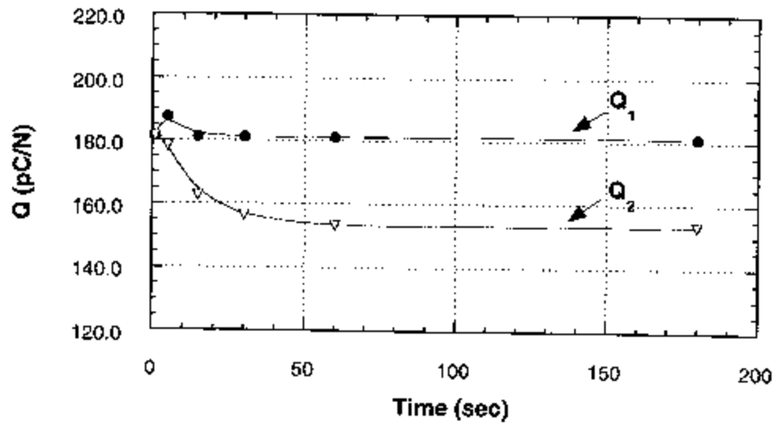

Figure 4.3 Charge measured on releasing pressure after applying pressure for different period of time. Q_1 and Q_2 are as defined in Figure 4.2c.

To verify that there were in-plane stresses induced by friction between the O-rings and the sample surfaces during the pressure changes in the cavities, the in-plane strain of a test specimen mounted on the pneumatic pressure rig was measured using strain gauges. Figure 4.4 shows the measured in-plane strain as a function of time during introduction or release of pressure. The in-plane strain followed a similar profile as the induced charge as a function of time. It peaks right after a pressure change, followed by a gradual decrease to a lower value. The in-plane strain was tensile when the cavities were pressurized and compressive after releasing the pressure. There was a remnant in-plane strain remaining at equilibrium, but it was much smaller than the peak value. These results agree very well with the above stress analysis, indicating further that there were friction-induced in-plane stresses imposed on the specimens which decreased with time due to O-ring sliding.

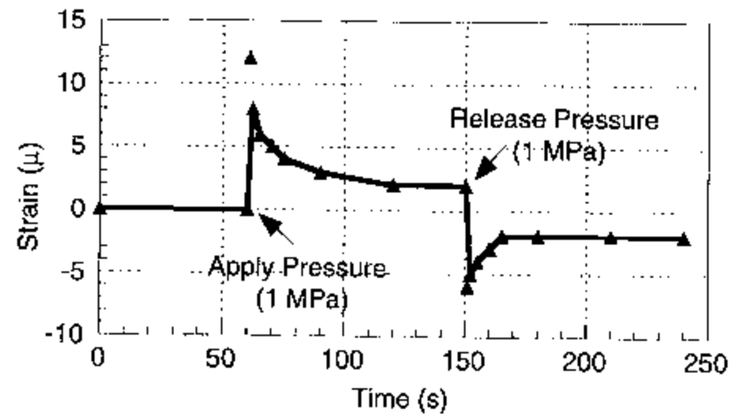

Figure 4.4 **In-plane strain as a function of time during pressure changes in the pneumatic pressure rig.**

4.4 Remnant In-Plane Stress Analysis

As the induced charge in response to a pressure change finally stabilized, the in-plane stress in the tested specimen was reduced to minimum because a majority of the friction had been released through O-ring deformation or recovery. The remnant in-plane stress level at stabilization was evaluated using a bulk PZT ceramic sample. The d_{33} coefficient of this sample was measured using both the Berlincourt method and double beam interferometry. Piezoelectric d_{33} measurements were made at several spots within the top electrode for both techniques and the average of the measured d_{33} values was used for the evaluation of remnant in-plane stress. The average d_{33} value given by the Berlincourt meter and the laser interferometry were 305 pC/N and 302 pm/V respectively, which experimentally confirmed that the piezoelectric coefficients from the direct piezoelectric effect and the converse piezoelectric effect were numerically equal to each other. The PZT bulk ceramic sample was then put into the pneumatic pressure rig and the pressure-induced charge at stabilization was measured. By comparing the total measured pressure-induced charge with the charge associated with the normal stress component, the charge produced by the remnant in-plane stress can be estimated. This charge is directly proportional to the remnant in-plane stress. Therefore the in-plane stress can be investigated through evaluating the charge which is associated with it. The charge associated with the normal stress component can be calculated using the known d_{33} value and the applied normal stress (which is equal to the change of the pressure in the cavities).

The remnant in-plane stress analysis showed that the total measured charge at stabilization was always larger than the calculated normal stress-induced charge, indicating that an appreciable amount of remnant in-plane stress was present even at the final stage. The remnant in-plane stress was found to be affected by the experimental conditions which influenced the friction between the O-rings and the sample surfaces. Typically, about 3-10% of the total induced charge at stabilization originated from the remnant in-plane stress.

Methods which can reduce the in-plane stress of the tested samples were investigated in an attempt to optimize the design and the operation of the pressure rig so that less error would be introduced in the calculated d_{33}. Since friction is the major concern in this application, the following factors were considered in the design of the pneumatic pressure rig: the O-ring groove dimensions, the O-ring cross section, and the compression of the O-rings.

In principle, the frictional force is given by $F = \mu N$, where μ is the friction coefficient between the two contacting surfaces and N is the force parallel to the surface. Therefore, friction is governed by the factors which affect either of these two parameters. Table 4.1 lists the friction factors in an O-ring seal. It should be noted that this is a general guideline and there are often anomalies and difficulties in the prediction of friction.

All of the relevant factors on friction were considered in this study. It was found that there were several factors which controlled the friction in our pneumatic pressure rig. Of them, the concentricity of the O-ring grooves and their dimensions are of the most importance. Misalignment of the O-ring grooves in the two aluminum parts could result

in substrate bending and must be avoided. The width of the O-ring groove should be adequately larger than the width of the O-ring cross-section to allow the O-ring to slide so that the friction can be released through O-ring deformation. However, excessive width of the O-ring groove should be avoided since the O-rings may be misaligned during sliding. The O-ring grooves can be a little bit deeper than that of the standard hydraulic reciprocating design since lower squeeze designs are permissible in low pressure pneumatic applications for friction reduction [109]. Since the temperature range is very small and a little leakage is not critical in this application, a float seal in which the depth of the O-ring groove is larger than the width of the O-ring cross-section is allowed. This design was expected to further reduce the friction because there was no compression in the O-ring. However, experiments showed that this design introduced other charge in response to the pneumatic pressure and might cause more error in the determination of d_{33}, possibly due to the solid contact between the sample and the aluminum housing. The design which gave the least in-plane stress in this study is shown in Figure 4.5.

O-ring compression (i.e. the percentage reduction in dimension in the clamping direction) is another important factor which controls the friction. Figure 4.6 shows how the measured pressure-induced charge was affected by O-ring compression. The results indicated that the remnant in-plane stress dropped with decreasing O-ring compression. This was due to a smaller strain when the O-ring was less clamped. Therefore very small O-ring compression was favorable in this application, as long as there is no clearance between the sample and the housing.

Table 4.1 **Friction factors in O-ring seals [109]. The last two factors listed are minor effects compared to the others.**

TO INCREASE FRICTION	FACTOR	TO DECREASE FRICTION
Increase →	Unit Load (squeeze) ←	Decrease
Increase RMS	Surface Finish (metal)	Decrease RMS
Increase	Durometer	Decrease
Decrease	Speed of Motion	Increase
Increase	Cross Section of O-Ring	Decrease
Increase	Pressure	Decrease
Omit	Lubrication	Use
Lower	Temperature	Increase
Decrease	Groove Width	Increase
Increase	Diameter of Bore or Rod	Decrease
Decrease	Surface Finish (O-Ring)	Increase
Stretch O-ring	Joule Effect*	Compress O-Ring
Lower Durometer of O-Ring	Coefficient of Friction†	Increase Durometer

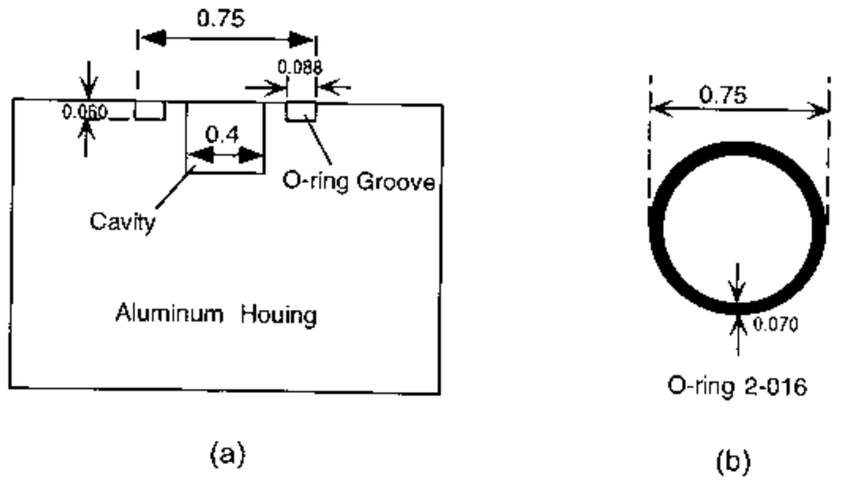

Figure 4.5 **The dimensions of: (a) the O-ring groove and (b) O-ring. Dimensions given in inches.**

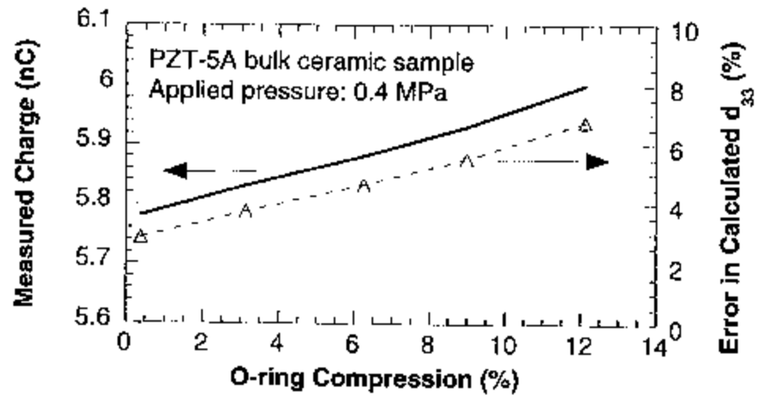

Figure 4.6 The effect of O-ring compression on the measured pressure-induced charge. O-ring compression was calculated as $(d_0 - d_c)/d_0$, where d_0 is its original diameter and d_c is the dimension in the clamped direction. The error in the calculated d_{33} was estimated by comparing the calculated d_{33} value with that measured by Berlincourt meter.

Since rubber has an inherently high friction coefficient with almost all metallic and non-metallic surfaces, adequate lubrication is very important, especially for pneumatic seal applications. It was found that the friction was greatly reduced by the application of lubricant, and reliable measurements were obtained only when the sample was properly lubricated. Since the surface of the PZT films were very smooth, the lubricant must be able to form a strong layer over the film surface which cannot be wiped away by the O-rings. The best result was obtained when Parker O-lube was used, since it clings tenaciously to the rubber or sample surfaces. Friction was also reduced by polishing the back of the substrates using 1μm alumina powder. The smoother the

surface, the smaller the remnant in-plane stress. Smaller remnant in-plane stresses were also obtained when an O-ring with a smaller cross-sectional area was used, since this reduced the pneumatic force acting on it. It was also found that friction was smaller when harder O-rings were used, probably due to the smaller friction coefficient.

Under the best experimental conditions used to reduce the in-plane stress component, the total measured pressure-induced charge exceeded the calculated normal stress induced charge by about 3-4%. This suggests that a d_{33} coefficient calculated using the total measured charge after equilibrium would have an error of less than 5%. However, this optimized condition was not always readily achievable. As a result, there was a relatively large scatter in the d_{33} value derived from this charge, and sometimes errors as large as 10-15% were observed.

4.5 Self-Compensation of the Remnant In-Plane Stress

To further improve the accuracy and more importantly, the reliability of the pneumatic pressure charge technique for d_{33} measurement, the charge resulting from the in-plane stress must be eliminated from the measured charge. To achieve that, a measurement procedure named remnant in-plane stress self-compensation (RIPSSC) method was developed. In this method, the charge contribution from the in-plane stress could be totally eliminated by manipulating the remnant in-plane stress levels. Figure 4.7 shows schematically how this method works.

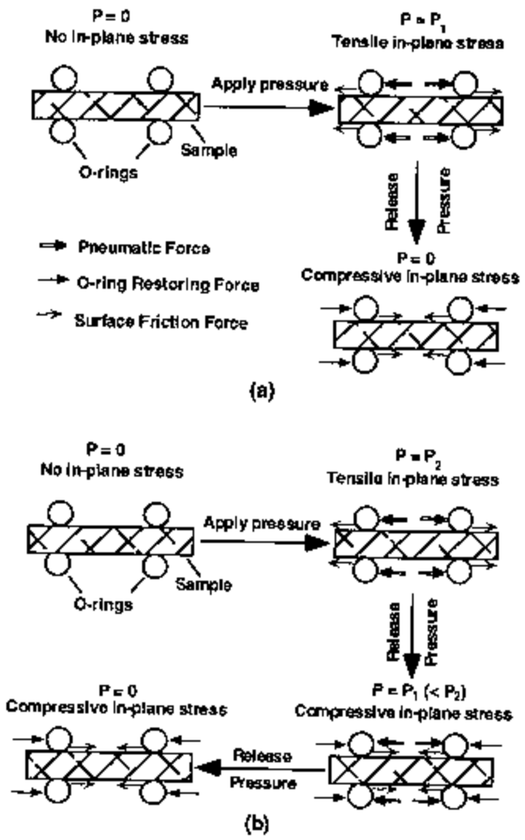

Figure 4.7 **Remnant in-plane stress produced by pneumatic pressure during:**

(a) procedure in which pressure was switched between 0 and P_1

(b) procedure with a remnant in-plane stress self-compensation mechanism

The charge induced by a pressure change is determined by the difference between the initial and final stress states. Therefore, it is the change in the remnant in-plane stress between the two states which governs the accuracy of the d_{33} measurement. In the

previous section, where the induced charge was measured during switching the pressure between P = 0 and P = P_1 (Fig 4.7a), the remnant in-plane stress at the two steady states were of opposite sign. Therefore a difference in in-plane stress between the two final states is unavoidable and is fundamentally responsible for the inflated d_{33} values. The idea of the RIPSSC method is to tailor the remnant in-plane stresses so that they are of the same sign and magnitude in the two steady states. When this condition is reached, there will be no change in in-plane stress between the two steady states. The induced charge is then only that due to the normal component of the stress. Thus accurate d_{33} values can be obtained. One way to reach this condition is to pre-load the cavities with a pressure P = P_2 which is higher than P_1 and then reduce the pressure to P = P_1 (Figure 4b). By doing so, a compressive remnant in-plane stress was imposed on the sample due to the O-ring recovery. After stabilization, the pressure is released again to P = 0 and the induced charge is measured between the steady states at P = P_1 and P = 0.

The remnant in-plane stress at P = P_1 as a function of the preloading level (P_2) was investigated in studying how to control the magnitude of the remnant in-plane stress. Fig 4.8 shows that the induced charge measured between P = P_1 and P = 0 decreased with an increase in the preloading pressure (i.e. as P_2 increased). The normal stress induced charge Q' (calculated using the d_{33} value obtained from the Berlincourt measurement) was equal to the total induced charge Q when the preloading pressure P_2 was about two times the value of P_1. This result suggests that the remnant in-plane stress can be controlled by adjusting the preloading pressure, and its magnitude is determined by the pressure change between the two steady states. This is reasonable since the friction is proportional to the pressure change. Thus, one might expect that the remnant in-plane

stress due to the friction would also be proportional to the change of pressure. Therefore, at $P_2 = 2P_1$, induced charge associated with the in-plane stresses was totally eliminated, and accurate d_{33} value was obtained.

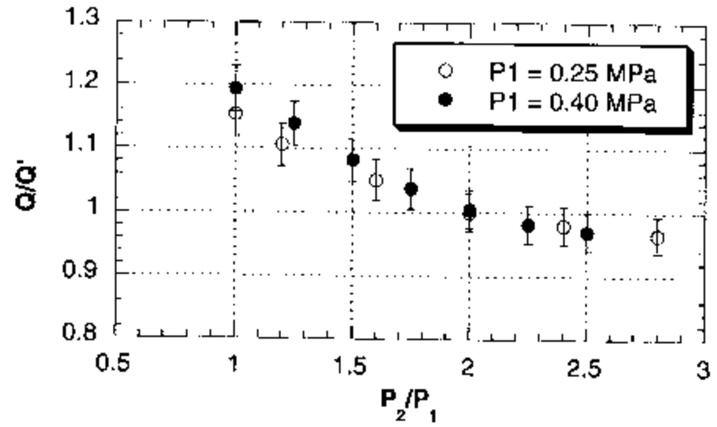

Figure 4.8 Influence of the pre-loading pressure P_2 on the measured charge for a pressure change from $P = P_1$ to $P = 0$. Q is the measured pressure-induced charge, and Q' is the charge due to the normal component of the stress evaluated using the d_{33} value measured by Berlincourt meter.

4.6 Calibration of the Pneumatic Pressure Charge Technique

The pneumatic pressure charge technique was calibrated using other established techniques. A PZT bulk ceramic sample was used for the calibration. As was expected, the measured induced charge was found to be proportional to the applied pressure using

the RIPSSC method (see Figure 4.9). The d_{33} coefficient for the bulk PZT ceramic sample derived from the slope of the curve was 304 pC/N, which was in very good agreement with the value obtained by both the Berlincourt method and interferometry, indicating that the influence of surface friction on the d_{33} measurement was eliminated by the RIPSSC method.

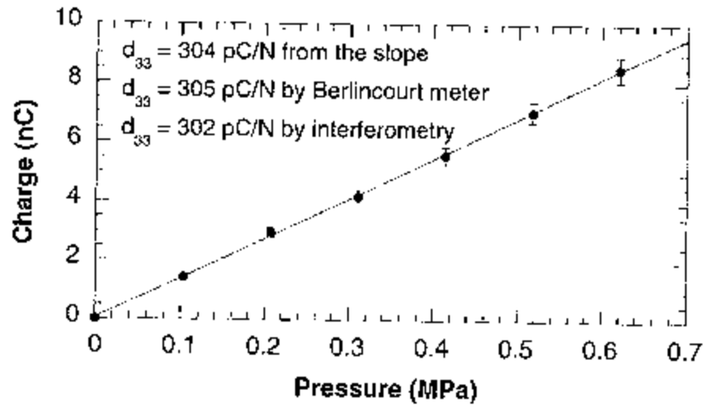

Figure 4.9 **Charge induced in a bulk PZT-5A ceramic specimen as a function of applied pressure. Measurements were made with the remnant in-plane stress self-compensation method. The applied normal stress is equal to the applied pressure.**

In addition to enhancing the measurement accuracy, the RIPSSC method also made the d_{33} measurement much less sensitive to variations in the remnant in-plane stress. Figure 4.10 shows the influence of the O-ring compression on the d_{33}

measurement with and without remnant in-plane stress self compensation. In this experiment, very large compressions (which were not used in actual d_{33} measurements) were intentionally applied to the O-rings to magnify the effect. As the O-ring compression increased, friction increased and so did the remnant in-plane stress, as indicated by a considerable increase (15%) in the calculated d_{33} value when the RIPSSC method was not employed. On the other hand, there was only a 2% variation in the measured d_{33} value from zero compression up to 17% compression when the RIPSSC method was used. Practically, this is very important in the routine application of the technique, making the measurements much more consistent and the measurement procedure much more convenient.

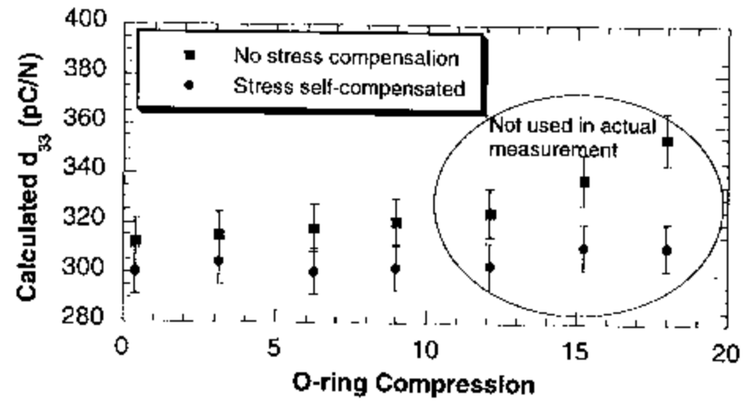

Figure 4.10 Influence of O-ring compression on the measured d_{33} coefficient of bulk PZT-5A. The effectiveness of stress compensation is clear.

4.7 Summary

1). A direct piezoelectric d_{33} measurement method which uses pneumatic pressure for the stress application was proposed. A pneumatic pressure rig was designed to enable measurement of bulk and thin film piezoelectric specimen.

2). In addition to the intended normal stress, in-plane stress was also generated by the pneumatic pressure due to the friction between the sample and O-ring. The majority of the in-plane stress, however, was released through O-ring sliding and recovery.

3). The change in remnant in-plane stress also produced charge through the transverse piezoelectric effect and this charge contributed 3-10% of the total measured charge.

4). The remnant in-plane stress was affected by a number of factors. Among them, the dimensions of the O-ring groove and the O-ring, the O-ring compression, lubrication, and surface finish are most important. By optimizing the design and operation of the pressure rig, charge associated with the surface friction could be reduced to less than 5% of the total charge.

5). The charge associated with the in-plane stress was eliminated using the RIPSSC method and an accurate d_{33} value could be obtained even if there was an appreciable amount of friction present.

6). The pneumatic pressure charge technique was calibrated using a bulk PZT sample. Excellent agreement among this technique, the Berlincourt method and double beam interferometry was obtained.

Chapter 5. The Piezoelectric Characteristics of Sol-Gel Derived PZT Films on Platinum-coated Silicon Substrates

In this chapter, the effective longitudinal piezoelectric coefficient (d_{33}) of sol-gel derived PZT films with compositions near the MPB were measured using the pneumatic pressure charge technique (described in chapter 4) and the double beam laser interferometer. The effects of the poling field, the film thickness, and the composition and preferred orientation of the films on the effective d_{33} of PZT films were investigated. A small difference between the effective d_{33} values measured using direct and converse methods was noticed and attributed to the different mechanical boundary conditions of the PZT films for the two measurements. The effect of substrate clamping on the effective d_{33} of PZT films was discussed.

5.1 Structural Analysis

The PZT films studied in this chapter were all prepared using 2-methoxyethanol solutions and rapid thermal annealing processes. Three different compositions near the MPB which had Zr/Ti ratios of 56/44, 52/48, and 48/52 respectively were chosen for this investigation. The films had thickness ranging from 0.2 μm to 3.4 μm.

Before RTA annealing, the pyrolyzed films were amorphous, showing only the substrate peaks in X-ray diffraction patterns. After annealing at 700°C, XRD showed that the films were crystallized into the perovskite phase with strong preferred orientation. No pyrochlore phase was detected. Depending on the texture of the Pt bottom electrode of the substrates used, the films were either <111> or <100> oriented (indices given for pseudocubic cell). Films deposited on substrates with <111> oriented Pt bottom electrodes were highly <111> oriented. On the other hand, films deposited on substrates with <100> oriented Pt bottom electrodes had strong <100> preferred orientation. Figure 5.1 shows the typical XRD patterns of both <111> and <100> oriented films. In either case, the relative intensities* of the preferred orientations (<111> or <100>) were greater than 90%. In the film thickness range studied, the relative intensities of the preferred orientations didn't change with film thickness for either <111> or <100> oriented PZT films [110].

The surface and cross-sectional microstructures of the PZT films were observed using field-emission SEM and TEM. The SEM surface morphology of as deposited films revealed a very fine structure at the top surface which showed features as small as 10-20 nm (Figure 5.2a). Through chemically etching the film surface using a very dilute solution of HF in 10% HCl for 5 to 10 seconds, the thin top layer was removed and microstructures with average grain sizes around 50-100 nm were observed (Figure 5.2b). This indicated that the average grain size of PZT films was about 50 nm to100 nm, and there was a very thin surface layer which was either amorphous or pyrochlore. Figure

* The relative intensity used in this work was defined as:
$(I/I^*)/[(I/I^*)_{111} + (I/I^*)_{110} + (I/I^*)_{100}]$
where I and I* are the integrated intensities of the peaks of XRD patterns of PZT films and powders.

5.2c is the plane view of a 0.7 μm <111> oriented PZT film which showed grain sizes ranging from 50 nm to 100 nm [100]. The cross-sectional TEM image of the films revealed a textured structure and a similar average grain size in the direction parallel to the film surface (Figure 5.2d). Electron diffraction patterns indicated that the <111> oriented texture was very strong near the bottom of the film and weak near the top of the film, which suggested that the nucleation of the perovskite phase during crystallization was strongly influenced by the Pt bottom electrode [99]. These results were consistent with the XRD pattern and the SEM surface morphology which also showed strong preferred orientation controlled by the orientation of the bottom electrode and small grain size in these films.

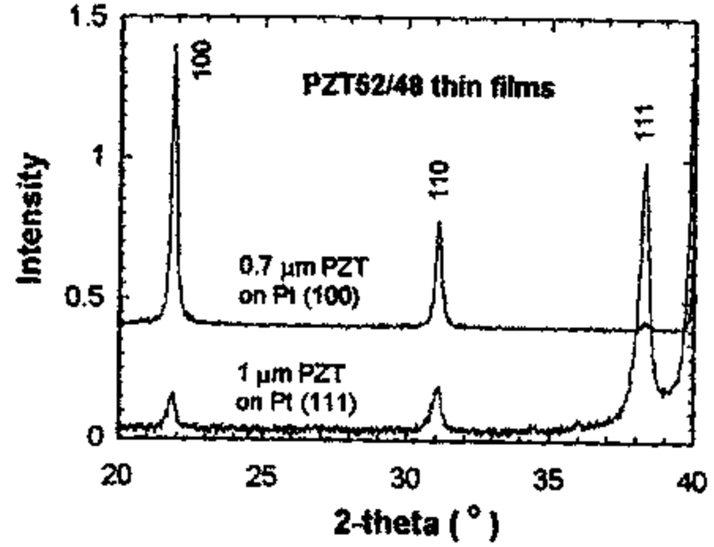

Figure 5.1 XRD patterns of PZT 52/48 films prepared using 2-methoxyethanol solution and RTA process on Si substrate with either <111> or <100> oriented Pt bottom electrodes.

From the SEM study, it was found that there was little change in the grain size of these PZT films with a change in the film thickness or composition. The grain size of <100> oriented films was slightly larger than that of <111> oriented films (about 100 nm to 200 nm), due to a larger grain size of <100> oriented Pt bottom electrodes.

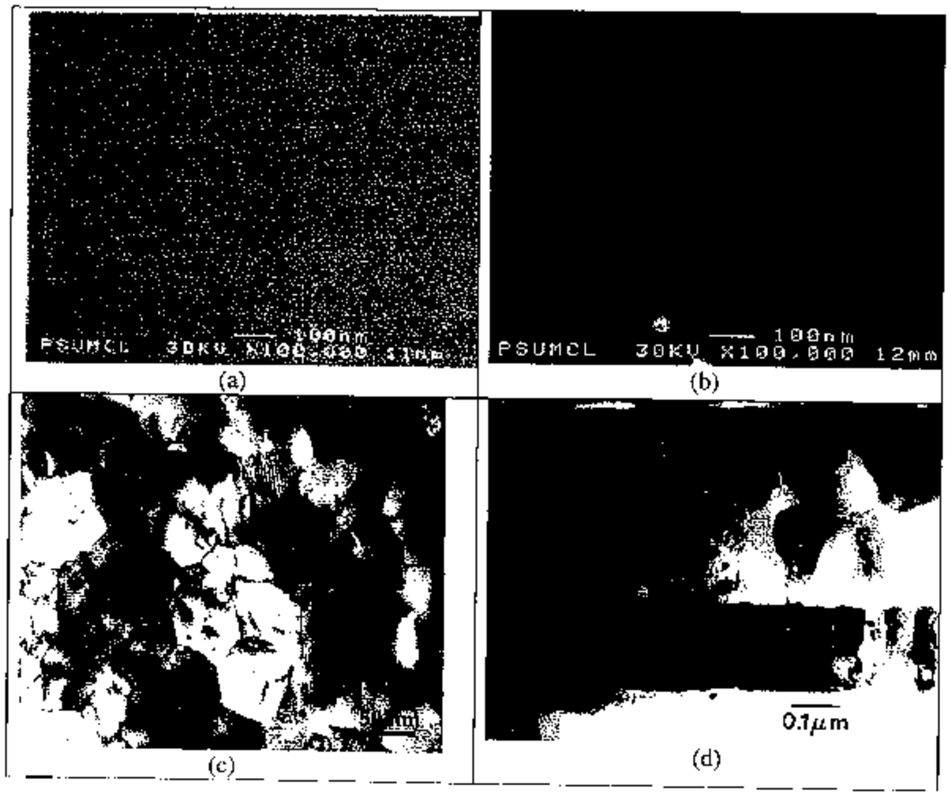

Figure 5.2 **Microstructure of <111> oriented 52/48 PZT film: (a) SEM surface morphology of as-deposited film (b) SEM surface morphology after chemical etching (c) TEM plan view image (Courtesy of Z. Xie et al.). (d) TEM cross-sectional image (Courtesy of S. C. Cheng).**

5.2 Dielectric and Ferroelectric Characterization

As described in chapter 2, the dielectric, ferroelectric, and piezoelectric properties of ferroelectric materials are interrelated. The intrinsic contribution to the longitudinal piezoelectric coefficient d_{33} is a function of both the intrinsic dielectric constant ε_3 and the spontaneous polarization P_s (Equation 2.10). The extrinsic contribution to the longitudinal piezoelectric coefficient d_{33} is mainly controlled by non-180° domain wall motion. This is also an important factor governing the extrinsic dielectric properties and the high field switching properties of ferroelectric materials. For a better understanding of the longitudinal piezoelectric behaviors of the PZT films, these properties must be also considered. Therefore, low and high field dielectric and ferroelectric characteristics of these films were investigated.

The weak field dielectric properties of the PZT films were investigated at 1 kHz under an ac field of 0.5 kV/cm. Figure 5.3 gives the thickness dependence of the dielectric constant for both <111> and <100> oriented PZT 52/48 films. The results showed that with an increase of film thickness, the dielectric constant of both <100> and <111> oriented films increased. For films with the same thickness, <100> oriented films had larger dielectric constants than <111> oriented films. In all the films, the dielectric loss was no larger than 5% and decreased from 5% to 2% as the film thickness increased from 0.25 μm to 3.4 μm.

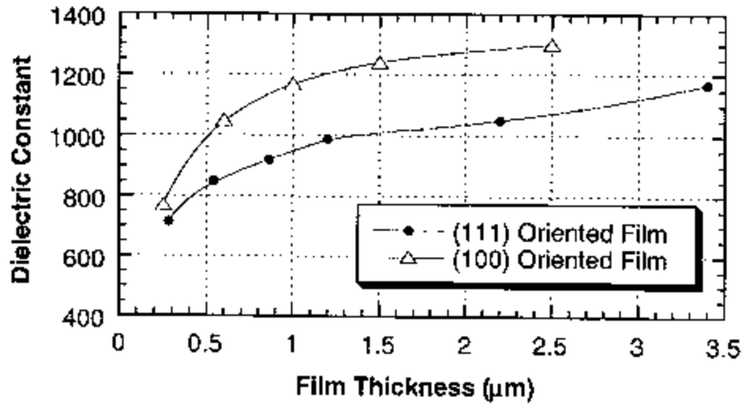

Figure 5.3 **Thickness dependence of the dielectric constant for <111> and <100> oriented PZT 52/48 films (pseudocubic indices).**

The increase of the dielectric constant with film thickness was believed to be due mainly to the increased extrinsic contribution to the dielectric response as film thickness increased (which will be discussed in Chapter 6). At small thicknesses, the thin second-phase layer at the top surface of the film was found to become important in reducing the dielectric constant. The reason for the decrease of the dielectric loss with increasing film thickness at room temperature is still not clear. Low temperature measurements (given in Chapter 6) showed that the dielectric loss at 4K was much lower than room temperature and it converged to about 0.6% for all the films. This result indicated that most of the loss at room temperature was from extrinsic or transport sources. Kim suggested that in fine grained undoped PZT ceramics, the dominant loss mechanism was due to the space charge accumulated at the grain boundary [7]. The same mechanism may also account for

the loss in PZT films. However, it was also found that the interface between the PZT and electrode played a very important role in dielectric loss. For films which had top Pt electrodes, the dielectric loss was about 50% lower after 6 months aging than the dielectric loss measured right after the top electrode was deposited. But if new top electrodes were deposited on these aged PZT films, the dielectric loss was almost the same as that in newly prepared films with fresh top electrodes.

The high field P-E hysteresis loop measurements showed that the remanent polarization (P_r) of both <111> and <100> oriented 52/48 films increased with film thickness (Figure 5.4). The coercive field was found to decrease as the film thickness increased. For films with the same thickness, <100> oriented films had smaller P_r and larger E_c than <111> oriented films.

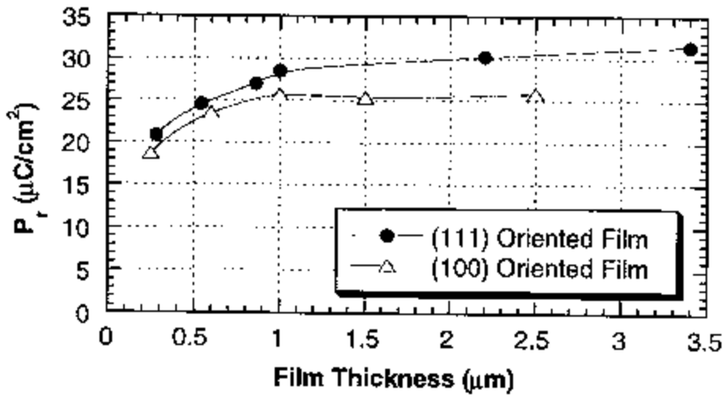

Figure 5.4 **Thickness dependence of the remanent polarization for <111> and <100> oriented PZT 52/48 films. The maximum electric field was 500 kV/cm.**

Compared to undoped bulk PZT ceramics, the hysteresis loops of PZT films were tilted, resulting in a larger difference between P_r and P_s. The maximum electric field required to saturate the polarization and E_c were much larger that those in bulk ceramics. In addition, P_r and P_s were smaller than those in bulk PZT ceramics. We believe the main reason for these behaviors is the small grain size and high defect density in PZT films. Kim has shown that in fine grain PZT ceramics (grain size < 1 μm) there was a sharp decrease of P_r and an increase in E_c with decreasing grain size [7]. In PZT films, it is likely that domain reversal through the applied electric field is much more difficult than in large grained ceramics due to the impediment offered to domain wall mobility by grain boundaries, pinning centers, incompatibility between domain structures in adjacent grains, and the reduced number of twinned domains. Therefore the switchable polarization is smaller and the electric field required to reverse the polarization is larger in these films. The large difference between P_r and P_s is the result of a significant amount of free domain reversal after the removal of the electric field. This could be due to domain walls having lower free energies at their original positions since they are stabilized by pinning centers such as space charges or point defects there. As suggested by the decrease of the dielectric constant with the decrease of the film thickness, the domain wall clamping may become stronger as films become thinner (possibly due to the stronger substrate effect). Therefore domain reversal also becomes more difficult, resulting in smaller P_r and larger E_c as film becomes thinner. In addition, the second-phase surface layer and the interfacial layer may also play roles in reducing P_r and increasing E_c in thin films.

The dielectric constant of the PZT 52/48 films was measured as a function of temperature from 25°C to 450°C. Figure 5.5 gives the temperature dependence of the dielectric constant for several films with different film thickness and orientation. As was expected, all the films showed a dielectric anomaly due to the ferroelectric-paraelectric phase transition. The temperatures where the dielectric constant reached the maximum (T_m) were all around 390°C for these films. This temperature is almost the same as the Curie temperature of the undoped PZT 52/48 bulk ceramics (386°C). However, the dielectric constant peak at T_m was much lower in these films than bulk PZT ceramics. The dielectric peaks were also very broad compared to the peak in bulk PZT ceramics. With an increase in film thickness, a modest increase in the maximum dielectric constant at T_m was observed. However, the film thickness seemed have no effect on T_m. In addition, the temperature dependence of the dielectric properties was found to be very similar for <100> oriented films and <111> oriented films.

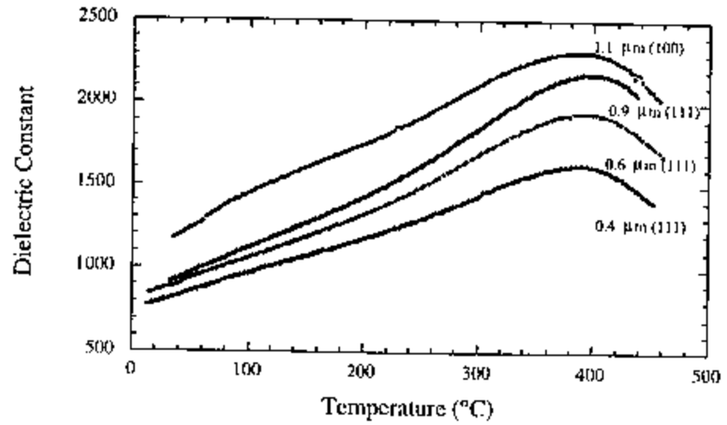

Figure 5.5 **Temperature dependence of the dielectric constant of PZT 52/48 films.**

In thin film ferroelectrics, there are two major factors which have been known to cause a shift in the Curie temperature. The first one is the space charge effect. In bulk PZT ceramics, it was found that space charge could result in a strong internal field which both favored the ferroelectric state and impeded domain wall motion, thus leading to an increase in the Curie temperature and a decrease in the dielectric constant [7, 77, 80]. This effect was also observed in PZT films. Due to the high volatility of PbO at the annealing temperature, Pb or O site vacancies may result in space charge in PZT films and lead to an increase in Curie temperature. However, by adding excess Pb to the sol-gel solution or by using an additional PbO top layer to compensate for the loss of PbO during annealing, the space charge effect on the Curie temperature in PZT films can be eliminated. Figure 5.6 shows how excess Pb in the sol-gel solution reduces T_m and enhances the dielectric constant of PZT thin films. The space charge effect was also manifested by the premature fatigue of the Pb-deficient PZT films. Figure 5.7 shows how the remanent polarization of a Pb-deficient PZT films decreases with the number of sequential measurements performed. The space charge in the film was rearranged by the high electric field applied during the P-E hysteresis measurement and therefore pinned the domain walls. By heating the film to a temperature higher than 300°C, the remanent polarization of the fatigued film was found to return to its original value (since the space charge trapped at domain walls and the alignment of the defect dipoles were disrupted). If the PbO loss during annealing was compensated by adding sufficient excess Pb in the solution (12%), then the premature fatigue was greatly reduced.

Another factor which can cause a change in the Curie temperature of ferroelectric films is a residual biaxial stress. There are large tensile biaxial stresses (around 100MPa)

in sol-gel derived PZT films deposited on Pt-coated Si wafers due to the thermal expansion coefficient mismatch between the film and the substrate [111]. Thermodynamic theory predicts that tensile biaxial stresses can lead to a decrease in the Curie temperature for those domains which have the polar axis perpendicular to the stress plane, and an increase in the Curie temperature for those whose polar axis is parallel to the stress plane [112]. The effect of biaxial stress on T_c has been observed experimentally in predominantly c-domain epitaxial PZT films grown on MgO substrates, in which the Curie temperature shifted up more than 50°C due to the compressive biaxial stress. Tuttle et al. have showed that if there are tensile biaxial stresses acting on PZT films at the Curie temperature, the films tend to develop into predominantly *a*-domain films to reduce the elastic energy [83].

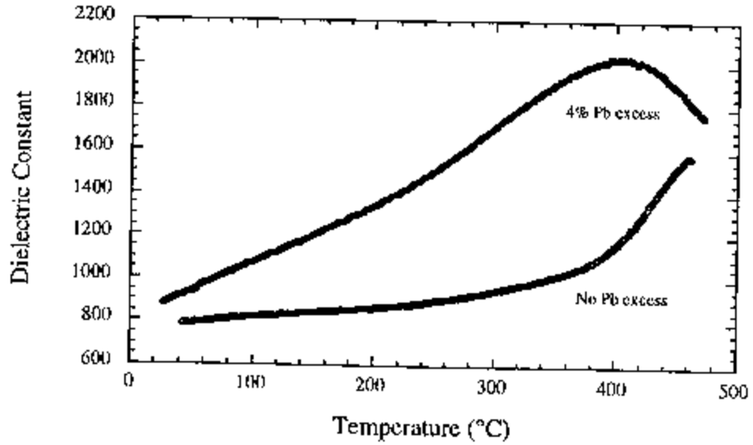

Figure 5.6 **The effect of excess Pb in solution on the Curie temperature of 52/48 PZT films.**

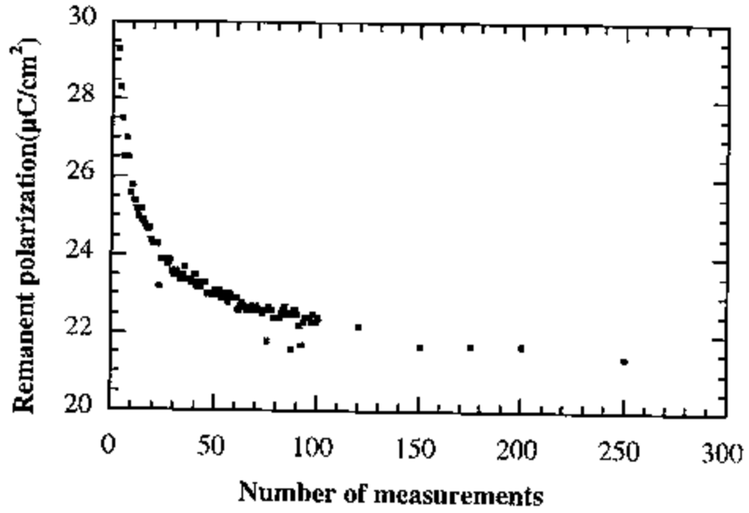

Figure 5.7 **The remanent polarization of a lead-deficient PZT 52/48 thin film as a function of the number of sequential measurements performed.**

Little shift in the Curie temperature was seen for the sol-gel PZT films in these studies, although all the films had tensile biaxial stresses acting on them [14]. This result suggested that there may be both *a*-domains and *c*-domains in our PZT films (although theoretically *a*-domains are easier to form), otherwise the Curie temperature would have shifted to higher temperatures due to the tensile biaxial stress. This was consistent with the fact that there were hysteresis loops and substantial remanent polarizations measured for all of the films. If the films were predominantly *a*-domain, the remanent polarization would be nominal given the fact that non-180° domain switching is negligible in these

films (as will be discussed in the next chapter). Since the tensile biaxial stress would cause an increase in the Curie temperature for *a*-domains and a decrease in the Curie temperature for *c*-domains, a split rather than a shift in the Curie temperature is expected in PZT films. However, each grain in the film may have a different amount of shift in the Curie temperature. This is because the crystallographic orientation of the grains is slightly different from one to another since it is distributed around the preferred orientation of the film. Therefore a diffused Curie temperature is expected in PZT films due to the different stress applied to different grains. In addition, variations in the local stress may also result in different shifts in the Curie temperature. The resulting diffuse phase transition temperature may be partially responsible for the depressed dielectric anomaly in polycrystalline ferroelectric films. It has been proposed that substrate clamping due to the tensile strain might also be responsible for the suppression of the dielectric constant of ferroelectric films near the transition temperature [113]. In addition, the existence of the secondary phase at the top surface or an interface between the PZT and one of the electrodes can act as a Curie point depressor, which will lead to a reduced and broadened peak of the dielectric constant. The temperature dependence of the dielectric constant of these layers is much smaller than that of PZT so that it reduces the measured dielectric constant of the film much more at the Curie temperature and apparently broadens the peak.

The difference in the dielectric constant and P_r between <111> oriented films and <100> oriented films suggests that the volume fraction of *a*-domains may be slightly larger in the <100> oriented films. Since the intrinsic ε_a is larger than ε_c, a larger volume fraction of *a*-domains can result in a larger dielectric constant. The same reason may also

account for the smaller P_r in <100> oriented films than in <111> oriented films. Since non-180° domain switching cannot be achieved during the P-E hysteresis measurements in these films, domains with their polar axes parallel to the film plane do not contribute to the switchable polarization during the hysteresis loop measurements. Therefore, the closer the polar axes of the domains are to the film plane, the smaller the switchable polarization, and the smaller the remanent polarization.

5.3 The Longitudinal Piezoelectric Properties

Due to the constraint of the substrate, the piezoelectric response of a thin film specimen to both electric fields and mechanical stresses is strongly dependent on the mechanical boundary conditions. In general, the ratio between the induced-charge and the applied stress in a direct piezoelectric measurement or the ratio between the induced strain and the applied field in a converse piezoelectric measurement does not represent the piezoelectric coefficients of the thin film itself (which should be measured under unclamped conditions by definition). Thus, the piezoelectric coefficient reported for a thin film is generally the effective coefficient under the particular boundary conditions for that measurement only.

The effective d_{33} of sol-gel derived PZT films was measured using the pneumatic pressure charge technique. The charge response of the films was very similar to that observed in bulk samples (Figure 5.8). This indicated that the state of stress applied to the thin films was similar to that of the bulk sample, i. e., a small remnant in-plane stress due

to friction was induced in addition to the designed normal stress. Therefore, the charge induced by the remnant in-plane stress must be eliminated in order to obtain accurate effective d_{33} for PZT thin films. PZT films with different thickness, orientation and composition were measured using this technique and the measured effective d_{33} was compared with the effective d_{33} measured using the double-beam interferometer.

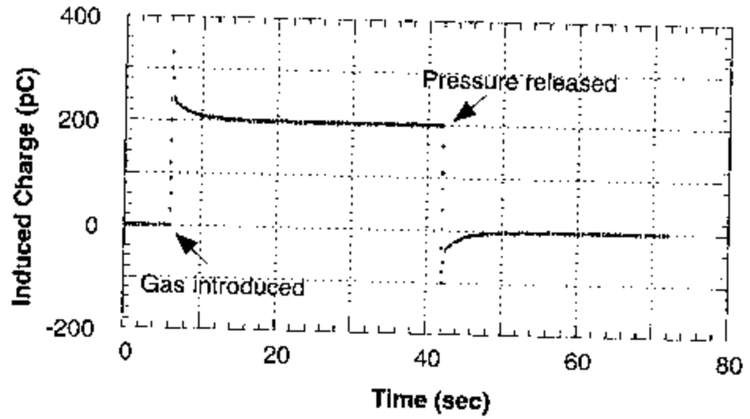

Figure 5.8 **Charge response of PZT films to the applied pressure measured by the pneumatic pressure charge technique.**

Using the RIPSSC procedure (which was described in Chapter 4), the charge induced by the normal stress was measured and used along with the applied pressure to calculate the effective d_{33} using Equation 3.1. For all the PZT films measured, a linear relationship was found between the applied pressure and the induced charge. Figure 5.9 shows the induced charge as a function of the pressure change for a 1μm PZT film poled

at 150 kV/cm for 1 min. From the slope of the line, the effective d_{33} value of the thin film was calculated to be 88 pC/N. Again it is evident that a 7% error in the effective d_{33} could be introduced if the RIPSSC method was not used to compensate for the in-plane stress.

Since double beam interferometry is currently the most widely accepted technique for thin film d_{33} measurement and most of the d_{33} values reported in the literature were obtained using that method, a direct comparison between the d_{33} value from our method and interferometry is necessary. The same electrode used for the data in Fig. 5.9 was also used to measure the effective d_{33} using double beam interferometry. A linear increase in the induced strain was observed with increasing electric filed and an effective d_{33} of 84 pC/N was obtained from this technique. The two measurement techniques gave very close d_{33} values, further confirming the validity of the charge measurement technique.

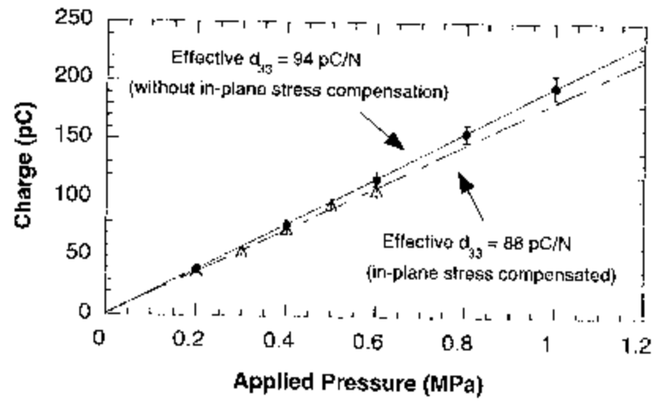

Figure 5.9 **Induced charge as a function of pressure change for a 1μm PZT film poled at 150 kV/cm for 1 min. The applied normal stress is equal to the applied pressure.**

For bulk PZT ceramic samples, the d_{33} coefficients measured by double-beam interferometry and the pneumatic pressure charge technique were found to be numerically equal to each other. However, it was noticed that for PZT films, the effective d_{33} measured by the pneumatic pressure charge technique was always slightly larger than that measured by the double-beam interferometry, even though the in-plane stress was compensated using the RIPSSC procedure. It is our belief that the small difference in the d_{33} value obtained from the two techniques was due to the different boundary conditions under which the two measurements were made. As was mentioned before, thin film piezoelectric measurements yield an effective value of the piezoelectric coefficient due to the clamping effect of the substrate. The effective d_{33} value of a thin film on a substrate is related to the unclamped d_{33} value via the elastic and piezoelectric constants of the film and the substrate in a manner which depends on the boundary conditions. Since the boundary conditions for the direct piezoelectric measurement used in the pneumatic pressure charge technique and a converse piezoelectric measurement such as interferometry are quite different, different effective d_{33} values are expected even when the same film is measured by the two techniques. Lefki and Dormans analyzed the boundary conditions for these two situations and predicted that the effective value given by the direct piezoelectric effect should be larger than the effective value given by the converse piezoelectric effect [106]. Their theoretical analysis supports our experimental result, which we believe is the first direct experiment to show the influence of boundary conditions on the effective d_{33} of piezoelectric thin films.

To quantitatively evaluate the difference in the effective d_{33} measured by direct and converse methods, the model developed by Lefki and Dormans was adopted as a first

approximation. In this model, the in-plane strain of the film was taken to be zero (assuming the film was totally clamped in-plane by the substrate) for the converse piezoelectric measurement, and was equal to the in-plane strain of the substrate (assuming the substrate was free to expand and isotropic) for the direct piezoelectric measurement. The effective d_{33} for these two boundary conditions are governed by [106]:

$$d'_{33}\,(cp) = d_{33} - 2d_{31}s^{E}_{13}/(s^{E}_{11} + s^{E}_{12}) \tag{5.1}$$

$$d'_{33}\,(dp) = d_{33} - 2d_{31}(s^{E}_{13} + \nu/Y)/(s^{E}_{11} + s^{E}_{12}) \tag{5.2}$$

here d'_{33} (cp) and d'_{33} (dp) represent the effective d_{33} measured by the converse and direct piezoelectric effect respectively, s^{E}_{ij} and d_{ij} are the compliances and piezoelectric coefficients of the thin film, and Y and ν are Young's modulus and Poisson's ratio of the substrate.

Because of the lack of compliance data for PZT thin films in the literature, data for an undoped bulk PZT ceramic with the same Zr/Ti ratio was used as a rough approximation [26]. For the calculation, the Young's modulus and Poisson's ratio of the substrate were taken as the average of the values in the <100> direction and <110> direction, which are the maximum and minimum in-plane values for a <100> silicon wafer [114]. Table 5.1 summarizes the values used for this work. Substituting them into equations (5.1) and (5.2) yields:

$$d'_{33}(cp) = d_{33} + 1.19d_{31} \tag{5.3}$$

$$d'_{33}(dp) = d_{33} + 0.96d_{31} \tag{5.4}$$

Subtracting (5.3) from (5.4) yields:

$$d'_{33}(dp) - d'_{33}(cp) = -0.23d_{31} \tag{5.5}$$

Since the typical d_{31} value for these PZT films was around -40pC/N to -50 pC/N [14], the difference in effective d_{33} measured by direct piezoelectric effect and converse piezoelectric effect was estimated to be around 9-10 pC/N using equation (5.5).

Table 5.1 Elastic properties of PZT and silicon substrate [26, 114]

$S^E_{11(PZT)}$ (10^{-12} m^2/N)	$S^E_{12(PZT)}$ (10^{-12} m^2/N)	$S^E_{13(PZT)}$ (10^{-12} m^2/N)	$Y_{Si<100>}$ (GPa)	$Y_{Si<110>}$ (GPa)	Y_{ave} (GPa)	$\nu_{Si<100>}$	$\nu_{Si<110>}$	ν_{ave}
13.8	-4.07	-5.80	130	169.5	149.7	0.28	0.064	0.172

However, in real measurements, the boundary conditions deviate somewhat from the conditions used in the above model. Experimental results from single beam interferometry measurements indicate that the substrate is bent by the piezoelectric thin film during electrical excitation [10, 104], making the assumption that the in-plane strain was zero during the converse piezoelectric measurement invalid. In addition, during the

direct piezoelectric measurement the substrate was not free to expand parallel to the plane because the periphery of the substrate was not subjected to the pneumatic pressure. Therefore, the model represents two extremes for the boundary conditions and gives a maximum for the difference in effective d_{33}. The discrepancies between the measurements for the two techniques should and do fit between these bounds.

Kholkin et al. also used the above model to explain the difference between the d_{33} coefficients of bulk ceramic and thin film in PZT and Ca-modified lead titanate (PCT) [115]. The d_{33} coefficient was significantly smaller in PZT thin films than that in PZT ceramics with the same composition, while in PCT, thin films and bulk material gave similar d_{33} values. This was attributed by the authors to the effect of the boundary conditions on the d_{33} coefficient obtained in a converse piezoelectric measurement. For thin films, the effective d_{33} value is related to both the unclamped d_{33} and d_{31} of the piezoelectric material in a way similar to that described in Equations 5.1 and 5.2. However PCT is a very anisotropic material and its d_{33} coefficient is about 20 times larger than the d_{31} coefficient. Therefore the difference in the unclamped d_{33} and the effective d_{33} in PCT is negligible, while it is significant in PZT due to the larger d_{31}.

In piezoelectric films, since the film is rigidly attached to a substrate, any measurement of the d_{33} coefficient is performed under at least partially clamped mechanical boundary conditions unless the substrate is totally released before the measurement. The above experimental results and analysis indicate that the effective d_{33} is always smaller than the value measured under free mechanical boundary conditions. The difference between the effective d_{33} and the unclamped one is determined by the exact boundary conditions and the elastic properties of both the film and the substrate.

However, there are few elastic properties reported on PZT films in the literature. The elastic properties of films may be different from those of the bulk PZT ceramics due to the small grain size and textured structure of PZT films. Furthermore, it is difficult to model the exact mechanical boundary condition for these measurements. Therefore, an accurate and quantitative evaluation of the unclamped d_{33} from the effective d_{33} is not possible at this point. Nevertheless, it is evident that clamping by the substrate is one of the reasons which causes a small effective d_{33} in PZT films.

The effective d_{33} coefficient of all the PZT thin films measured before poling was in the range between 0 and 10 pC/N. This result indicated that there was little or no pre-existing alignment of the domains in the as-deposited films although all the films had strong preferred crystallographic orientation. The d_{33} increased with both poling time and poling field. Figure 5.10 shows the induced charge as a function of the poling field for a 1.3μm PZT film with <111> preferred orientation. The coercive field of this sample was about 42 kV/cm. As expected, a considerable increase in the induced charge was observed as the poling field approached the coercive field of the film. The induced charge started to saturate at a poling field of about three times the coercive field. Poling the film in the opposite direction led to a reversal in the sign of the induced charge, but the d_{33} value was almost the same for the two poling directions.

As the film thickness increased from 0.25 μm to 3.4 μm, the effective d_{33} of PZT films was found to increase (similar to observations on the dielectric constant and remanent polarization). Figure 5.11 is the thickness dependence of the effective d_{33} of <111> oriented PZT 52/48 films. All the films measured were poled at 150 kV/cm for ten min and the measurements were made after one-day's aging.

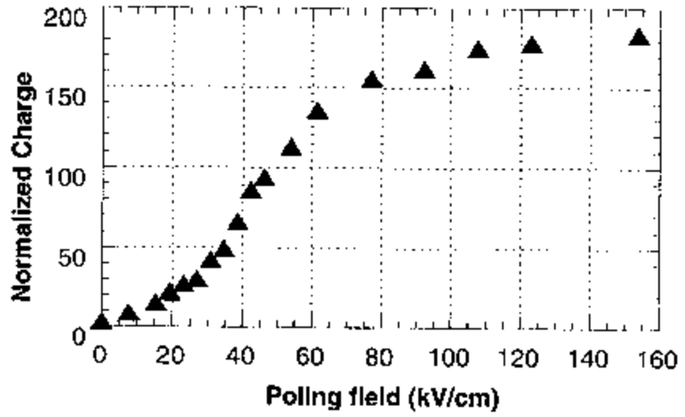

Figure 5.10 Induced charge as a function of the poling field of a 1.3 μm thick <111> oriented PZT 52/48 film. The coercive field of the film is 42 kV/cm.

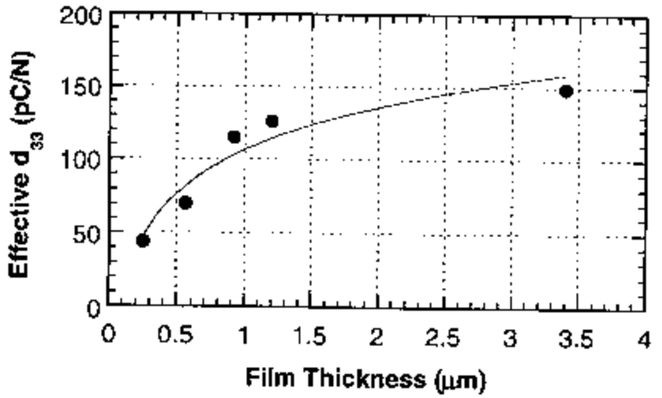

Figure 5.11 Effective d_{33} as a function of film thickness for 52/48 PZT films with <111> preferred orientation.

The piezoelectric coefficient d_{33} of ferroelectric materials is composed of both intrinsic and extrinsic contributions. The intrinsic part is from the contribution of the single domain properties and can be related to the spontaneous polarization and the dielectric constant of the single domain through the electrostrictive effect (see Section 2.7). For a multi-domain polycrystalline ferroelectric material, the intrinsic contribution to the piezoelectric coefficient d_{33} is the average of the intrinsic piezoelectric coefficient d_{33} of all the domains. In PZT films, the polarization vectors of the domains are clustered along several specific directions due to the strong preferred orientation of the grains. Domains whose polarization vectors are along directions close to the film plane contribute little to the intrinsic d_{33} of the films. The intrinsic d_{33} of the films arises mainly from the longitudinal piezoelectric response of domains with polarization vectors close to the normal of the film (i.e., c-domains). For both tetragonal and rhombohedral phases, the c-domain d_{33} is proportional to the spontaneous polarization and the intrinsic dielectric constants:

Tetragonal $$d_{33} = 2\,\varepsilon_0\eta_{33}Q_{11}P_3 \qquad (5.6)$$

Rhombohedral $$d_{33} = 2\,\varepsilon_0(\eta_{11}Q_{11} + 2\eta_{12}Q_{12})P_3 \qquad (5.7)$$

Since the intrinsic dielectric constants of PZT films are believed to be very similar for all the films (see Chapter 6), the average of the single domain d_{33} of these films is proportional to the intrinsic dielectric constant and the remanent polarization of the films. Therefore, with an increase in the film thickness, the intrinsic contribution to d_{33} in PZT

films increases due to the increase of the remanent polarization. This results in the effective d_{33} increasing with film thickness. As will be shown in the next chapter, the non-180° domain wall motion is strongly pinned in these films due to their small grain size and film thickness, thus the extrinsic contribution to d_{33} is limited in these PZT films.

The influence of the Zr/Ti ratio and preferred orientation on the piezoelectric properties of PZT films was also investigated. Table 5.2 lists the dielectric constant, P_r and d_{33} of PZT films with Zr/Ti ratios of 48/52, 52/48, and 56/44 for both <100> and <111> oriented films. All the films were 1 μm thick and poled at 150 kV/cm for 10 min at room temperature. The d_{33} was measured using the pneumatic pressure charge technique.

Table 5.2 Typical values for the dielectric constant, remanent polarization and d_{33} of 1 μm thick PZT films with different Zr/Ti ratios near the MPB

Orientation	<111>			<100>		
Composition	48/52	52/48	56/44	48/52	52/48	56/44
ε_3 (before poling)	950-1000	950-1000	950-1000	1030-1080	1150-1200	1000-1050
P_r ($\mu C/cm^2$)	23-26	27-30	20-23	21-24	24-27	17-20
d_{33} (pC/N)	100-105	110-120	80-85	90-95	95-105	75-80

In PZT ceramics, the room temperature dielectric constant and the piezoelectric coefficients are all found to reach their maximum at compositions near the MPB

composition (Zr/Ti ratio of 52/48). From the phenomenological theory, a peak in the dielectric constant occurs near the MPB composition (Zr/Ti 50/50) in single domain PZT due to the structural instability brought about by the coexistence of the tetragonal and rhombohedral phases [37]. Owing to the large dielectric constant at the MPB, the intrinsic piezoelectric coefficients also peak at the same composition [37]. In our PZT films, it was found that for the three compositions studied near the MPB, both the remanent polarization and the piezoelectric coefficient d_{33} had the largest values at a Zr/Ti ratio of 52/48, which is the closest composition to the MPB of bulk PZT. Chen et al. also observed the same behavior in conventional furnace annealed PZT films and concluded that the MPB of PZT films coincided with that of bulk PZT ceramics [98]. Since the spontaneous polarization of single domain PZT does not have a peak at the MPB composition, the peak of remanent polarization in PZT films is believed to be due to the high poling efficiency at the MPB. Because the two phases coexist at this boundary, an electric field induced phase transition may occur and thus increase the reversible polarization that can be achieved in these films. As was discussed for the thickness dependence of d_{33}, the enhancement in the effective d_{33} at the MPB may also be attributed to the enhanced remanent polarization at this composition. The dielectric constant also had its largest value at a Zr/Ti ratio of 52/48 for <100> oriented films, similar to the bulk PZT ceramics and conventional furnace annealed PZT films which also had strong <100> preferred orientation. However, for <111> oriented films, the difference in dielectric constant were small for the three compositions near the MPB. It was also noticed that the tetragonal 48/52 PZT film had a larger effective d_{33} than the

rhombohedral 56/44 PZT film, possibly due to the larger remanent polarization of the 48/52 PZT film.

A comparison between the properties of <111> and <100> oriented PZT films showed that all the <111> oriented PZT films had larger effective d_{33} than the <100> oriented films with the same composition. We believe that this is due to the larger intrinsic d_{33} in <111> oriented films since <111> oriented films had larger remanent polarizations than <100> oriented films. The extrinsic contribution to the piezoelectric properties played little role here because it was very limited in these films.

5.4 Summary

Sol-gel derived PZT films were deposited on Pt-coated silicon wafers using rapid thermal annealing. The films had either <111> or <100> preferred orientation depending on the orientation of the Pt bottom electrodes. All the films had very small grain size, about 50nm to 100 nm for <111> oriented films and 100 nm to 200 nm for <100> oriented films. When the film thickness increased from 0.25 μm to 3.4 μm, there was no change in the grain size and preferred orientation. Both the dielectric constant and the remanent polarization were found to increase with film thickness. The temperature dependence of the dielectric constant showed that there was no shift in the Curie temperature observed in these films, which suggested that both *a*-domains and *c*-domains were developed in the films. The broadened and reduced peak of the dielectric constant

formed at the Curie temperature could be the result of the diffuse Curie temperature, the tensile biaxial stress, and the surface/interfacial layers in these films.

The longitudinal piezoelectric measurements showed that the effective d_{33} from direct measurements was slightly larger than that from converse measurements. A consideration of the mechanical boundary conditions for these measurements indicated that the clamping effect of the substrate is the reason for this difference. Theoretical analysis showed that substrate clamping is an important cause of the small effective piezoelectric coefficients in PZT films. The as-deposited PZT films showed very weak piezoelectricity, indicating there is no pre-existing alignment of the domains. The effective d_{33} increased with both poling time and field and saturated as the poling field exceeded three times the coercive field. With an increase of film thickness, the effective d_{33} increased, primarily due to the increase of the remanent polarization. The maximum effective d_{33} was measured at a Zr/Ti ratio of 52/48, which suggested that the MPB of PZT films coincided with that of the PZT ceramics. The effective d_{33} was larger on the tetragonal side of the MPB than on the rhombohedral side of the MPB. It was also found that PZT films with <111> preferred orientation had larger effective d_{33} than films with <100> preferred orientation due to the larger remanent polarization in these films.

Chapter 6. Domain Wall Motion and its Contribution to the Dielectric and Piezoelectric Properties of PZT Films

It is well known that there are both intrinsic and extrinsic contributions to the dielectric and piezoelectric responses in ferroelectric materials at room temperature, of which the intrinsic contributions refer to the single domain properties and the extrinsic contributions are mainly attributed to domain wall motion. In ferroelectric PZT ceramics, the large extrinsic contributions to the dielectric and ferroelectric properties at room temperature are important factors in the superior dielectric constants and piezoelectric coefficients. Recently, it has been found that the measured longitudinal and transverse piezoelectric coefficients of PZT films are much smaller than those of their bulk counterparts, especially when the film thickness is small [10, 14, 116]. In the last chapter, it was shown that this is due, in part, to clamped mechanical boundary conditions. However, it has also been suggested that the limited extrinsic contributions to the piezoelectric properties (due to the inability to activate the non-180° domain wall motions) may also be responsible [14,15]. In this chapter, the domain wall motions and their contributions to the dielectric and piezoelectric properties of sol-gel derived PZT films were investigated. To separate the intrinsic and the extrinsic dielectric responses, measurements at 4K were made to freeze the domain wall motion. The extrinsic contribution to the piezoelectric properties in PZT films was investigated by studying the stress and electric field dependence of the piezoelectric coefficients. In addition, through studying the influence of uniaxial stress and dc electric field on the dielectric properties,

both the ferroelectric and ferroelastic activities of the non-180° domain walls in these films were evaluated. The effect of grain size and film thickness on domain wall motion in PZT films will be illustrated.

6.1 Film Preparation and Properties

The PZT films investigated were all deposited on Pt-coated Si substrates with a Zr/Ti ratio of 52/48. Three different sol-gel processes were used to prepare the PZT films to allow large variations in film thickness, grain size, and preferred orientation. The first sol-gel method used was a 2-methoxyethanol solution and RTA process, which was already described in Chapter 5. The films prepared by this method had small grain size (50 nm-100 nm) and strong preferred orientation (see section 5.1). The dielectric, ferroelectric, and piezoelectric properties of the films prepared by this method were described in Chapter 5 and will not be repeated here.

The second sol-gel method used in this investigation was an acetylacetone modified 2-methoxyethanol solution and RTA process. PZT films with thicknesses up to 10 μm were prepared by this method on <111> oriented Pt coated Si wafers. XRD patterns showed that there was a gradual change in the preferred orientation in these films with increasing film thickness (Figure 6.1). When the film thickness was small (<2μm), the PZT films had <111> preferred orientation, indicating nucleation from the bottom electrode. With increasing film thickness, the films became more and more randomly oriented as the influence of the Pt/PZT interface was reduced [96]. The grain size of these films was around 0.1 μm as observed by SEM and didn't change with increasing film

thickness. The cross-sectional pictures of the SEM images showed a layered structure for the thick films, in which each layer corresponded to one crystallization step (Figure 6.2). There was no columnar growth found in these films, which was in agreement with the randomly oriented XRD patterns. Electrical characterizations showed that the dielectric constant, remanent polarization, and the effective piezoelectric d_{33} coefficient all increased monotonically as the film thickness increased from 0.25 μm to 7 μm. On the other hand, the dielectric loss and coercive field initially decreased with increasing film thickness, then saturated for films thicker than two micrometers [96].

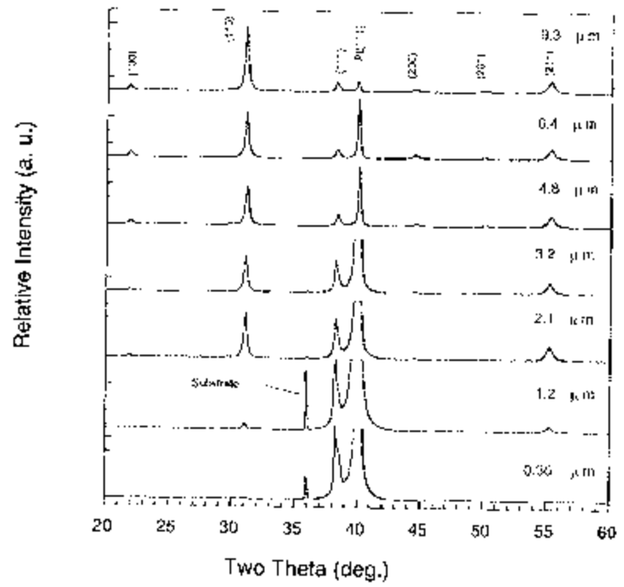

Figure 6.1 **XRD patterns of PZT films deposited using acetylacetone modified 2-mothoxyethanol solution and RTA process (Courtesy of W. Ren).**

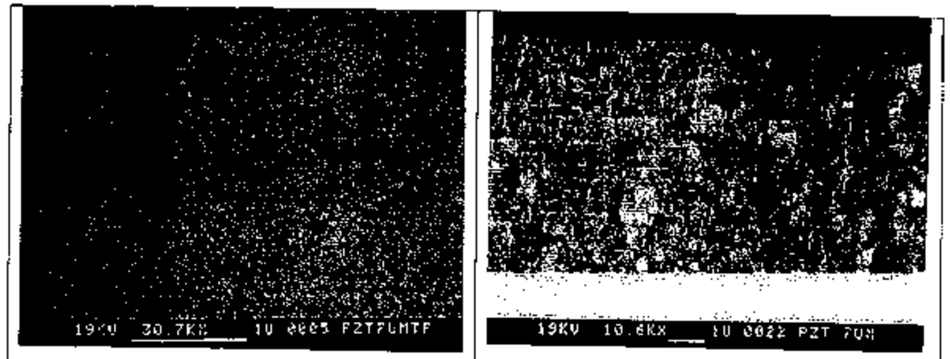

(a) Surface morphology (b) Cross-section

Figure 6.2 SEM pictures of a 7 μm thick PZT 52/48 film prepared using acetylacetone modified 2-mothoxyethanol solution and RTA process (Courtesy of W. Ren)

The third sol-gel method for PZT film preparation was an acetic acid solution and conventional furnace anneal process. PZT films up to 10 μm thick were deposited on Pt(111)/Ti/SiO_2/Si(100) substrates. Despite the <111> preferred orientation of the bottom electrodes, XRD patterns showed that all the films prepared using this method were strongly <100> oriented. The relative intensity of the <100> peak was found to increase with increasing film thickness [117]. Unlike the films prepared using RTA, films prepared by this method (crystallized using the conventional box furnace) had larger grain sizes. The average grain size increased with the film thickness, typically ranging from 300 nm to 700 nm. Figure 6.3 is the AFM surface image of a three μm thick <100> oriented PZT 52/48 film prepared using this method. An average grain size of 500 nm was obtained from this picture. It was also found from cross-sectional SEM study that dense layered structures with well defined grains and columns were observed [117]. The

dielectric constant and effective piezoelectric d_{33} coefficient were found to increase with film thickness in the range from 0.5 to 10 μm, but the remanent polarization increased with film thickness up to 3 μm and then saturated as the film thickness continued to increase.

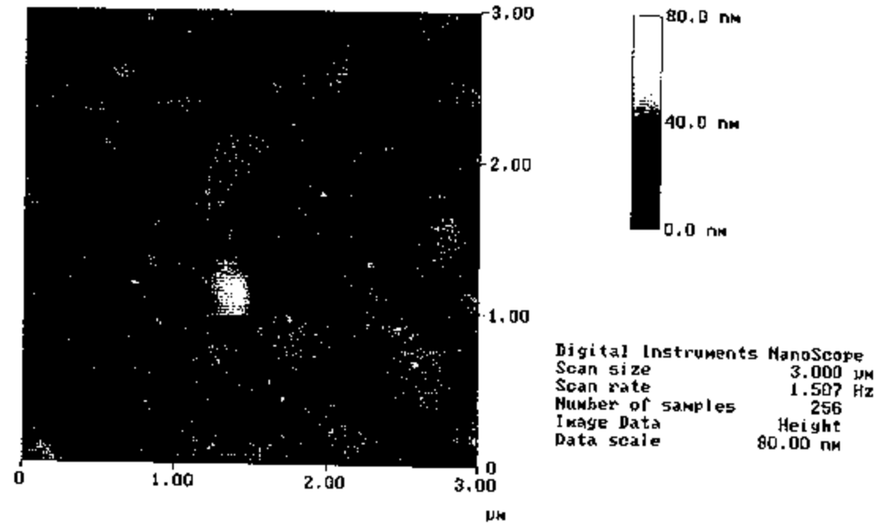

Figure 6.3 AFM picture of the film surface of a 3 μm thick <100> PZT 52/48 film prepared using acetic acid solution and conventional furnace anneal process.

6.2 Temperature Dependence of the Dielectric and Ferroelectric Properties

The temperature dependence of the low and high field electrical characteristics of the PZT films were investigated from room temperature down to 4.2 K. This was done for films with different thicknesses, orientations and grain sizes, as shown in Figure 6.4.

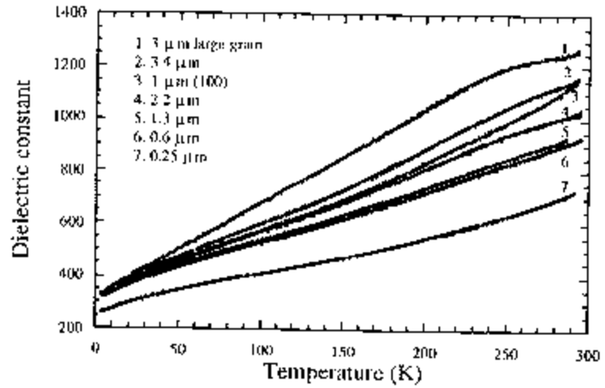

Figure 6.4 Temperature dependence of the dielectric constant of sol-gel PZT 52/48 films at 1kHz.

At room temperature, there are large differences observed for the dielectric constants of the various PZT films investigated. The dielectric constant increases with film thickness for films with the same orientation and grain size, and is larger in films with larger grain sizes. As the temperature decreases, the dielectric constants of all the films decrease. However, the temperature coefficients of capacitance are different.

Eventually the dielectric constants of all these films converge to approximately the same value as the temperature approaches to 0 K (except films < 0.5 μm thick).

As has been pointed out, the extrinsic contribution to the dielectric response in ferroelectric materials is mainly from domain wall motion, phase boundary motion, and defect reorientation. These processes are thermally activated and thus can be frozen out as the temperature approaches 0 Kelvin. Therefore the dielectric constant measured at 4.2 K is almost solely from the intrinsic dielectric response. Figure 6.4 indicates that although the sol-gel PZT films have much different dielectric constants at room temperature due to the difference in thickness and grain size, they all have similar intrinsic contributions to the dielectric constant near 0 K. A close look at the dielectric constant at 4 K showed that there is still a weak dependence of the intrinsic dielectric constant on the film thickness. This is probably due to the effect of the top surface layer, as has been observed by SEM, and/or an interfacial layer between the PZT and the bottom electrode. These layers usually have lower dielectric constants than ferroelectric PZT, and thus can result in a smaller apparent intrinsic dielectric constant. If the surface and interfacial layers have a combined capacitance of C_{int} for all the films, then the apparent capacitance of the film C_{tot} is related to C_{int} as follows:

$$1/C_{tot} = 1/C_{film} + 1/C_{int} \tag{6.1}$$

where C_{film} is the actual capacitance of the PZT films. Since C_{film} is determined by:

$$C_{film} = \varepsilon_0 \varepsilon S/t \tag{6.2}$$

therefore,

$$1/C_{tot} = t/\varepsilon_0\varepsilon S + 1/C_{int} \qquad (6.3)$$

in the above equations, t is the film thickness and S is the area of the top electrode. This assumes that the interfacial layer is negligibly thin compared to the measured thickness. Figure 6.5 shows the plot of $1/C_{tot}$ versus film thickness t for <111> oriented fine-grained PZT films. The linear relationship between $1/C_{tot}$ and t along with the non-zero intercept for the plot support the hypothesis that the thickness dependence of the dielectric constant at 4 K is mainly due to the surface and interfacial layers. It is expected that with improved film processing this effect could be eliminated, or at least substantially lessened.

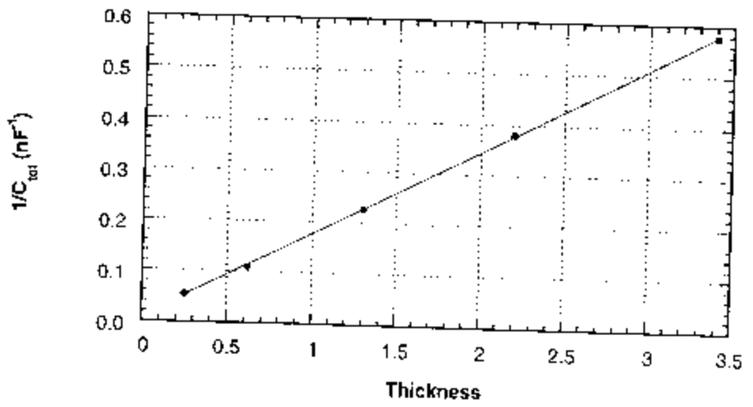

Figure 6.5 Reciprocal of the measured capacitance as a function of film thickness for <111> oriented fine-grained PZT films.

Since all the films have similar intrinsic dielectric constants at 4 K, it is reasonable to expect that they also have similar intrinsic contributions to the dielectric constant at room temperature. Some of the difference in dielectric constants at room temperature can be attributed to the surface and interfacial layers. However, deviation in the linear relationship between the reciprocal capacitance and the film thickness was found at room temperature. This suggests that the extrinsic contributions to the dielectric response also contribute to a difference in dielectric constant at room temperature. To quantitatively separate the effect of the surface and interfacial layer on the dielectric constant of the films at room temperature, the capacitance of the surface and interfacial layers must be determined. This was attempted, however, it was not possible to determine the intercept in $1/C_{tot}$ versus t line at 4 K accurately enough, due to the lack of dielectric data in the very thin film thickness range. Very small variations in this number lead to very large over or under corrections of the room temperature dielectric data in thin films. In addition, the temperature coefficient of the dielectric constant of the surface and interfacial layers is also unknown, which adds more complexities in the calculations. In any event, it is clear that the interfacial layer does not account for all of the difference in room temperature dielectric constants for the films as a function of thickness.

The existence of extrinsic contributions to the dielectric constant in PZT films is manifested in the ac driving-field dependence of the dielectric constant at room temperature and 4 K (Figure 6.6). At 4 K, the non-linearity of the dielectric constant is very small, reflecting the characteristic of the intrinsic dielectric response of the material. However, at room temperature, the dielectric constant increases with the amplitude of the applied electric field, showing a large dielectric non-linearity in these films. This

dielectric non-linearity is believed to be associated with extrinsic sources and can be attributed to domain wall motions [59, 60].

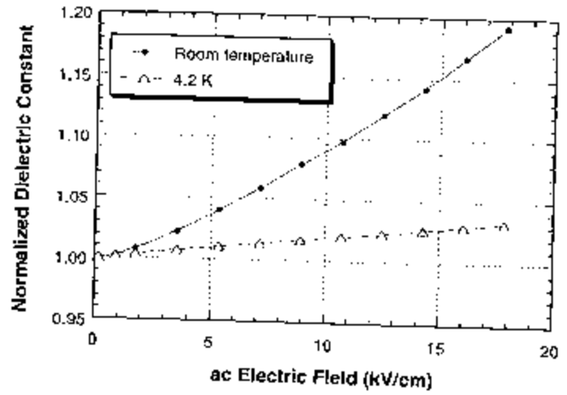

Figure 6.6 **The dependence of the dielectric constant of PZT films on the amplitude of the ac electric driving field.**

Despite the large difference in the texture and grain size between the PZT films and bulk ceramics, the dielectric constant of PZT films was similar to that of PZT bulk ceramics when measured at 4 K. There are a number of factors which might lead to a variation in the measured intrinsic dielectric constant between bulk and thin film PZT specimens. Firstly, the PZT films have strong preferred orientation; therefore the polarization vectors in these films are concentrated along several specific directions relative to the electrodes. This may give different averages of the intrinsic dielectric constant for films with different textures, and for thin films and bulk PZT. Secondly, with a decrease in grain size, there is an increase in the internal stress due to the difficulty in forming non-180° domains. Therefore the intrinsic dielectric constant should increase as

the grain size decreases. It was found that the dielectric constant of bulk PZT ceramics increased with decreasing grain size at temperature near 0 K, and was attributed to the increased internal stress in fine grain ceramics [7]. This effect would result in a larger dielectric constant in thin films than in bulk ceramics, and would also tend to increase the dielectric constant in fine-grained films. Thirdly, due to the constraints of the substrates, the measured dielectric constant of PZT films is at least partially clamped (clamping should decrease ε_r). Finally, since the thickness of the PZT films is much smaller than bulk samples, low dielectric constant layers at the PZT/electrode interfaces can cause a noticeable decrease in the measured dielectric constant of thin films while they have virtually no effect on bulk samples. The experimental results indicates that these factors are either very modest or that they counterbalance each other. Thus, the intrinsic dielectric constant are similar for bulk ceramics and most of the thin film PZT's.

From the phenomenological theory developed for PZT, the intrinsic contribution to the dielectric constant at room temperature for PZT 52/48 bulk ceramics was calculated to be about 670 [7]. Using this value as an approximation for the intrinsic contribution to the dielectric constant of PZT films at room temperature, it was estimated that 25% to 50% of the total dielectric constant at room temperature in these films from the extrinsic sources. The extrinsic contribution to the dielectric constant is likely to increase with film thickness, and is larger in films with larger grain size.

As will be shown in the next two sections, non-180° domain wall motion in the small grain (<0.2 μm) and thin (thickness smaller than 3 μm) PZT films is negligible. Therefore the extrinsic contribution to the dielectric constant in these films was most probably from 180° domain wall motions or from phase boundary motion. The reason for

the increase in extrinsic contribution to the dielectric constant with film thickness is not clear. One possibility is that there may be pinning centers located at the interface between the bottom electrode and the PZT film. In thicker films, fewer grains are affected by these pinning centers. Therefore the 180° domain wall or phase boundary motion becomes easier. There is also evidence from TEM study that the domain wall density was lower near the film surface (see section 6.5). The increased extrinsic contribution to the dielectric constant in large grained films is believed to be due to the high domain wall density and less domain wall pinning. It has been shown in bulk PZT ceramics that the domain wall density decreases with decreasing grain size in the deep sub-micron range [7]. There is also more grain boundary area in the fine-grained films where space charge tends to be trapped. As a result, domain wall pinning is expected to be stronger in fine grained films. In addition, non-180° domain wall motion may contribute to the dielectric constant in thick and large grained films, as indicated by the extrinsic contribution to the piezoelectric coefficient in these films (see Section 6.3).

The dielectric loss of the PZT films was also measured as a function of temperature from room temperature to 4.2 K (shown in Figure 6.7). Compared to the dielectric constant, the temperature dependence of the loss factor was more complicated. In general, there was a broad anomaly in the loss factor centered at temperatures between 200 K to 250 K. For films with thicknesses larger than 1 μm, the dielectric loss at temperature around 200 K was larger than its room temperature value. As the temperature dropped below 50 K, a rapid decrease of the loss factor was observed in all films. When the temperature approached 0 K, the dielectric loss in these films converged to about 0.6%, though there was a little variation.

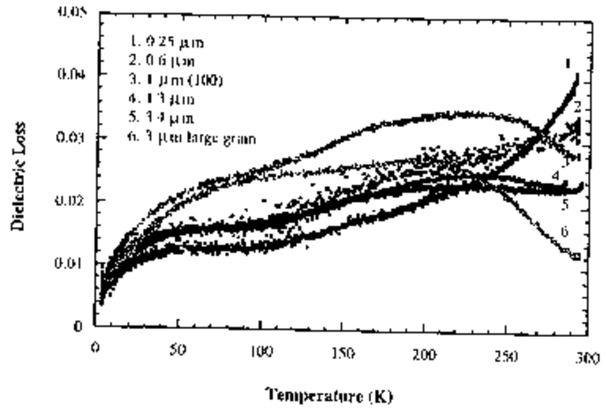

Figure 6.7 **Temperature dependence of the dielectric loss of PZT 52/48 films.**

The behavior of the dielectric loss with temperature is still not well understood. Similar behavior of the dielectric loss was also observed in PZT bulk ceramics [58]. The authors suggested that there are several relaxation processes depending on composition and doping. The relaxation processes could be connected with the impurity ions and with domain walls or phase-boundary motions. At temperatures near zero K, these thermally activated processes were frozen out, therefore the intrinsic single-domain properties dominated the measured dielectric loss [58]. A similar mechanism may also be responsible for the dielectric loss behavior in PZT films.

The P-E hysteresis loop of PZT films was also measured as a function of temperature from room temperature to 4 K (Figure 6.8a). Figure 6.8b shows the temperature dependence of the saturation polarization and remanent polarization of a 0.6 μm PZT 52/48 film. The saturation polarization was almost independent of temperature between 300 K and 50 K. As the temperature continued to decrease, there was a slight

decrease in the saturation polarization. In contrast, the remanent polarization showed a much larger change with the temperature. It monotonically increased with decreasing temperature. As a result, the difference between the saturation polarization and the remanent polarization decreased at low temperatures. Figure 6.9 shows the coercive field of the 0.6 μm PZT film as a function of temperature. The coercive field was found to increase with decreasing temperature. As the temperature dropped below 50 K, a very rapid increase in the coercive field with the decrease of temperature was observed.

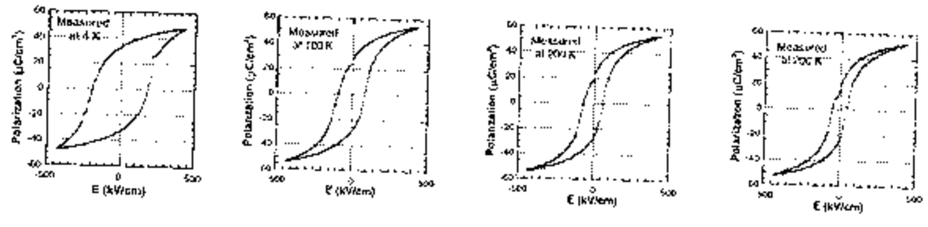

(a)

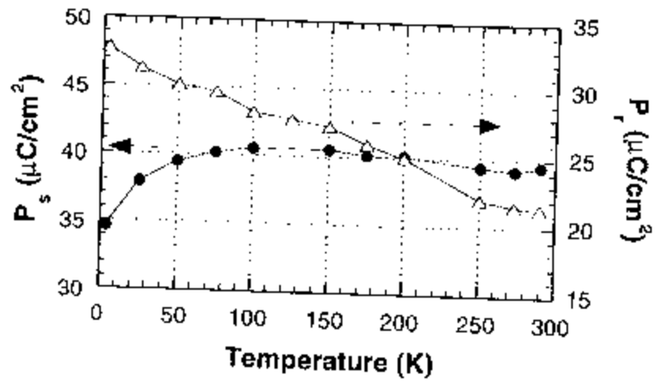

(b)

Figure 6.8 **(a) P-E hysteresis loops at different temperatures. (b) Saturation and remanent polarizations as a function of temperature. Data measured from a 0.6 μm <111> oriented PZT 52/48 film at maximum field of 500 kV/cm.**

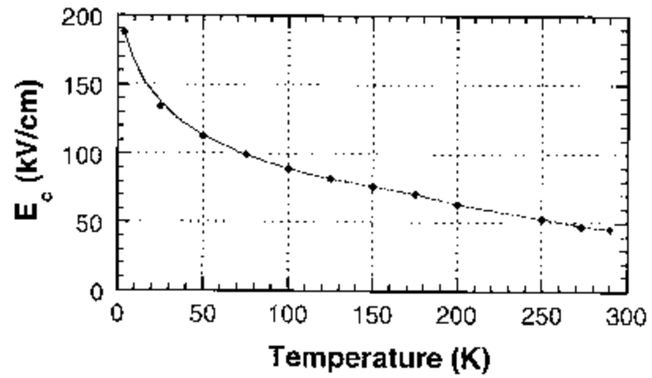

Figure 6.9 **The coercive field of a 0.6 μm <111> oriented PZT film as a function of temperature. The maximum field applied was 500 kV/cm.**

The temperature dependence of the coercive field indicates that domain reversal in PZT films becomes more difficult as the temperature decreases. Since non-180° domain reorientation is very limited in these films, domain reversal is mainly achieved by 180° domain wall motion. With decreasing temperature, the domain wall motion become more difficult, and thus a larger electric field is needed to accomplish it. The rapid increase of the coercive field at temperature below 50 K indicated a dramatic decrease in the 180° domain wall mobility, which is also illustrated by the rapid decrease in the dielectric loss in this temperature range. The increase of the remanent polarization with decreasing temperature may also be due to the reduced domain wall mobility. As was suggested earlier, the large difference between saturation and remanent polarizations in PZT films is most likely a result of significant domain reversal after the removal of the electric field. At low temperatures, the back switching of the domains is partially frozen

out. This, therefore results in a small difference between the saturation and remanent polarizations. The slight decrease in the saturated polarization at temperature near zero K can be attributed to the inability to reverse all the domains at that temperature, using a 500 kV/cm excitation field.

6.3 Stress and Field Dependence of Dielectric and Piezoelectric Properties

In order to investigate the ferroelastic activity of the non-180° domain walls, the low and high field electrical characteristics of <111> PZT films crystallized by the RTA process were measured as a function of applied uniaxial stress perpendicular to the film plane. Figure 6.10 shows the effect of the applied normal stress on the dielectric constant of a poled 1 μm thick <111> PZT film which has an average grain size of about 0.05 μm to 0.1 μm. The result shows that the dielectric constant has a very weak stress dependence, increasing less than 2% for an applied normal stress up to 20 MPa. The change of the dielectric constant with applied stress is also reversible, i.e., removal of the applied stress results in the full recovery of the dielectric constant. On the other hand, the dielectric loss is almost independent of the applied stress within the stress range used in this investigation. The ferroelectric P-E hysteresis loop was also measured during the application of normal stress. There was no noticeable change found in either the remanent polarization or the coercive field with applied stresses up to 20 MPa. Both high field and low field measurements were performed on several films with film thickness ranging from 0.5 μm to 3 μm. Similar results were obtained on all the sample tested.

In poled PZT bulk ceramics, it was found that for an applied compressive uniaxial stress of 20 MPa there were 12% and 5% increases in the dielectric constant of hard and soft PZT respectively [86]. This behavior was attributed to stress-induced non-180° domain wall motion which resulted in increased domain wall contributions to the dielectric response [90]. In hard PZT bulk ceramics, there are defect dipoles which tend to align with the polarization vectors of the domains to stabilize the domain structure. They act as pinning centers to prevent domain wall motions due to external excitation, resulting in small extrinsic contributions to the dielectric constant. By applying a uniaxial stress, ferroelastic domain wall motion occurs in PZT bulk ceramics, which results in a metastable domain configuration. Therefore both the dielectric constant and loss increase with applied stress as a result of the increased extrinsic response associated with the depinning of the domain walls in bulk PZT ceramics. Since domain wall pinning is more severe in hard PZT, a larger stress dependence of the dielectric constant was found in hard PZT over this stress range.

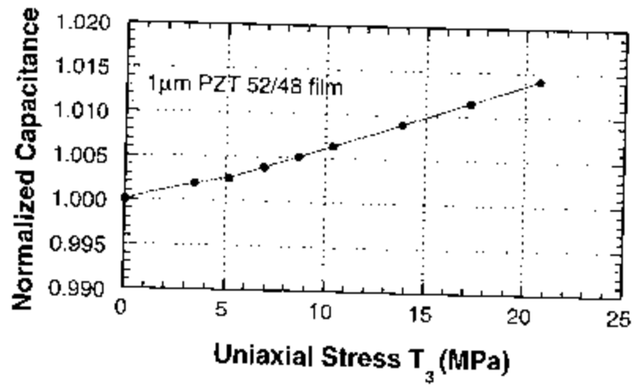

Figure 6.10 **The effect of applied normal stress on the dielectric constant of a poled <111> PZT 52/48 film which has an average grain size of about 50 nm to 100 nm.**

The stress dependence of the dielectric constant of the poled PZT films was much smaller than in bulk PZT ceramics. In addition, there was no increase in the dielectric loss with the applied stress. These results suggest that non-180° domain wall motion in response to the applied stress is negligible in these films for this stress range. Since strong domain wall pinning in these films is expected due to their small grain size and to interfacial effects, a large dependence of the dielectric constant and loss on the applied stress would be expected if the non-180° domain walls were ferroelastically active.

The effect of normal stress on the high field characteristics of the PZT films also suggests that the ferroelastic activity of the non-180° domain walls is negligible in these films. Otherwise, a decrease in the remanent polarization and a change in the coercive field would be expected. However, they were not observed in our experiments.

Both the low and high field electrical measurements as a function of the normal stress are consistent with the hypothesis that ferroelastic motion of the non-180° domain walls is limited. In an investigation on the effect of biaxial stress on the properties of PZT thin films, it was also proposed that non-180° ferroelastic domain wall motion played little role in the thin film properties [14]. It is believed that the submicron grain structure is the one critical reason for this behavior in sol-gel PZT films [14, 15]. Besides, the reduced domain wall density and strong pinning by the film/substrate interface, point defects (such as lead and oxygen vacancies) may also play roles in reducing the non-180° domain wall activity in PZT films [14].

Since the extrinsic contribution to the piezoelectric response in ferroelectric materials is mostly from non-180° domain wall motion, little extrinsic contribution to the piezoelectric coefficient is expected in PZT films in which non-180° domain wall motion

is limited. To investigate whether this was the case, the effective d_{33} of the PZT films was measured using the pneumatic pressure charge technique as a function of the amplitude of the applied stress. Figure 6.11 shows the effect of stress amplitude on the d_{33} coefficients of both a 1 μm thick <111> PZT film with 50 nm to 100 nm average grain size and a PZT-5A bulk ceramic sample.

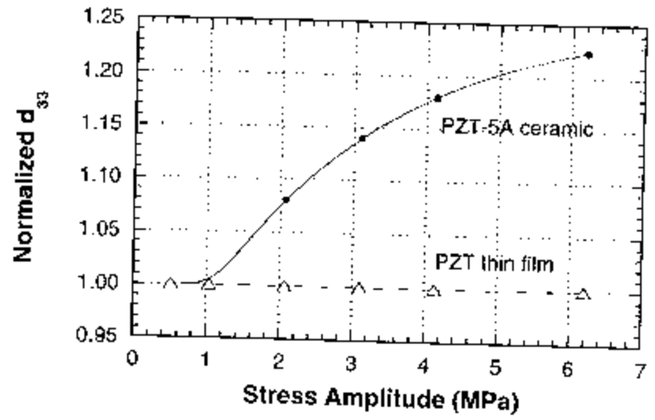

Figure 6.11 The effect of stress amplitude on the d_{33} coefficients of a 1 μm thick <111> oriented PZT film (50 nm to 100 nm average grain size) and a PZT-5A bulk ceramic.

The d_{33} of the bulk PZT ceramic was found to increase with the stress amplitude, showing a significant piezoelectric non-linearity. The non-linearity of the piezoelectric response in ferroelectric materials is believed to be of extrinsic nature and can be attributed to non-180° domain wall motion [59, 60]. This behavior was observed in both PZT and barium titanate bulk ceramics and was used to identify the extrinsic

piezoelectric response in these materials. It was found in barium titanate ceramics that both the d_{33} coefficient and its non-linearity with stress amplitude decreased as the grain size decreased, due to the reduction of non-180° domain wall motion in fine grain ceramics [118]. Measurements on the fine grained (50 nm to 100 nm in grain size) PZT thin films (thickness less than 2 μm) showed that there was no increase in the effective d_{33} with an increase of the applied stress amplitude up to 6 MPa. This result is again a strong indication that the ferroelastic motion of the non-180° domain walls in these films is limited.

The piezoelectric non-linearity of the PZT films was also measured as a function of the applied electric driving field using double-beam laser interferometry. The PZT films studied here were prepared using the acetylacetone modified 2-methoxyethanol solution and RTA process. The film thickness was between 1.5 and 6.7 μm. These films had an average grain size of 100 nm and almost random orientation. The effective d_{33} of the films was also found to increase with film thickness under an ac field of 2 kV/cm and 1kHz (Figure 6.12). To investigate the ferroelectric non-linearity of the effective d_{33}, measurements were made as a function of sub-coercive ac electric field (Figure 6.13). For films with small thickness (1.5 μm), the effective d_{33} remained unchanged as the applied ac field increased to 10 kV/cm. Above that, only a small increase in the effective d_{33} was measured. For the 6.7 μm thick film, the onset of the piezoelectric non-linearity occurred below 4 kV/cm, and the effective d_{33} increased much more rapidly with the ac electric field. Similar behavior was also observed by Kholkin, in which a 7 μm thick <111> oriented PZT film showed large non-linearity in the effective d_{33} while a 0.3 μm thick PZT showed very small piezoelectric non-linearity [12].

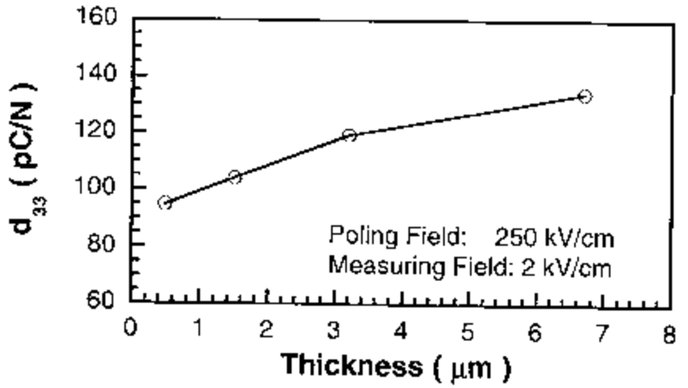

Figure 6.12 The effective d_{33} of PZT films as a function of film thickness at 1kHz. The films had an average grain size on the order of 0.1 μm and were poled at room temperature under an electric field of 250 kV/cm.

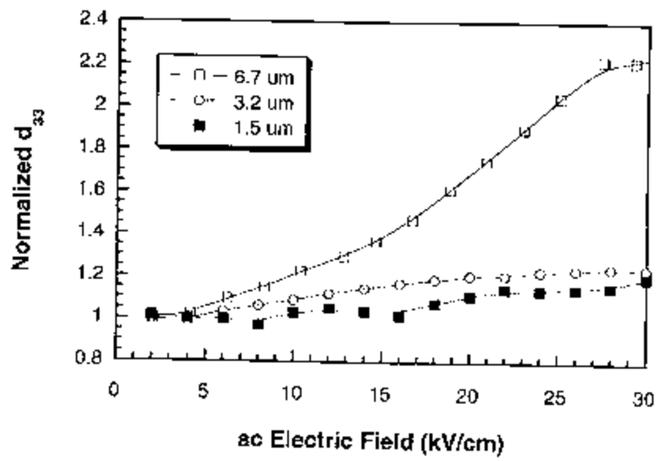

Figure 6.13 Normalized effective d_{33} of PZT films as a function of sub-coercive ac electric field at 1kHz. The films had an average grain size on the order of 0.1 μm and were poled at room temperature under an electric field of 250 kV/cm.

The large piezoelectric non-linearity in thick PZT films suggests that there is significant irreversible non-180° domain wall motion at sufficiently high ac electric fields. The decrease of the threshold field for piezoelectric non-linearity with film thickness suggests that the degree of non-180° domain wall pinning becomes less severe as the films become thicker. This, in turn, suggests that there is an increasing tendency to have extrinsic contributions to the piezoelectric response as the films become thicker. Again, the large threshold field for piezoelectric non-linearity and the small degree of piezoelectric non-linearity in thin PZT films agrees with the hypothesis that there is strong non-180° domain wall pinning and thus little extrinsic contribution to the piezoelectric coefficient in thin PZT films.

Unlike the effective d_{31}, which showed small non-linearity with ac field, the dielectric constant of all PZT films showed very large amplitude dependence (Figure 6.14). All the films displayed a significant dielectric non-linearity, which was found to increase with the film thickness. As has been pointed out before, domain walls in a ferroelectric material can be categorized into two types: 180° domain walls and non-180° domain walls. 180° domain wall motion contributes only to the dielectric response, while non-180° domain wall motion contributes to both the dielectric and piezoelectric properties. The large difference between the non-linearity in piezoelectric coefficients and dielectric constants suggests that 180° domain wall motion is much more significant than non-180° domain wall motion. As a result, a majority of the extrinsic contribution to the dielectric constant in PZT films is due to the 180° domain wall motion. The increase in the dielectric non-linearity with film thickness suggests that the extrinsic contribution to the dielectric constant also increases with film thickness, which is in consistent with

the results from the temperature dependence of the dielectric constant measurements. Kholkin also observed a large difference in the non-linear behavior of dielectric constants and piezoelectric coefficients in PZT films [12]. However, he attributed this difference to the geometry of the PZT films. It was proposed that the large dielectric non-linearity was due to extensive non-180° domain wall motion, and the small non-linearity in effective d_{33} was due to the <111> orientation and the tetragonal structure of the films. He argued that since all the allowed polarization vectors have equal projections onto the substrate normal, 90° domain wall motion should not produce any mechanical strain, and therefore didn't contribute to the piezoelectric response [12]. However, this argument is not applicable to the randomly oriented, MPB films used in this investigation. In addition, if 90° domain wall motion is important in tetragonal PZT films, then the effective d_{33} of <100> PZT films is expected to be larger than <111> PZT films due to extrinsic contribution in <100> films. However, our experimental results showed that this was not the case.

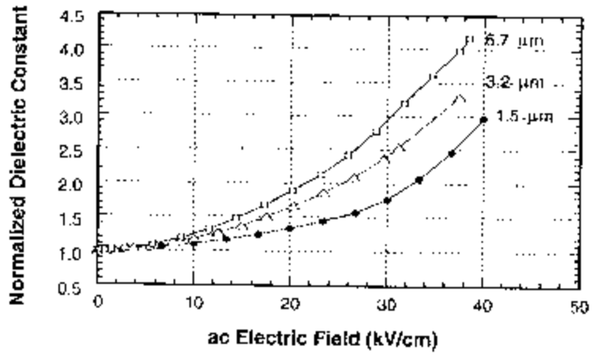

Figure 6.14 **The normalized dielectric constant of PZT films as a function of ac electric field at 1 kHz. Films were randomly oriented and had an average grain size of 0.1 μm.**

6.4 Non-180° Domain Switching in PZT Films

It is well known that the piezoelectric properties of bulk PZT ceramics can be improved by enhancing non-180° domain wall motion. In small grain PZT films the experimental results in the last section indicated that the extrinsic contribution to the effective d_{33} is small due either to strong pinning of the non-180° domain walls or to a low density of ferroelastic walls in the films. However, it was also found that with an increase in film thickness, non-180° domain wall motion might contribute to the piezoelectric response. It has been suggested that the degree of non-180° domain wall pinning is strongly influenced by the grain size of the PZT films [15]. In this section, the activity of the non-180° domain walls of the PZT films and their relationship with the film thickness and grain size were investigated.

The activity of non-180° domain walls can be related to the ease of non-180° domain switching. In general, domain switching occurs via domain wall motion driven by the external field. Therefore the smaller the degree of domain wall pinning, the more extensive domain wall motion should be, thus the more easily domain switching should occur. Domain switching can be identified by monitoring the change of the relative intensity of the <001> and <100> peaks in the XRD patterns for tetragonal PZT ceramics and thin films [15, 119]. This method, though, cannot be used for PZT films at the MPB composition due to the overlap of the <001> and <100> peaks in the XRD pattern. However, single domain PZT with the MPB composition has very large anisotropy in the dielectric properties, i.e., *a*-domains have much larger dielectric constants than *c*-domains [37]. Therefore a large change in the intrinsic contribution to the dielectric constant is

expected as a result of non-180° domain switching. This can be used to identify non-180° domain switching in PZT films.

The effect of dc poling on the dielectric constant of the PZT films was investigated at room temperature first. Dielectric measurements were made under small field (0.5 kV/cm) without dc bias. PZT films were poled at different dc fields for one minute at room temperature. A five minute aging time was allowed before measuring the dielectric constant. Figure 6.15 shows the dielectric constant as a function of dc poling field.

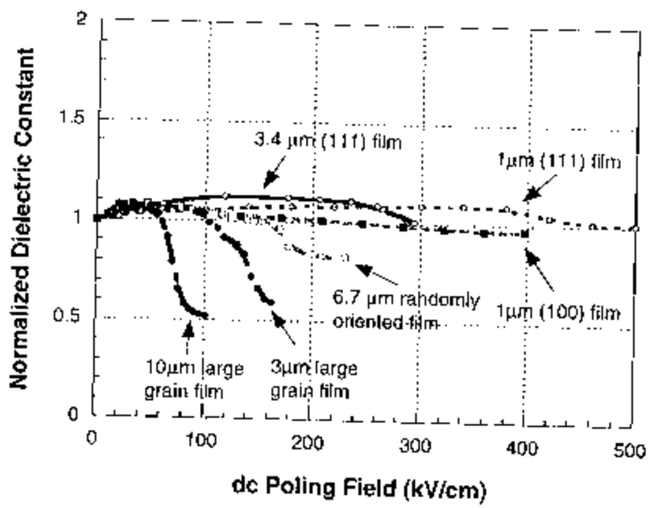

Figure 6.15 **Weak field dielectric constant of PZT films as a function of dc poling field.**

For poling fields below the coercive field, all the films showed small increases in both the dielectric constant and loss immediately after poling. The dielectric constant and

loss gradually decreased with the increase of aging time, and finally returned to their original values after about 72 hours aging. This observation suggests that the initial increases in the dielectric constant and loss result from de-aging. 180° domain walls may be de-pinned by the dc poling field through the formation of a metastable domain structure or redistribution of the defect dipoles, thus leading to larger 180° domain wall contributions to the dielectric response in these films. Similar de-aging behavior was also observed after heat treatment at temperatures above the Curie temperature, in which the domain structure and space charge distributions were also changed.

As the dc poling field continued to increase, the dielectric constant remained flat for small grained PZT films when the film thickness was less than two micrometers. The dielectric constant changed little through dc poling in either <100> or <111> oriented PZT thin films up to the breakdown fields. This behavior suggests that the non-180° domain wall pinning is so strong in these films that the ferroelectric switching of non-180° domain is not achievable at room temperature. However, in thicker films, a decrease in the dielectric constant was observed when the poling field exceeded a certain level. Little change was observed in the dielectric loss. When heated above T_c the dielectric constant recovered to its original value, so the change was not due to cracking or electrode delamination. The decrease in the dielectric constant can be explained by non-180° domain switching. Under a dc poling field normal to the film plane, *c*-domains are energetically more favorable than *a*-domains in PZT films. Since the dielectric constant of *a*-domains is much larger than that of *c*-domains, non-180° domain switching will result in a decrease of the dielectric constant in the direction measured. Since the non-180° domain walls are strongly pinned in PZT films, some minimum electric field is

required to overcome the potential barrier to realize extensive domain wall motion. Therefore the threshold field for the non-180° switching (the onset of the decrease of the dielectric constant) can be used as an indication of the degree of non-180° domain wall pinning in PZT films. It was found that for films with similar average grain sizes on the order of 0.1 μm, the threshold field decreased with increasing film thickness, indicating a reduction in the degree of the non-180° domain wall pinning (Figure 6.16). The percentage change in the dielectric constant through dc poling increased slightly in thicker films and was less than 20% in all the fine grain PZT films, indicating that only a small fraction of *a*-domains could be switched to *c*-domains by the electric field.

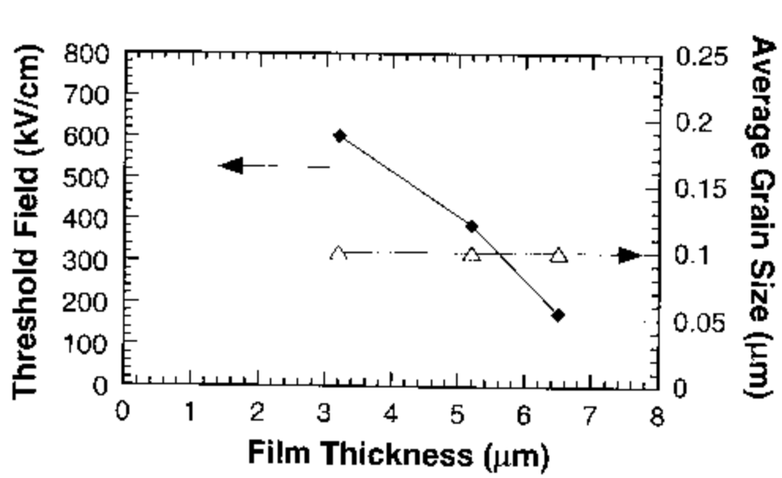

Figure 6.16 The threshold electric field for non-180° domain switching as a function of film thickness. The PZT films are randomly oriented and have an average grain size on the order of 0.1 μm.

Compared to the film thickness, the grain size of the films had a much stronger effect on ferroelectric non-180° switching in PZT films. The large grain PZT films prepared using conventional furnace annealing showed much more significant decreases in the dielectric constant (40-50%) at a much smaller threshold field. The large decrease in dielectric constant suggests that there is a significant volume fraction of *a*-domains which are switched to *c*-domains by dc poling when the poling field exceeds the threshold field. The small threshold field for non-180° domain switching indicates that the pinning of non-180° domain walls in these large grain films is much less severe than that in the small grained films. It was also found that with an increase in grain size, there was a decrease in the threshold field (Figure 6.17).

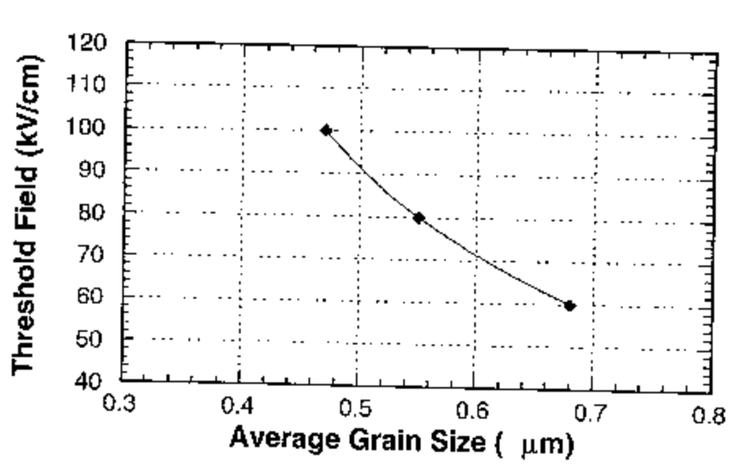

Figure 6.17 The threshold electric field for non-180° domain switching as a function of grain size. The PZT films are <100> oriented with film thicknesses between 3 and 10 μm.

To verify that there is non-180° domain switching accompanying the decrease of the dielectric constant with dc poling, the dielectric constant of the PZT films was measured as a function of temperature before and after poling. Since the dielectric constant at room temperature is composed of both intrinsic and extrinsic contributions, a variation in the extrinsic contribution to the dielectric constant may also result in a change in the room temperature dielectric constant. The domain configuration of the PZT films can be changed by dc poling, and this could as well lead to a change in the extrinsic contribution to the dielectric constant. On the other hand, non-180° domain switching changes the observed dielectric constant of the PZT films via the intrinsic contribution. Figure 6.18 shows the temperature dependence of the dielectric constant of a 3 μm thick conventional furnace annealed PZT film which had an average grain size of 0.5 μm. The large decrease of the dielectric constant at 4 K after dc poling clearly showed that the intrinsic contribution to the dielectric constant was reduced. This result indicated that non-180° domain switching accompanied the decrease of the room temperature dielectric constant in coarse grained PZT films. In contrast, there was little change in the dielectric constant either at room temperature or 4 K for fined grain thin films, again suggesting no non-180° domain switching in these films.

6.5 Direct Observation of Microstructure and Domain Structures

The effect of film thickness and grain size on the domain configurations was also investigated by direct methods. PZT films prepared by different sol-gel methods were

sent to John Hopkins University for TEM observation (courtesy of Z. Xie and K. Hemker). The microstructures of 0.3 μm, 0.7 μm and 1 μm thick PZT 52/48 films prepared by the 2-methoxyethanol solution and RTA have been studied by TEM plane view. The TEM samples were prepared by mechanical dimpling from the silicon substrate, followed by ion milling from the substrate side. The conditions of ion milling were as follows: voltage = 5 kV, current = 0.5 mA, at 12.5° with a liquid nitrogen cooling stage. To reduce possible contamination, the thin film surface was protected while ion milling.

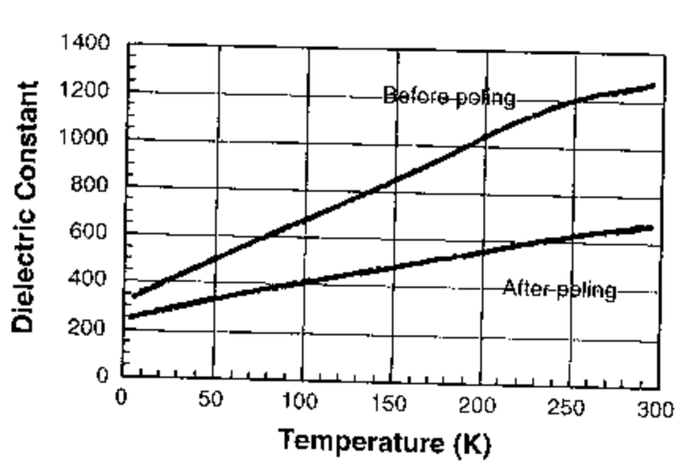

Figure 6.18 Temperature dependence of the dielectric constant before and after dc poling. The film was 3 μm thick annealed by conventional furnace. dc poling was performed at room temperature under 150 kV/cm.

TEM micrographs of PZT films showed that the films were composed of equiaxed perovskite grains ranging from 50 nm to 100 nm in size (see Figure 5.2c). No change of the grain size with the film thickness was noticed in these samples. By ion milling the PZT films from both sides of the sample for different times, microstructures at different depths in the films were observed. Near the film surface, very few grains which had domain structures inside them were observed. In addition, dislocations were clearly seen inside grains and along grain boundaries. In contrast, domain fringes were observed in the middle of the films for all the samples. No distinct difference in the domain configurations was found for the three thin films. The vast majority of the grains which showed domain fringes only had one set of parallel stripes, as shown in Figure 6.19a. However, in some large grains (about 100 nm), more complex domain structures were observed. Figure 6.19b is a TEM picture which shows a grain with four variants related to each other by nearly 90°. The investigation of PZT films prepared by the other two sol-gel methods is still under way and hopefully will provide more information on the effect of grain size on the domain configuration.

The TEM results described above indicated that the domain assemblages in PZT films changed with both the film thickness and grain size. The lower probability for non-180° domain wall formation at the top surface of the films can result in a small domain wall density. This, along with the fact that the probability of forming multi-variant grains decreased with the film thickness, may be responsible for the difficulty of non-180° domain switching in thinner PZT films. The relative ease in switching non-180° domains in large grained PZT films is possibly related to the complex domain structure (more domain variants) formed in larger grains [7]. Domain structures have also been observed

in the literature in fine grain PZT films using TEM. Twins 5-10 nm in width were found in sol-gel PZT films with average grain size of 0.1 μm [50]. As for the grain size effect, Tuttle et al. found [120] that many of the grains with dimensions on the order of 80 nm in PZT 20/80 films exhibited single 90° domain lamella, while it was difficult to find 90° domain images in smaller grains (50-70 nm).

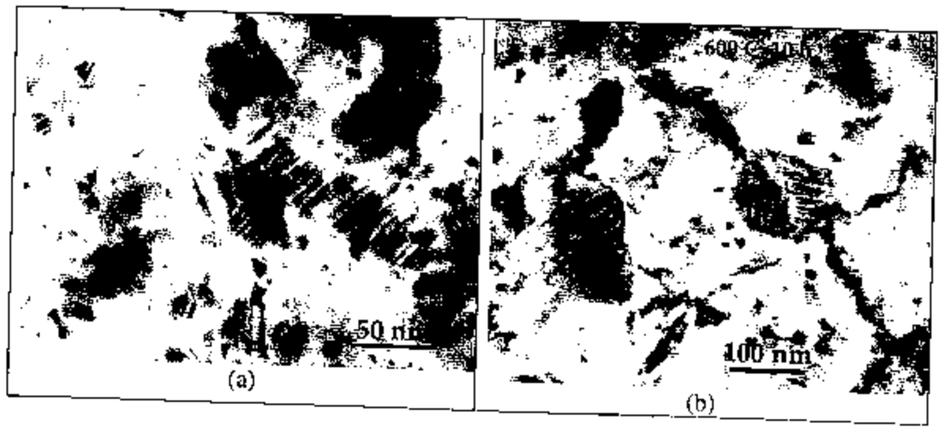

Figure 6.19 TEM Plane view of PZT 52/48 films prepared using 2-methoxyethanol precursor solution and RTA.

(a) Domain fringes which have one set of parallel stripes.

(b) Domain fringes which have four sets of variants related to each other by nearly 90°.

6.6 Summary

Domain wall motions and the extrinsic contributions to the dielectric and piezoelectric response in sol-gel derived PZT films were investigated. The temperature dependence of the dielectric properties showed that although PZT films had much different dielectric constants at room temperature for films with different film thickness, grain size, and preferred orientation, they all had similar intrinsic contributions to the dielectric constant. It was estimated that at room temperature 25% to 50% of the dielectric response of PZT films arises from the extrinsic contribution. The extrinsic contribution to the dielectric constant in PZT films was mostly attributed to 180° domain wall motion, and was likely to increase with both film thickness and grain size.

On the other hand, ferroelastic non-180° domain wall motion was found to be limited in fine grain PZT films, as was indicated by the small effect of normal stress on the low and high field electrical characteristics of the films and the linear relationship between the piezoelectric response and the stress excitation amplitude. This, in turn, suggested that the extrinsic contribution to the piezoelectric coefficient in the fine grain PZT films was small. However, as the films became thicker (> 5 μm), non-linear behavior between the piezoelectric coefficient and the electric driving field was observed. This indicated that there was significant ferroelectric non-180° domain wall motion under high external excitation in thicker films, which suggested that either the degree of non-180° wall pinning decreased or the concentration of ferroelastic walls rose with increasing film thickness.

The activity of the non-180° domain walls was studied through the characteristics of non-180° domain switching. For fine grained films with film thicknesses less than two μm, non-180° switching was negligible, indicating that either the pinning of non-180° domain walls was very strong or that there were few present in the films. As the films became thicker, a decrease in the dielectric constant was observed when the poling field exceeded a threshold field. The drop in dielectric constant was attributed to non-180° domain switching, as indicated by dielectric measurements at 4.2 K. The threshold field was found to decrease with an increase in film thickness, suggesting larger non-180° domain wall mobility in thicker films. The non-180° domain switching in the large grained PZT films was found to be much easier and more significant than that in fine grain PZT films. With an increase in the grain size, a decrease in the threshold field was observed.

Domain structures were studied in PZT films using TEM. Initial results on PZT films prepared by 2-methoxyethonal solution and RTA showed that domain fringes were observed in the middle of the films for all the samples from 0.3 μm to 1 μm thick. The majority of the grains which showed domain fringes only had two variants. Multi-variants domain fringes were observed in some large grains. Near the films surface, very few grains which had domain structures were found.

Chapter 7. Conclusions and Recommendations for Future Work

7.1 Conclusions

7.1.1 Pneumatic Pressure Charge Technique for Piezoelectric d_{33} Measurement

The pneumatic pressure charge technique was developed for characterization of the effective d_{33} of piezoelectric films using the direct piezoelectric effect. In this method, a normal stress was applied to the tested specimen and the stress-induced charge was measured for evaluation of the d_{33} coefficient. Using a pneumatic pressure rig for stress application, substrate bending was avoided and a self-aligned normal stress was obtained. However, it was found that in addition to the intended normal stress, in-plane stresses were also applied to the specimen by the pneumatic pressure due to the friction between the sample and O-ring. Although the majority of the in-plane stresses were released through O-ring sliding, a small amount of remnant in-plane stresses still existed, which tended to give an inflated d_{33} value by inducing additional surface charge through the transverse piezoelectric effect. It was found that the remnant in-plane stresses were controlled by a number of factors. Among them, the dimensions of the O-ring groove and the O-ring, the O-ring compression, lubrication, and surface finish were most important. By optimizing the design and operation of the pneumatic pressure rig, the remnant in-plane stress induced charge was reduced to less than 5% of the total measured charge. To further improve the accuracy and reliability of this technique, a remnant in-plane stress

self-compensation method was developed. In this method, surface charge associated with the in-plane stresses was eliminated through manipulating the in-plane stresses during the measurement. Using this method, accurate d_{33} values were obtained even if there was an appreciable amount of friction present. Calibrations of the pneumatic pressure charge technique were made using the Berlincourt method and double beam interferometry. d_{33} coefficients of 304 pC/N, 305 pC/N and 302 pC/N were obtained for a bulk PZT specimen by these three techniques respectively.

7.1.2 The Piezoelectric Characteristics of Sol-Gel Derived PZT Films

Sol-gel derived PZT films were deposited on Pt-coated silicon wafers using a 2-methoxyethanol precursor solution and rapid thermal annealing. SEM, TEM and XRD studies showed that the films had small grain size (50 to 200 nm) and strong preferred orientation with a very thin second phase layer at the film surface. Films deposited on substrates with <111> oriented Pt bottom electrodes were <111> oriented and films deposited on substrates with <100> oriented Pt were <100> oriented. As the film thickness increased from 0.25 μm to 3.4 μm, there was no change in the grain size and preferred orientation observed. However, both the dielectric constant and the remanent polarization were found to increase with film thickness. The temperature dependence of the dielectric constant showed that there was a very broad dielectric anomaly peaked at T_m of about 390°C in these films due to the ferroelectric-paraelectric phase transition. The peak value of the dielectric constant was much lower in these films than in bulk PZT ceramics and slightly increased with film thickness. However, no change in T_m with film

thickness was found. The modest shift in the Curie temperature suggested that both *a*-domains and *c*-domains were present in these films. The broadened and reduced peak in the dielectric constant at the Curie temperature could result from tensile biaxial stress, and surface/interfacial layers in these films.

The effective d_{33} of the PZT films was measured using both the pneumatic pressure charge technique and the double beam laser interferometer. Results showed that the effective d_{33} from direct measurements was slightly larger than that from converse measurements. This was attributed to the difference in the mechanical boundary conditions for the two measurements. Since the films were clamped by the substrates, thin film piezoelectric measurements gave effective d_{33} values which were related to the unclamped value via the boundary conditions. Theoretical analysis indicated that substrate clamping is partially responsible for the small effective piezoelectric coefficients in PZT films.

The as-deposited PZT films showed very weak piezoelectricity with an effective d_{33} less than 10 pC/N, indicating there is no or little pre-existing alignment of the domains. The effective d_{33} increased with both poling time and field and saturated as the poling field exceeded three times the coercive field. With an increase of film thickness, the effective d_{33} increased, primarily due to the increase of the remanent polarization. The maximum effective d_{33} was measured at Zr/Ti ratio of 52/48, which suggested that the MPB of PZT films coincided with that of the PZT ceramics. For a 1 μm PZT film at this composition, typical effective d_{33} values between 100 pC/N to 120 pC/N were measured. The effective d_{33} was larger on the tetragonal side of the MPB than on the rhombohedral side of the MPB. It was also found that PZT films with <111> preferred orientation had

larger effective d_{33} than films with <100> preferred orientation due to the larger remanent polarization in these films.

7.1.3 Domain Wall Motion and Extrinsic Contributions to the Dielectric and Piezoelectric Properties of PZT Films

Domain wall motion and the extrinsic contributions to the dielectric and piezoelectric response in sol-gel derived PZT films were investigated. The temperature dependence of the dielectric properties showed that although PZT films had much different dielectric constants at room temperature for films with different film thickness, grain size, and preferred orientation, they all had similar intrinsic contributions to the dielectric constant. It was estimated that at room temperature 25% to 50% of the dielectric response of PZT films arises from the extrinsic contribution. The extrinsic contribution to the dielectric constant in PZT films was mostly attributed to 180° domain wall motion, and was likely to increase with both film thickness and grain size.

On the other hand, ferroelastic non-180° domain wall motion was found to be limited in fine grained PZT films, as was indicated by the small effect of normal stress on the low and high field electrical characteristics of the films and the linear relationship between the piezoelectric response and the stress excitation amplitude. This, in turn, suggested that the extrinsic contribution to the piezoelectric coefficient in the fine grained PZT films was small. However, as the films became thicker (> 5 μm), non-linear behavior between the piezoelectric coefficient and the electric driving field was observed. This indicated that there was significant ferroelectric non-180° domain wall motion under

high external excitation in thicker films, which suggested that either the degree of non-180° domain wall pinning decreased or the concentration of ferroelastic walls rose with increasing film thickness.

The activity of non-180° domain walls was studied through non-180° domain switching. For fine grained films with film thickness less than 2 μm, non-180° switching was negligible, indicating that either the pinning of non-180° domain walls was very strong or that there were few present in the films. As the films became thicker, a decrease in the dielectric constant was observed when the poling field exceeded a threshold field. The drop in dielectric constant was attributed to non-180° domain switching, as indicated by dielectric measurements at 4.2 K. The threshold field was found to decrease with an increase in film thickness, suggesting larger non-180° domain wall mobility in thicker films. The non-180° domain switching in the large grained PZT films was found to be much easier and more significant than that in fine grain PZT films. With an increase in the grain size, a decrease in the threshold field was observed.

Domain structures were studied for PZT films using TEM. Initial results on PZT films prepared by 2-methoxyethonal solution and RTA showed that domain fringes were observed in the middle of the films for all the samples from 0.3 μm to 1 μm thick. The majority of the grains which showed domain fringes only had one set of parallel stripes. More complex domain fringes were observed in some large grains. Near the films surface, very few grains which had domain structures were found.

7.2 Recommendations for Future Work

Investigations performed through this thesis indicated that there are several important factors which have a strong influence on the dielectric and piezoelectric properties of PZT films, such as grain size, orientation, film thickness, and substrate clamping. All these factors act together on PZT films and determine the effective dielectric and piezoelectric properties. For a better understanding of the piezoelectric behavior of PZT films, quantitative analysis of the effect of each of the above factors on the intrinsic and extrinsic properties of PZT films is desirable. However, due to insufficient experimental data and the complexity of polycrystalline PZT films, such analysis is still not possible at this moment. The future work should be aimed at quantitative evaluations of both the intrinsic and extrinsic contributions to the dielectric and piezoelectric properties of PZT films, and how they are affected by each of the individual factors.

It has been shown that the partially clamped mechanical boundary condition leads to a small effective d_{33} in PZT films. Theoretical evaluation of this effect is not available due to the uncertainty in the boundary conditions and the lack of elastic constant data for the film. However, the effect of substrate clamping on thin film piezoelectric constants can be evaluated experimentally by releasing the film from the substrate. Suspended cantilevers or beams of PZT film with only very thin electrodes can be formed through selective etching. The unclamped piezoelectric coefficients can then be determined by the resonance method. Comparing this value with the clamped piezoelectric coefficients measured using static methods, the effect of clamped boundary conditions can be

evaluated. Using the resonance method, the unclamped piezoelectric coefficients of the PZT films could be measured at 4 K to give the intrinsic piezoelectric coefficients. An investigation into the temperature dependence of the piezoelectric coefficients of PZT films will provide direct experimental information on how the intrinsic and extrinsic contributions to the piezoelectric response in these films are affected by factors such as film thickness, grain size and orientation. In addition, elastic constants of the PZT films may also be obtained from the resonance measurements. Such data are required for the design of PZT MEMS devices and may enable modeling and simulation of the mechanical boundary conditions of the PZT films in real applications.

The effect of stress, orientation, and clamped mechanical boundary conditions on the intrinsic dielectric and piezoelectric properties of PZT can be investigated using single crystal specimens. Due to the unavailability of large single crystal PZT, lead based perovskite crystals such as $Pb(Zn_{1/3}Nb_{2/3})O_3$-$PbTiO_3$ or $Pb(Mg_{1/3}Nb_{2/3})O_3$-$PbTiO_3$ are suggested for this study. Since these crystals have very similar structures as PZT, it is expected that they will also have similar dielectric and piezoelectric behaviors. The effect of uniaxial, biaxial, and hydrostatic stresses on the intrinsic properties of single domain single crystal specimens at various cutting angles would be useful for understanding the intrinsic properties of PZT films. Information about the clamping effect on the intrinsic properties can also be obtained from this investigation. In addition, by tailoring the domain patterns in these specimens, the extrinsic contributions to the dielectric and piezoelectric properties can be investigated. For example, the single domain specimen can be partially depoled by injecting a controlled amount of opposite surface charge to introduce 180° domain walls into the specimen. By measuring the dielectric constant at

frequencies both below and above the thickness resonance frequency, the effect of piezoelectric clamping on the intrinsic dielectric constant and the 180° domain wall contribution to the dielectric constant of the crystal can be evaluated, as was reported in barium titanate by Fousek [121]. Of particular interest is whether lead based compositions show the same degree of piezoelectric clamping as $BaTiO_3$. Another interesting experiment is to apply uniaxial stress to the single domain specimen to introduce only non-180° domains into it. By comparing the dielectric and piezoelectric properties before and after the introduction of non-180° domains, the relative contributions of the non-180° domain wall motion to the dielectric and piezoelectric response may be evaluated.

Experimental results showed that limited domain wall contributions to the piezoelectric properties in PZT films are partially responsible for the small piezoelectric response in PZT films. There is evidence that both 180° and non-180° domain wall contributions increase with film thickness and grain size. For a more detailed investigation on the domain wall contributions to the properties of PZT films, a more thorough TEM study would be very helpful. In particular, TEM studies may provide quantitative statistics on how the domain assemblage and domain wall density vary with film thickness, grain size, and orientation. To investigate the thickness dependence of the grain size and domain structure, cross-sectional TEM observations should be performed. It is also important to study how the domain structures change with dc poling. This may be achieved by TEM with both unpoled and poled PZT films. To distinguish the 180° domains and non-180° domains in these films, a high-resolution TEM study is recommended.

In addition to TEM, X-ray diffraction is also very useful in analyzing the microstructure and domain structures of the PZT films. From the width of the peaks in XRD patterns, the average coherence length of the crystallites may be determined. This coherence length could be determined by the grain size, the domain width, or the defect distribution of the films. Comparison between the measured coherent diffraction length and the actual grain size might give another indication of the domain size in PZT films. An investigation of the X-ray coherent length of the PZT films may also provide information on how the domain structures vary with film thickness, average grain size, orientation, and composition. By measuring XRD from room temperature to above the Curie temperature, the temperature dependence of the coherence length may be obtained, from which the evolution of the domain structures of PZT films with temperature may be deduced. Use of a synchrotron source would enable higher resolution measurements, as well as a very small spot size, so that the peak shape could also be tracked as a function of the applied electric field. A more comprehensive understanding of the domain structures of the PZT films should be achieved by combining the TEM and XRD results.

It is evident that there are non-180° domain walls in PZT thick films and non-180° domain switching can be achieved at high fields in these films. However, the non-180° domain walls are strongly pinned in PZT films so that they have low mobility under small driving fields. Therefore the extrinsic contribution to the piezoelectric response may be smaller even in thick PZT films in which the degree of non-180° domain wall pinning is much smaller than in thin PZT films. In bulk PZT ceramics, the domain wall pinning can be reduced through adding soft dopants such as Nb into the materials. In thin PZT films, donor doping is not effective in enhancing wall mobility. But there is no

previous work on donor-doped thick films. Therefore, it may be possible to reduce the degree of non-180° domain wall pinning in thick PZT films by soft doping. If the non-180° domain wall pinning can be reduced to such an extent that some of the non-180° domain walls can be activated at relatively small excitation, then an enhancement in the piezoelectric properties of PZT films would be achieved.

In many applications, it is required that the PZT films have low dielectric and piezoelectric losses. However, the loss mechanism in PZT films is still not well understood yet. It has been shown in this thesis that most of the dielectric loss at room temperature is from extrinsic or transport sources, and it is greatly influenced by the interface between the PZT film and the top electrode. To investigate whether the Schottky barrier between the PZT film and the electrode plays a role in the dielectric loss, top electrodes may be deposited on PZT films using various metals which have different work functions. By changing the height of the Schottky barrier using different top electrodes, its influence on the dielectric loss of PZT films may be illustrated.

References

[1] K. R. Udayakumar, J. Chen, A. M. Flynn, S. F. Bart, L. S. Tavrow, D. J. Ehrlich, L. E. Cross, and R. A. Brooks, *Ferroelectrics*, **160**, 347 (1994).

[2] D. L. Polla and L. F. Francis, *MRS Bulletin*, **July**, 59 (1996).

[3] J. J. Bernstein, S. L. Finberg, K. Houston, L. C. Niles, H. D. Chen, L. E. Cross, K. K. Li, and K. Udayakumar, *IEEE Transactions on Ultrasonics, Ferroelectrics, and Frequency Control*, **44**, 960 (1997).

[4] Y. Nemirovsky, A. Nemirovsky, P. Muralt, and N. Setter, *Sen. and Act.*, **A56**, 239 (1996).

[5] T. Itoh, J. Chu, I. Misumi, K. Kataoka, and T. Suga, *Proc. Transducers 97*, 459 (1997).

[6] P. Muralt, M. Kohli, T. Maeder, A. Kolkin, K. Brooks, N. Setter, and R. Luthier, *Sen. and Act.*, **A48**. 157 (1995).

[7] N. Kim, "Grain size effect on the dielectric and piezoelectric properties in compositions which are near the morphotropic phase boundary of lead zirconate titanate based ceramics", *Ph. D. Thesis*, The Pennsylvania State University (1994).

[8] F. Jona, and G. Shirane, *Ferroelectric Crystals*, Pergamon Press, New York (1962).

[9] W. P. Mason, *Piezoelectric Crystals and their Application to Ultrasonics*, D. Van Nostrand Company Inc., New York (1955).

[10] A. L. Kholkin, C. Wutchrich, D. V. Taylor, and N. Setter, *Rev. Sci. Instrum.*, **67**, 1935 (1996).

[11] W. Y. Pan and L. E. Cross, *Rev. Sci. Instr.*, **60**, 2701 (1989).

[12] A. Kholkin, Submitted to *Ferroelectrics* (1998).

[13] P. Luginbuhl, G. A. Racine, P. Lerch, B. Romanowicz, K. G. Brooks, N. F. de Rooij, P. Renaud, and N. Setter, *Sen. and Act.*, **A54**, 530 (1996).

[14] J. F. Shepard, The Investigation of Biaxial Stress Effects and the Transverse Piezoelectric (d_{31}) Characterization of Lead Zirconate Titanate Thin Films, *Ph.D. Thesis*, The Pennsylvania State University (1998)

[15] M. O. Eatough, D. Dimos, B. A. Tuttle, and W. L. Warren, *Mat. Res. Soc. Symp. Proc.* **361**, 111 (1995).

[16] S. Trolier-McKinstry, J. F. Shepard, Jr., T. Su, G. Zavala, and J. Fendler, *Ferroelectrics* **206**, 381 (1997).

[17] K. Petersen, *Sen. and Act.*, **A56**, 143 (1996).

[18] K. Petersen, *Proc. of the IEEE*, **70**, 420 (1982).

[19] W. S. N. Trimmer and K. J. Gabriel, *Sen. and Act.*, **11**, 189 (1987).

[20] H. Chen, M. Bao, H. Zhu, and S. Shen, *Sen. and Act.* **A63**, 19 (1997).

[21] M. Bao, and W. Wang, *Sen. and Act.* **A56**, 135 (1996).

[22] M. Petersen, W. Dlthuis, and P. Bergveld, *Sen. and Act.* **A63**, 97 (1997).

[23] P. Krause, E. Obermeier, W. Wehl, *Sen. and Act,* **A53**, 405 (1996).

[24] P.P.A. Syms, B. M. Hardcastle, R. A. Lawes, *Sen. and Act,* **A63**, 61 (1997).

[25] M. H. Kiang, O. Solgaard, R. S. Muller, and K. Y. Lau, *IEEE Photonics and Technology Letters*, **8**, 57 (1996).

[26] B. Jaffe, J. W. R. Cook, and H. Jaffe, *Piezoelectric Ceramics*: R. A. N. (1971).

[27] *Landolt Bornstein Tables*, vol. II. Berlin: Springer-Verlag, (1979).

[28] D. L. Polla, *Proc. IEEE Ultrasonics Symposium*, 127 (1992).

[29] M. Kurosawa, T. Morita, and T. Higuchi, *Proc. IEEE Ultrasonics Symposium*, 549 (1994).

[30] P. Muralt, A. Kholkin, M. Kohli, T. Maeder, and N. Setter, *Microelectronic Engineering*, **29**, 67 (1995).

[31] C. Lee, T. Itoh, and T. Suga, *IEEE Transactions on Ultrasonics, Ferroelectrics, and Frequency Control*, **43**, 533 (1996).

[32] W. P. Robbins, *Integrated Ferroelectrics*, **11**, 179 (1995).

[33] W. G. Cady, *Piezoelectricity*, First Edition, Third Impression, New York (1946).

[34] J. F. Nye, *Physical Properties of Crystals*, Oxford University Press, New York (1985).

[35] A. F. Devonshire, *Phil. Mag. Suppl.*, **3**, 85 (1954).

[36] P. W. Forsbergh, Jr., *Piezoelectricity, Electrostriction and Ferroelectricity, Handbuch der Physik*, **17**, 264, Springer-Verlag, Berlin (1956).

[37] M. J. Haun, *Ph.D. Thesis*, The Pennsylvania State University, (1988).

[38] L. A. Shuvalov, *J. Phys. Soc. Jpn., Supplement24*, 38 (1970).

[39] W. D. Kingery, H. K. Bowen, and D. R. Uhlmann, *Introduction to Ceramics*, Second Edition, John Wiley and Sons, New York (1976).

[40] M. E. Lines and A. M. Glass, *Principles and Applications of Ferroelectrics and Related Materials*, Oxford University Press, New York (1977).

[41] H. D. Megaw, *Ferroelectricity in Crystals*, Methuen Co., London (1975).

[42] L. E. Cross and K. H. Härdtl, *Encyclopedia of Chemical Technology*, **10**, 1, Third Edition, Edited by Kirk Othmer, John Wiley & Sons, New York (1980).

[43] T. Mitsui and J. Furuichi, *Phys. Rev.*, **90**, 193 (1953).

[44] Weilie Zhong, *Physics of Ferroelectrics*, Scientific Press, Beijing, China (1996).

[45] G. Arlt, *Ferroelectrics*, **104**, 217 (1990).

[46] G. Arlt, *J. Mater. Sci.*, **25**, 2655 (1990).

[47] G. Arlt, D. Hennings, and D. de With, *J. Appl. Phys.*, **58**, 1619 (1985).

[48] C. A. Randall, N. Kim, W. Cao, and T. R. Shrout, in *Proc. 7th US-Japan Seminar on Dielectric and Piezoelectric Ceramics*, Nov. 14-17, (1995).

[49] W. Cao, and C. Randall, *J. Phys. Chem. Solids*, **57**, 1499 (1996).

[50] L. D. Madsen, E. M. Griswold, and L. Weaver, *J. Mater. Res.*, **12**, 2612 (1997).

[51] R. Herbiet, U. Robels, H. Dederichs, and G. Arlt, *Ferroelectrics*, **98**, 107 (1989).

[52] Q. M. Zhang, H. Wang, N. Kim, and L. E. Cross, *J. Appl. Phys.*, **75**, 454 (1994).

[53] D. Damjanovic, M. Demartin, F. Chu, and N. Setter, in *Proc. of 10th International Symp. on Applications of Ferroelectrics*, New Brunswick, NJ, (1996).

[54] L. E. Cross, in *Ferroelectric Ceramics*, p. 1, Edited by N. Setter and E. Colla, Birkhauser, Basel, Switzerland (1993).

[55] E. I. Bondarenko, V. Yu. Topolov, and A. V. Turik, *Ferroelectr. Lett. Sect.*, **13**, 13 (1991).

[56] O. Kersten, and G. Schmidt, *Ferroelectrics*, **67**, 191 (1986).

[57] U. Bottger, and G. Arlt, *Ferroelectrics*, **127**, 95 (1992).

[58] X. L. Zhang, Z. X. Chen, L. E. Cross, and W. A. Schulze, *J. Mater. Sci.*, **18**, 968 (1983).

[59] S. Li, W. Cao, and L. E. Cross, *J. Appl. Phys.*, 69, 7219 (1991).

[60] D. Damjanovic, *J. Appl. Phys.*, 82, 1788 (1997).

[61] D. Damjanovic, and M. Demartin, *J. Phys.:Condens. Matter.*, 9, 4934 (1997).

[62] G. Arlt, and N. A. Pertsev, *J. Appl. Phys.*, 70, 2283 (1991).

[63] J. Grindlay, *An Introduction to the Phenonmenological Theory of Ferroelectricity*, Pergamon Press, Oxford (1970).

[64] E. Fatuzzo, W. J. Merz, *Ferroelectricity*, North-Holland, Amsterdam (1967).

[65] T. Mitsui, I. Tatsuzaki, E. Nakamura, *An Introduction to the Physics of Ferroelectrics*, Gordon and Breach, New York (1976).

[66] V. A. Isupov, *Soviet Physics – Solid State*, **12**, 1084 (1970).

[67] V. A. Isupov, *Soviet Physics – Solid State*, **19**, 783 (1977).

[68] K. Carl, and K. H. Hardtl, *Phys. Stat. Sol.*, **A8**, 87 (1971).

[69] A. Amin, *Ph.D. Thesis*, The Pennsylvania State University (1979).

[70] A. Amin, M. J. Haun, B. Badger, H. A. McKinstry, and L. E. Cross, *Ferroelectrics*, **65**, 107 (1985).

[71] T. R. Halemane, M. J. Haun, L. E. Cross, and R. E. Newnham, *Ferroelectrics*, **62**, 149 (1985).

[72] M. J. Haun, E. Furman, S. J. Jang, H. A. McKinstry, and L. E. Cross, *J. Appl. Phys.*, **62**, 3331 (1987).

[73] G. H. Haertling, and W. J. Zimmer, *Am. Ceram. Soc. Bull.*, **45**, 1084 (1966).

[74] G. H. Jonker, *Ber. Deut. Keram. Ges.*, **44**, 265 (1967).

[75] H. J. Gesemann, *Ber. Deut. Keram. Ges.*, **42**, 60 (1965).

[76] A. H. Webster, and T. B. Weston, *Canadian Ceram. Soc. J.*, **37**, 41 (1968).

[77] K. Okazaki, and K. Nagata, *J. Am. Ceram. Soc.*, **56**, 82 (1973).

[78] H. T. Martirena, and J. C. Burfoot, *J. Phys C: Solid State Sci.*, **7**,3182 (1974).

[79] T. Yamamoto, *Ceram. Bull.*, **71**, 978 (1992).

[80] M. Takahashi, *Japn. J. Appl. Phys.*, **9**, 1236 (1970).

[81] S. B. Desu, *J. Electrochem. Soc.*, **140**, 2981 (1993).

[82] G. A. C. M. Spierings, G. J. M. Dormans, W. G. J. Moors, M. J. E. Ulenaers, and P. K. Larsen, *J. Appl. Phys.*, **78**, 1926 (1995).

[83] B. A. Tuttle, J. A. Voigt, T. J. Garino, D. C. Goodnow, R. W. Schwartz, D. L. Lamppa, T. J. Headly, and M. O. Eatough, *Proc. Of 8th International Symposium on Applications of Ferroelectrics*, **344** (1992).

[84] R. F. Brown, *Can. J. Phys.*, **39**, 741 (1961).

[85] R. F. Brown, and G. W. McMahon, *Can. J. Phys.*, **40**, 672 (1962).

[86] H. H. A. Krueger, *J. Acoust. Soc. Am.*, **42**, 636 (1967).

[87] H. H. A. Krueger, *J. Acoust. Soc. Am.*, **43**, 576 (1967).

[88] H. H. A. Krueger, *J. Acoust. Soc. Am.*, **43**, 583 (1967).

[89] R. Y. Nishi, *J. Acoust. Soc. Am.*, **40**, 486 (1966).

[90] Q. M. Zhang, J. Zhao, K. Uchino, and J. Zheng, *J. Mater. Res.*, **12**, 226 (1997).

[91] B. A. Rotenberg, *Soviet Physics Solid State*, **1**, 1627 (1960).

[92] X. Du, J. Zheng, U. Belegundu, and K. Uchino, *Appl. Phys. Lett.*, **72**, 2421 (1998).

[93] B. A. Tuttle, T. J. Garino, J. A. Voigt, T. J. Headley, D. Dimos, and M. O. Eatough, in *Science and Technology of Electroceramic Thin Films*, **117** (1995).

[94] K. D. Budd, S. K. Dey, and D. A. Payne, *Brit. Ceram. Proc.*, **36**, 107 (1985).

[95] K. Brooks, M. Kohli, D. V. Taylor, T. Maeder, I. Reaney, A. Kholkin, P. Muralt, and N. Setter, in *Proc. of 10th International Symposium on Applications of Ferroelectrics*, New Brunswick, NJ, (1996).

[96] W. Ren and S. Trolier-McKinstry, unpublished work (1998).

[97] G. Yi, Z. Wu, and M. Sayer, *J. Appl. Phys.*, **64**, 2717 (1988).

[98] H. D. Chen, K. R. Udayakumar, C. J. Gaskey, and L. E. Cross, *Appl. Phys. Lett.*, **67**, 3411 (1995).

[99] S. C. Cheng, T. Su, and S. Trolier-McKinstry, to be published in *Microscopy and Microanalysis* (1999).

[100] Z. Xie, Johns Hopkins University, unpublished work (1999).

[101] *IEEE Standard on Piezoelectricity*, ANSI/IEEE, Std. (1988).

[102] S. Sherrit, H. D. Wiederick, B. K. Mukherjee, and M. Sayer, *Ferroelectrics*, **193**, 88 (1997).

[103] M. Lukacs, private communication (1999).

[104] F. Xu, and S. Trolier-McKinstry, in *Proceedings of the 10th International Symposium on Applications of Ferroelectrics*, New Brunswick, NJ, (1996).

[105] Z. Surowiak, D. Czekaj, A. M. Margolin, E. V. Sviridov, V. A. Aleshin, and V. P. Dudkevich, *Thin Solid Films*, **214**, 78 (1992).

[106] K. Lefki, and G. J. M. Dormans, *J. Appl. Phys.*, **76**, 1764 (1994).

[107] K. Lefki, Private Communication (1996).

[108] W. Ren, H. Zhou, X. Wu, L. Zhang, and X. Yao, *Materials Letters*, **31**, 185 (1997).

[109] *Parker O-ring Handbook*, Parker Seal Group, Lexington, KY

[110] F. Chu, F. Xu, J. Shepard, Jr., and S. Trolier McKinstry, *Mat. Res. Soc. Symp. Proc.* **493**, 409 (1995).

[111] J. F. Shepard, Jr., S. Trolier-McKinstry, M. A. Henderickson, and R. Zeto, in *Proceedings of the 10th International Symposium on Applications of Ferroelectrics*, New Brunswick, NJ, (1996).

[112] S. K. Streiffer, C. Basceri, C. B. Parker, S. E. Lash, and A. I. Kingon, submitted to *J. Appl. Phys.* (1999).

[113] N. A. Pertsev, A. G. Zembilgotov, S. Hoffmann, R. Waser, and A. K. Tagantsev, *J. Appl. Phys.*, **85**, 1698 (1999).

[114] W. A. Brantley, *J. Appl. Phys.*, **44**, 534 (1973).

[115] A. L. Kholkin, M. L. Calzada, P. Ramos, J. Mendiola, and N. Setter, *Appl. Phys. Lett.* **69**, 3602 (1996).

[116] F. Xu, F. Chu, and S. Trolier-McKinstry, *J. Appl. Phys.*, **86**, 588 (1999).

[117] H. D. Chen, Ferroelectric Thin and Thick Films for Sensing and Decoupling Functions, *Ph.D. Thesis*, The Pennsylvania State University (1996).

[118] M. Demartin, and D. Damjanovic, *Appl. Phys. Lett.*, **68**, 3046 (1996).

[119] M. Kohli, P. Muralt, and N. Setter, *Appl. Phys. Lett.*, **72**, 3217 (1998).

[120] B. A. Tuttle, T. J. Headley, H. N. Al-Shareef, J. A. Voigt, M. Rodriguez, J. Michael, and W. L. Warren, *J. Mater. Res.*, **11**, 2309 (1996).

[121] J. Fousek, Czech. *J. Phys. B*, **15**, 412 (1965).

Vita

Fei Xu was born in Xingjiang, China on August 12th, 1967. He received his Bachelor of Science degree in Electrical Engineering in 1988 from Jilin University in Changchun, China. He earned his Masters of Science degree in Electrical Engineering from Shanghai Institute of Metallurgy, The Chinese Academy of Science in 1991. Mr. Xu then joined the faculty of the Department of Materials Science at Fudan University as an assistant professor in Shanghai, China. In 1995, he came to the Materials Research laboratory at the Pennsylvania State University and conducted research on ferroelectric thin films. Mr. Xu received his Ph.D. in August of 1999.